Consequences of Fuel Failure on Criticality Safety of Used Nuclear Fuel

Fuel Cycle Research & Development

Prepared for
U.S. Department of Energy
Fuel Cycle Technologies Program
W. J. Marshall
J. C. Wagner
Oak Ridge National Laboratory
September 2012
ORNL/TM-2012/325
FCRD-UFD-2012-000262

EXECUTIVE SUMMARY

This report documents work performed for the Department of Energy's Office of Nuclear Energy (DOE-NE) Fuel Cycle Technologies Used Fuel Disposition Campaign to assess the impact of fuel reconfiguration due to fuel failure on the criticality safety of used nuclear fuel (UNF) in storage and transportation casks. This work was motivated by concerns related to the potential for fuel degradation during extended storage (ES) periods and transportation following ES, but has relevance to other potential causes of fuel reconfiguration.

Commercial UNF in the United States is expected to remain in storage for longer periods than originally intended. Extended storage time and irradiation of nuclear fuel to high-burnup values (>45 GWd/t) may increase the potential for fuel failure during normal and accident conditions involving storage and transportation. Fuel failure, depending on the severity, can result in changes to the geometric configuration of the fuel, which has safety and regulatory implications for virtually all aspects of a UNF storage and transport system's performance. The potential impact of fuel reconfiguration on the safety of UNF in storage and transportation is dependent on the likelihood and extent of the fuel reconfiguration, which is not well understood and is currently an active area of research. The objective of this work is to assess and quantify the impact of postulated failed fuel configurations on the criticality safety of UNF in storage and transportation casks. Although this work is motivated by the potential for fuel degradation during ES periods and transportation following ES, it has relevance to fuel reconfiguration due to the effects of high burnup. Regardless of the ultimate disposition path, UNF will need to be transported at some point in the future.

To investigate and quantify the impact of fuel reconfiguration on criticality safety limits, which are given in terms of the effective neutron multiplication factor, k_{eff}, a set of failed fuel configuration categories was developed and specific configurations were evaluated. The various configurations were not developed to represent the results of specific reconfiguration progressions; rather, they were designed to be bounding of any reconfiguration progressions that could occur. The configuration categories considered in this analysis include the following:

- clad thinning/loss – reduced cladding thickness up to the total removal of all cladding material
- rod failures – removal of one or more fuel rods from the assembly lattice
- loss of rod pitch control – rod pitch contraction and expansion within the storage cell
- loss of assembly position control – axial displacement of fuel assemblies
- gross assembly failure – rubblized fuel within the storage cells with varying degrees of moderation
- neutron absorber degradation – gaps of varying location and size; thinning of absorber panels.

Within each category, a number of specific configurations were modeled to calculate the corresponding k_{eff} values and the associated consequences of those configurations relative to the reference intact configuration. The consequence of a given configuration is defined as the difference in the calculated k_{eff} values for the given configuration and the reference intact configuration, with a positive value indicating an increase in k_{eff} as compared to the reference configuration. Several of the specific configurations are not considered credible but are included in the analyses for completeness (e.g., to fully understand trends and worst-case situations). Pending improved understanding of the various material degradation phenomenon, and subsequent determination and justification for what configurations are and are not credible, the assessment of the credibility of configurations provided herein is based on engineering judgment. The credibility of configurations and the impact of the configurations on criticality safety are dependent on many factors, including storage and transportation conditions, the fuel assembly characteristics, and the storage and/or transportation system characteristics. Therefore, the assessment and analysis of credible configurations for a specific cask system would need to be performed as part of the safety analysis for licensing that system.

Representative pressurized water reactor (PWR) and boiling water reactor (BWR) fuel assembly designs loaded in representative cask systems were considered in this report. The two fuel assembly designs selected for this analysis represent a large portion of the current inventory of discharged UNF and/or a significant portion of the fuel designs currently in use. The cask systems selected for this analysis are high-capacity 32-PWR-assembly general burnup credit cask (GBC-32) and 68-BWR-assembly multipurpose canister (MPC-68) cask designs based on the Holtec International HI-STAR 100 system. The depletion conditions used in this analysis are considered representative of those used in a burnup credit criticality safety evaluation. The analysis focuses on typical discharge fuel conditions (e.g., fuel initial enrichment, discharge burnup, and post-irradiation decay time) that could be loaded into storage and transportation casks. Additional burnup and extended post-irradiation cooling times are considered in this analysis for both PWR and BWR fuel to establish the sensitivity of reconfiguration impacts to these parameters.

For the configurations judged by the authors to be potentially credible, the maximum increase in k_{eff} for the PWR cask system (GBC-32) was nearly 4%, corresponding to a nonuniform pitch expansion configuration due to a loss of fuel rod pitch control, and that for the BWR cask system (MPC-68) was 2.4%, corresponding to a configuration with multiple rod failures. It is important to emphasize that these results are contingent on the authors' judgment relative to the potential credibility of configurations, which includes not only whether a configuration category is credible but also whether the resulting configurations within a given category are credible for a specific cask system. For example, for the PWR cask system, axial assembly displacement such that assemblies extended more than 7.5 cm above or below the neutron absorber panel was not considered credible because of the presence of fuel assembly hardware and cask assembly spacers. If it were determined that such a configuration is credible, then that configuration and its specific characteristics may be limiting. Similarly, for the BWR cask system, the fuel assembly channel is assumed to be present and capable of constraining fuel rod pitch expansion. If the channel is not present or unable to constrain rod pitch expansion, then that configuration may be limiting. In addition to representative conditions for fuel burnup and post-irradiation decay time, the effects of higher burnup and longer cooling times were also investigated and found to be smaller than the reduction in k_{eff} associated with the higher burnup or cooling time.

Because a wide range of credible and non-credible configurations were analyzed, the calculated consequences also varied widely. For the PWR cask system (GBC-32), the calculated k_{eff} increase varied from 0.1% to almost 22.25% Δk_{eff}. For the BWR cask system (MPC-68), the calculated increase varied from 0.3% Δk_{eff} to as much as almost 36% Δk_{eff}. Some configurations in both cask systems result in decreases in k_{eff}. As the Nuclear Regulatory Commission (NRC) Standard Review Plans, which provide guidance for demonstrating compliance with the applicable regulations, recommend that k_{eff} should not exceed 0.95 under all credible conditions during storage and transportation, such large increases are concerning. However, as noted, a number of the configurations analyzed are not considered credible.

The magnitude of the potential increases in k_{eff} and the sensitivity of the potential increases in k_{eff} to the determination of the credibility of configurations highlight the importance of being able to determine and justify which configurations are credible under a given set of conditions for a given cask system. It is anticipated, at least in the near term, that these determinations will be done on a case-by-case basis for each cask system and associated licensing conditions.

Given the establishment of a set of credible failed fuel configurations for a given cask system and assuming that one or more of the configurations result in an increase in k_{eff} (above the regulatory limit of

0.95), the consequence of this potential increase in k_{eff} must be addressed. There are a number of potential options, the viability of which depends on the magnitude of the increase in k_{eff}. For example, a cask design and/or fuel assembly loading conditions could be modified to ensure that the current k_{eff} limit of 0.95 is satisfied for all credible failed fuel configurations. Separate assembly loading criteria (e.g., loading curves) based on a reduced k_{eff} limit could be developed for fuel assemblies that may have questionable integrity. In the context of high-burnup fuel or ES durations, a separate loading curve based on a lower k_{eff} limit could be developed and applied to fuel assemblies with burnup greater than 45 GWd/MTU and/or with a post-irradiation storage period beyond some specified value. Alternatively, depending on the probability of fuel reconfiguration, it may be possible that a separate higher limit could be established to allow margin for the increased reactivity effect associated with fuel reconfiguration. This latter approach would be similar to the higher limit (i.e., 0.98) allowed for the unlikely optimum moderation condition in dry storage of fresh fuel under 10 CFR 50.68. In this case, the customary k_{eff} limit would still apply to all conditions involving intact fuel. Limits above 0.95 are also allowed in some facilities regulated by the NRC Fuel Cycle Safety and Safeguards Division, and hence precedents for this type of approach exist. For casks that have already been loaded prior to implementation of a generic mitigation strategy, the analysis basis may be extended to include or expand burnup credit, providing mitigation for potential consequences of fuel reconfiguration.

Although the results indicate that the potential impacts on subcriticality can be rather significant for certain configurations, it can be concluded that the consequences of credible fuel failure configurations from ES or transportation following ES are manageable. Some examples for how to address the potential increases in k_{eff} in a criticality safety evaluation were provided. Future work to further inform decision-making relative to which configurations are credible, and therefore need to be considered in a safety evaluation, is recommended.

CONTENTS

Page

CONTENTS (continued)

FIGURES

Page

FIGURES (continued)

Page

FIGURES (continued)

TABLES

TABLES (continued)

TABLES (continued)

TABLES (continued)

ACRONYMS

BWR	boiling water reactor
CRC	commercial reactor critical
DOE-NE	Department of Energy’s Office of Nuclear Energy
EIS	environmental impact statement
EPRI	Electric Power Research Institute
ES	extended storage
FIP	fuel integrity project
GBC	generic burnup credit cask
GE	General Electric
GWd/MTU	gigawatt days per metric ton uranium
HAC	hypothesized accident conditions
ICNC	International Conference on Nuclear Criticality Safety
LWR	light water reactor
MPC	multipurpose canister
NRC	United States Nuclear Regulatory Commission
OFA	optimized fuel assembly
PATRAM	International Symposium on the Packaging and Transportation of Radioactive Materials
PRA	probabilistic risk assessment
PWR	pressurized water reactor
SAR	safety analysis report
SFST	Division of Spent Fuel Storage and Transportation, U.S. Nuclear Regulatory Commission
SRP	standard review plan
UNF	used nuclear fuel
WABA	wet annular burnable absorber
w/o	weight percent

FUEL CYCLE TECHNOLOGIES PROGRAM

CONSEQUENCES OF FUEL FAILURE ON CRITICALITY SAFETY OF USED NUCLEAR FUEL

1. INTRODUCTION AND BACKGROUND

This report documents work performed for the Department of Energy's Office of Nuclear Energy (DOE-NE) Fuel Cycle Technologies Used Fuel Disposition Campaign to assess the impact of fuel reconfiguration due to fuel failure on the criticality safety of used nuclear fuel (UNF) in storage and transportation casks. The consequences of degradation of neutron absorber panels and cask assembly spacers within the casks are also considered. This work is motivated by concerns related to the potential for fuel degradation during extended storage (ES) periods and transportation following ES, but has relevance to other potential causes of fuel reconfiguration.

Fuel reconfiguration could adversely impact virtually all aspects of a UNF storage and transport system's performance, including thermal, radiation dose, criticality safety, containment, structural, and fuel handling and retrievability, and hence is being studied in research and regulatory activities [1–6]. The likelihood and potential extent of fuel reconfiguration during ES and the subsequent impact of reconfiguration on the safety of the UNF are not well understood. Uncertainties related to the mechanical properties of fuel cladding and other structural materials at high burnups (>45 GWd/MTU) and after ES exacerbate these concerns.

A key element of understanding the impacts of ES is related to ensuring that regulatory requirements are met. These requirements address safety-significant aspects of UNF storage and transportation systems, including criticality safety performance and related operational requirements pertaining to UNF handling and retrievability. The results of this study may be used to develop an effective approach to address criticality safety associated with UNF after ES.

This work is an expansion of NUREG/CR-6835, Ref. 7, and includes the same overall strategy. This strategy is to identify relevant potential fuel degradation configurations, quantify the impact of these configurations on k_{eff}, and evaluate potential mitigation strategies to meet criticality safety requirements. This work expands on Ref. 7 by including irradiated (or used) boiling water reactor (BWR) fuel as well as used pressurized water reactor (PWR) fuel, considers longer cooling times, and expands the scope of reconfigurations considered.

The criticality safety requirements for dry storage and transportation of UNF are contained in 10 CFR Parts 72 and 71, respectively Refs. 8 and 9. Standard Review Plans (SRPs), Refs. 10–12, provide guidance for meeting the regulatory requirements, such as the k_{eff} limit of 0.95 for ensuring the regulatory requirement associated with criticality safety. Estimates of the change in k_{eff} (Δk) due to credible failed fuel configurations are generated in this analysis. A set of failed fuel configuration categories was developed and specific configurations are analyzed to provide a conservative assessment of the impact on k_{eff}. The potential credibility of these configurations is also considered, and only those judged to be potentially credible are considered in the development of mitigation strategies. The change in k_{eff} due to credible reconfigurations can be used in at least two different ways. A cask design and/or fuel assembly loading conditions could be modified to ensure that the current k_{eff} limit of 0.95 is satisfied for all credible failed fuel configurations. The Δk caused by reconfiguration would be accounted for in the determination of the loading curve to meet the regulatory limit. It is also possible that a separate higher limit could be established to allow margin for the Δk associated with fuel reconfiguration. This latter approach would be similar to the higher limit allowed for the optimum moderation condition applied to dry storage of fresh fuel (i.e., $k_{eff} \leq 0.98$), or the unborated condition in a spent fuel pool that credits soluble boron to demonstrate compliance (i.e., $k_{eff} < 1.0$) under 10 CFR 50.68, Ref. 13. In this case, the customary k_{eff} limit would still apply to all conditions involving intact fuel.

The results of this work may also be used to focus future materials research efforts. The configurations that lead to the highest k_{eff} increases may be precluded or determined not to be credible with appropriate material research and testing coupled with mechanical analyses of the UNF.

In addition to criticality safety, the regulatory requirements for UNF storage and transport systems address safety-significant aspects such as structural, thermal, containment and radiation shielding, as well as related operational requirements pertaining to UNF handling and retrievability, such as those contained in the following Sections of 10 CFR 72. 122 (h) *Confinement barriers and systems*:

- (1) "The spent fuel cladding must be protected during storage against degradation that leads to gross ruptures or the fuel must be otherwise confined such that degradation of the fuel during storage will not pose operational safety problems with respect to its removal from storage. This may be accomplished by canning of consolidated fuel rods or unconsolidated assemblies or other means as appropriate."

- (5) "The high-level radioactive waste and reactor-related GTCC waste must be packaged in a manner that allows handling and retrievability without the release of radioactive materials to the environment or radiation exposures in excess of part 20 limits. The package must be designed to confine the high-level radioactive waste for the duration of the license."

Because it is possible that, within potential ES time periods, SNF may be transported under 10 CFR 71, and then returned to dry storage (e.g., at another utility or a national interim storage site) under 10 CFR 72, demonstration of compliance with the current handling and retrievability requirements in 10 CFR 72 may pose a significant challenge.

2. REVIEW OF LITERATURE

A review of previous work that is potentially relevant to the scope of this report was conducted. The information reviewed provides a historical context for consideration of fuel reconfiguration during transportation, the extent of reconfiguration that may be expected based on material test data, and an indication of the magnitude of reactivity consequences observed involving configurations similar to those considered in this report.

The documents reviewed are grouped by source into four categories: NRC documents, Electric Power Research Institute (EPRI) documents, International Symposium on the Packaging and Transportation of Radioactive Materials (PATRAM) proceedings, and others. NUREG/CR-6835, Ref. 7, is not specifically reviewed as this report is an update and expansion of that work. The primary differences between this analysis and Ref. 7 are discussed in Section 3.

2.1 NRC Documents

The first source of documents reviewed from the NRC was the Division of Spent Fuel Storage and Transportation (SFST) technical exchange meeting held on November 1, 2011. The technical exchange meeting featured presentations from various members of the industry as well as NRC staff members. The NRC gave a presentation, Ref. 14, related to the reactivity impact of fuel reconfiguration. The presentation discussed pin deformation modeling but did not provide estimates of the k_{eff} increase associated with this type of fuel damage. In general, the presentation focused on the development and qualification of models to predict the potential deformation that could occur. Some perspectives on the k_{eff} changes caused by fuel reconfiguration were presented that referred to NUREG/CR-6835, Ref. 7, and an EPRI study of the reactivity consequence of fuel reconfiguration, Ref. 15. The presentation provided useful information regarding current NRC positions relative to fuel reconfiguration effects in storage/transportation casks.

Other documents reviewed include NUREG/CR-6672, NUREG/CR-4829, and NUREG-0170, Refs. 16–18. These documents provide generic analyses for package response during transportation accidents. NUREG/CR-6672, Ref. 16, includes updated methodologies and data for analyzing truck and rail cask accidents compared to NUREG/CR-4829, Ref. 17, which was an update of the methodologies used in NUREG-0170, Ref. 18. NUREG-0170 is the original environmental impact statement (EIS) for the transportation of radioactive materials. These documents discuss the impact of failed used fuel rods on source terms but do not include reactivity effects.

Overall, based on the NRC documents reviewed, no new information pertinent to modeling fuel reconfiguration conditions for criticality safety evaluations was identified.

2.2 EPRI Reports

EPRI has sponsored research culminating in several reports related to shipping UNF. The reports of interest for this effort tend to cover closely related and frequently overlapping areas. Three reports – *Fuel Relocation Effects for Transportation Packages* ,Ref. 15, *Transportation of Commercial Spent Nuclear Fuel: Regulatory Issues Resolution*, Ref. 19, and *Criticality Risks during Transportation of Spent Nuclear Fuel: Revision 1*, Ref. 20 – were referenced in the EPRI presentation at the 2011 SFST Technical Exchange meeting, Ref. 21, that are considered relevant to this work.

Reference 15 is largely a critique of NUREG/CR-6835, Ref. 7, and is focused on demonstrating that fuel reconfiguration effects are small and have minimal impacts on the criticality safety of transportation packages. Qualitative arguments were used to eliminate configurations as not practical in many places. The study provides references to additional EPRI reports to support some suppositions about the performance of fuel cladding in the transportation casks. Some lessons learned from radiochemical assay campaigns are also referred to in establishing the impracticality of many of the extreme configurations studied in Ref. 7.

Computational results are also provided for a number of similar configurations that are evaluated in this report. The k_{eff} change associated with pitch expansion over the entire length of the fuel array for PWR fuel is reported as 3.1% Δk_{eff}. The removal of all cladding material is reported as causing a k_{eff} increase of 3.3% Δk_{eff} in a generic 32-PWR-assembly capacity cask. The pellet array configurations considered were significantly different from those evaluated in this report as described in Section 3.1.5.2.

Reference 19 presents several proposed resolutions to various regulatory issues perceived by EPRI to be particularly problematic for licensing transportation packages characterized as high capacity, containing high-burnup UNF, or both. The document discusses several considerations including moderator exclusion, expanded burnup credit, the robust design of used fuel transportation casks, and systematic analyses based on defense-in-depth. The report summarizes other EPRI-sponsored efforts to investigate the performance of fuel cladding during accident conditions, including a summary of the analysis provided in Reference 15. The criticality analysis section includes a discussion of potential benefits from burnup credit and moderator exclusion, but no new information pertaining to accident configurations or computational results was provided.

Reference 20 contains a probabilistic risk assessment (PRA) quantifying the frequency of criticality accidents during railway shipment of UNF. The results of this research indicate a very low probability for a criticality accident based on several factors, including the low likelihood of severe rail accidents, large safety margins in the determination of the loading curve used in the certificate of compliance, and the difficulty of generating a critical configuration even with severe accident conditions. No new accident configurations or quantitative k_{eff} calculations were presented in this report.

The three reports discussed above provide a synopsis of the information contained in several other EPRI documents containing the majority of the information generated by EPRI-sponsored work related to fuel reconfiguration.

2.3 PATRAM Proceedings

The PATRAM symposium is the primary international meeting related to packaging and shipping of radioactive materials. The proceedings for the last four PATRAM symposia dating back to 2001 were reviewed, and a summary of the relevant papers to the work in this report is presented in the following subsections.

2.3.1 PATRAM 2010

Several papers in the 2010 PATRAM proceedings were identified as providing information related to modeling of fuel reconfiguration and the k_{eff} consequences of such events. The papers of interest with regards to this report are "Accelerated Corrosion Testing of Aluminum Carbide Metal Matrix Composite in Simulated PWR Spent Fuel Pool Solution," Ref. 22, and "Description of Fuel Integrity Project Methodology Principles," Ref. 23. Papers that did not provide detailed information about fuel deformation or damage and the effects of that damage on k_{eff} are not included in this discussion.

Reference 22 provides information related to corrosion testing of B_4C/Al neutron absorber materials in PWR spent fuel pool environments. This information is not directly relevant to the work performed here but provides some indication that the neutron absorber degradation configurations described in Section 3.1.6 should provide a reasonable upper bound of the potential consequences of neutron absorber degradation during dry storage.

Reference 23 presents progress and a proposed methodology resulting from the Fuel Integrity Project (FIP). The FIP is a joint research program executed between various British and French interests over the last decade. The particular companies and entities involved have evolved somewhat with industry activity over the years, but the project continued during the time period covered by the four PATRAM symposia discussed in this report. The methodology that has been developed as a result of the FIP applies to both fresh and irradiated fuel transported within Europe. Tests were performed on irradiated rod segments to determine the behavior of irradiated cladding specimens under various loadings. The results of various buckling and crushing tests have been used to validate the resulting models. The final results indicate that the three major causes of fissile material relocation with significant potential k_{eff} impacts are axial displacement, plastic deformation of fuel rods, and rod ruptures resulting in fuel release. All three of these mechanisms are considered in the configurations documented in this report. Axial displacement is discussed in Section 3.1.4, plastic deformation is bounded by the models discussed in Section 3.1.3, and fuel rod rupture is discussed in Sections 3.1.1, 3.1.2, and 3.1.5. Reference 23 is the most recent and most complete description of fuel reconfiguration modes and modeling approaches identified in the entire literature review.

2.3.2 PATRAM 2007

Several papers in the PATRAM 2007 proceedings were identified as providing information on modeling fuel reconfiguration and associated k_{eff} consequences. The relevant papers of interest are *Method to* "Evaluate Limits of Lattice Expansion in Light Water Reactor Fuel from an Axial Impact Accident during Transport," Ref. 24, and "Influence of the Accident Behaviour of Spent Fuel Elements on Criticality Safety of Transport Packages – Some Basic Considerations," Ref. 25.

Reference 24 focused on the effect of fuel assembly deformation caused by axial drops on the ends of the fuel assembly. Both PWR and BWR fuel assemblies are considered in the analysis. BWR fuel rods are typically attached to the assembly end fittings, while PWR rods typically are not. This leads to different response in the assembly during the end drop. The pitch in a BWR bundle tends to be compressed near the drop end, while the pitch in a PWR assembly tends to increase in the same transient. This increased fuel pin pitch is considered for both fuel assembly types in this work, as discussed in Section 3.1.3. The axial variation in the pitch change can also lead to regions of expanded pitch and regions of contracted pitch; the effect is referred to as "birdcaging." A sketch showing this birdcaging effect is provided in Figure 1. Some limited modeling of this phenomenon was also performed as discussed in Section 3.1.3.2. The results presented in Reference 24 ultimately relate to simulation of the distortion of the fuel assembly during the end drop accident. The results presented demonstrate good agreement between the structural computational model and the testing results and more importantly indicate that the modeling approach used in this report is adequate to represent the expected results of such a condition.

Reference 25 investigates the consequences of several accident configurations. The approach described is similar in many respects to the strategy used in the development of configurations for this report in that general accidents are considered in a conservative manner to estimate consequences on k_{eff}. Assembly pitch expansion is considered over various lengths, up to the full length of the fuel rods. The reported k_{eff} change associated with this full-length expansion is approximately 3.25% Δk_{eff}, which is similar to the results reported by EPRI in Reference 15. The results reported for the accumulation of fissile material inside the cask body, but outside the poisoned area of the basket, are quite different from those described in this report. The configuration described in Ref. 25 is quite different from that described in Section 3.1.5.1, so direct comparison is not possible. The primary value of this paper relative to the current effort is in providing quantitative k_{eff} changes for assembly pitch expansion and axial displacement for comparison with results presented in Section 5.

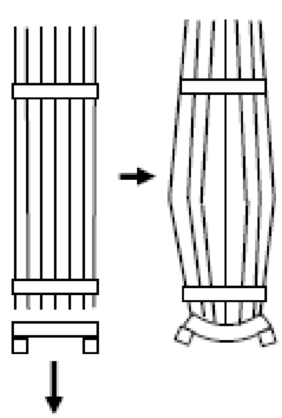

Figure 1. Sketch showing "birdcaging" as the result of an end drop [*Source*: Ref. 24 (Reprinted from P. Purcell, "Method to Evaluate Limits of Lattice Expansion in Light Water Reactor Fuel from an Axial Impact Accident During Transport" PATRAM 2007. Reprinted with permission.]

2.3.3 PATRAM 2004

The proceedings of PATRAM 2004 contained three papers related to the k_{eff} consequences of fuel reconfiguration in storage and/or transportation casks – “Criticality Assessment of Fuel Assemblies with Missing Fuel Rods – An Intractable Problem?,” Ref. 26, “Nuclear Criticality Safety Analysis for the Traveler PWR Fuel Shipping Package,” Ref. 27, and “Harmonisation of Criticality Assessments of Packages for the Transport of Fissile Nuclear Fuel Cycle Materials,” Ref. 28.

Reference 26 examined the practicality of determining an optimum fuel assembly configuration with missing rods. Two techniques were introduced for performing a missing rod analysis. The simple approach proposed in Reference 26 is similar to the approach used in this report, but was performed manually as described in Section 3.1.2.2. No quantitative results were presented that are comparable to configurations included in this report.

Reference 27 presents the criticality safety analysis for a cask for shipping fresh PWR assemblies. Some of the accident configurations considered included uniform pitch expansion restrained by the storage cell wall that is similar to the modeling described in Section 3.1.3. Individual rod axial displacements are considered but shown to have no impact on k_{eff}. The axial displacement of the entire assembly was not considered credible. Partial flooding of the cask body was also considered. The results presented are not directly comparable to the results generated in this report because the cask studied in Reference 27 was a single assembly cask; however, the methods used support the basis for some of the configurations used in this report. The trends in the k_{eff} consequences of uniform pitch expansion and neutron absorber panel load reduction are similar to the results presented for PWR fuel in Section 5.1.

Reference 28 examines potential accident modeling approaches for k_{eff} calculations and discusses elements to consider regarding standardizing scenarios for which analysis is needed. As with Ref. 24, the differences in fuel pin behavior in PWR and BWR assemblies are discussed. Both references contain unreferenced statements supporting the conclusion that PWR pins are likely to be displaced into an increased pitch. Both Refs. 28 and 24 also indicate that BWR pins are likely to decrease in pitch. Ref. 24 cites two instances to support the conclusion for BWR fuel: one was the unrestrained drop of a BWR bundle at a German nuclear power plant and the other was in drop testing being performed as part of package testing. These results were generalized in Ref. 24 to considerations that fuel pins might bend, break, or both. These observations are consistent with the configurations described in Sections 3.1.3, 3.1.4, and 3.1.5. It was also deemed possible that damage to the storage basket or neutron absorber material could result from package-handling accidents. Initial results reported for fuel pin axial displacement indicate that the displacement of some pins within an assembly will not increase k_{eff}. This configuration is not considered in this report.

2.3.4 PATRAM 2001

Within the proceedings of PATRAM 2001 a few papers were identified that provide information related to fuel reconfiguration and the k_{eff} consequences – “Drop Tests with the RA-3D Shipping Container for the Transport of Fresh BWR Fuel Assemblies,” Ref. 29, “Drop Test for the Licensing of the RA-3D Package in the Transport of BWR Fresh Fuel Assemblies,” Ref. 30, and “Effects of Impact Accidents on Transport Criticality Safety Cases for LWR Packages – A New Approach,” Ref. 31.

References 29 and 30 provide the results of drop testing a container intended for shipping fresh BWR bundles. Two containers were each put through a series of drops and evaluated after sequential impacts. The results indicate that some significant assembly distortion is possible, with one assembly suffering a radial rotation (twist) of nearly 45° along its length. Both papers indicate that the general cross section of the bundle was not changed, that is, the pitch was nearly unchanged, but a fairly lengthy section was twisted by the series of impacts. The drop testing was performed with natural enrichment un-irradiated fuel, and no rod failures were detected.

Reference 31 describes the initial plan for the FIP discussed in Ref. 23. As with other studies discussed before, the initial plan for the FIP includes studying deformation, axial displacement, and rupture as three primary fuel degradation mechanisms. Reference 31 also proposed a PWR pitch expansion configuration in which the outer row of pins is held in place along the storage basket but the inner rows continue to expand towards an optimum pitch. These configurations are considered in Section 3.1.3.1.

2.4 Other Sources

Other sources were also reviewed for relevant information related to modeling impact of fuel reconfiguration on criticality safety.

"New Approach to Evaluate Lattice Expansion of Light Water Reactor Fuel Elements on Criticality Safety of Transport Packages under Impact Accidents," Ref. 32, examined pin pitch deformation in LWR fuel assemblies during transportation accident conditions. The paper proposed a method for generating a regular, nonuniform array of fuel rods with the outer row restrained by the basket walls and the pitch of the inner rows progressively expanded or contracted. This method leads to a larger reactivity increase than uniform pitch expansion and, when combined with similar observations from Ref. 31, motivated the analysis of the nonuniform pitch expansion cases described in Section 3.1.3.1.

2.5 Literature Review Summary

A wide range of potentially relevant literature has been reviewed to provide guidance on modeling of fuel reconfiguration after ES and estimate consequences of some configurations. Documents that discuss potentially relevant degraded fuel configurations include Refs. 22–32. A limited number of papers, including Refs. 15 and 25, provide estimates of the consequence of reconfiguration on k_{eff}. The PATRAM proceedings contain the largest number of relevant papers, with several directly applicable papers presented at each symposium. The EPRI reports, taken together, may contain the largest quantity of directly applicable information for this analysis. Most of the discussion in the available literature focuses on what reconfigurations could occur with less emphasis made on the direct impacts on k_{eff}. Those papers that include calculated k_{eff} results tend to take a similar approach to this effort and consider a range of potential configurations to establish a bounding increase in k_{eff} without regard for credibility.

3. FAILED FUEL CONFIGURATIONS

A set of failed fuel configuration categories was developed, and specific configurations within each category were evaluated. The various configurations represent stylized analyses designed to be bounding of different reconfiguration progressions that could occur, but were not developed to represent the results of any specific reconfiguration progression. The configuration categories considered in this analysis are the following:

- clad thinning/loss – reduced cladding thickness up to the total removal of all cladding material
- rod failures – removal of one or more fuel rods from the assembly lattice
- loss of rod pitch control – rod pitch contraction and expansion within the storage cell
- loss of assembly position control – axial displacement of fuel assemblies

- gross assembly failure – rubblized fuel within the storage cells with varying degrees of moderation
- neutron absorber degradation – gaps of varying location and size; thinning of absorber panels.

Within each category, specific configurations were modeled to calculate the corresponding k_{eff} values and the associated consequences of those configurations relative to the reference intact configuration. The consequence of a given configuration is defined as the difference in the calculated k_{eff} values for the given configuration and the reference intact configuration, with a positive value indicating an increase in k_{eff} as compared to the reference configuration. Several of the specific configurations are not considered credible but are included in the analyses for completeness (e.g., to fully understand trends and worst-case situations and to provide results for configurations that may later be judged to be credible). Pending improved understanding of the various material degradation phenomena, and subsequent determination and justification for what configurations are and are not credible, the assessment of the credibility of configurations provided herein is based on engineering judgment. The credibility of configurations and the impact of the configurations on criticality safety are dependent on many factors, including storage and transportation conditions, the fuel assembly characteristics, and the storage and/or transportation characteristics. The credibility assessment for the specific configurations considered here is presented at the end of this section. The assessment and analysis of credible configurations for a specific cask system would need to be performed as part of the safety analysis for licensing that system.

Each of the configurations is considered with all the assemblies in the cask degraded. As discussed in Section 3.2, a subset of the configurations is also considered for a range of assemblies experiencing degradation. These calculations allow an examination of the impact of reconfiguration as a function of the number of degraded assemblies. Section 3.3 describes the limited number of configurations modeled as a combination of two individual degradations. These models are intended to investigate the potential impact of combined degradation mechanisms occurring within the same cask.

At the end of this section, each of the configurations is reviewed for credibility and applicability. The assessments are based on engineering judgment and are not directly supported by any analysis. Ultimately, the strategies developed to mitigate the consequences of fuel reconfiguration will depend on the classification of each configuration as credible or not credible and the severity of the consequences.

3.1 Fuel and Cask Reconfiguration Descriptions

This subsection presents the configurations considered in these analyses. Each of these configurations is considered for each cask design under the assumption that each and every fuel assembly has undergone the reconfiguration discussed. The majority of the cases directly reconfigure fuel, but some consider changes to cladding, neutron absorber material, or fuel assembly axial position. The configurations described in this subsection are used in Section 3.2 to examine the impact of a range of numbers of assemblies experiencing reconfiguration, and in Section 3.3 to investigate the effect of multiple simultaneous degradation mechanisms. Figures demonstrating most of the configurations for each cask are provided in Section 5.

3.1.1 Clad Thinning/Loss

The complete loss of all cladding material without subsequent collapse of fuel material is a nonphysical condition but is included in these analyses to provide a bounding estimate of the increase in k_{eff} caused by fuel cladding thinning or removal. A series of calculations is also performed to investigate the impact of clad thinning. The reduction of fuel cladding thickness results in an increase in reactivity due to increased moderation within the assembly lattice (cladding material is replaced by water) and the reduced absorption in the cladding. The moderation effect is the larger of the two components. In the models, all

Zircaloy material is replaced with water, including the instrument and guide tubes and water rods. The orientation of the canister, be it horizontal, vertical, or in between, has no impact on the modeling or analysis of this configuration.

3.1.2 Rod Failures

Fuel rod failure could result if the fuel rod cladding has failed. After ES periods or as a result of high burnup, or both, fuel rod cladding may become brittle, as discussed in Ref. 1. Cladding failure could be the result of a static or dynamic load. Configurations involving both single and multiple rod failures are included and discussed in more detail below.

3.1.2.1 Single Rod Failure

The single rod failure configuration is predicated on the collapse of an entire fuel rod, potentially due to cladding failure. Regardless of the cause of rod collapse, the fuel and cladding material would be displaced from the assembly lattice, thus leaving an empty rod location. In many internal locations within a fuel assembly lattice, this results in an increase in reactivity in the fully flooded condition due to increased internal moderation. The collapsed rod itself is not modeled as rubble on the bottom of the cask. The fissile material would form a fairly thin, severely undermoderated heap below the fuel assembly if the cask is in a vertical configuration. If the cask is in some other non-vertical configuration, the debris pile will have a larger surface area and thus more neutron leakage. The increase in leakage will increase the margin to criticality in the debris bed. Regardless of configuration, the rubble would have much lower reactivity than the assembly itself.

Separate calculations are performed with each unique rod location replaced with water for both the PWR and BWR fuel assemblies. The assembly and cask symmetries are accounted for in the determination of unique locations, neglecting exceptions for peripheral storage locations.

3.1.2.2 Multiple Rod Failure

Within the multiple rod failure configurations, rods are removed in small groups until an optimum reactivity is achieved. As with the single rod failure cases, the debris at the bottom of the cask is not modeled nor are other cask configuration expected to have a significant impact on the results of the analysis of this configuration. For the larger number of rods removed to achieve optimum reactivity, this assumption is likely conservative as a significant amount of debris material will be accumulating within the assembly storage cell. The homogeneous rubble configuration of gross assembly failure, described in Section 3.1.5.1, provides estimates of the effect of debris collection in the bottom of the fuel storage basket.

For each number of rods removed, a series of potentially limiting configurations is generated to determine the most reactive configuration with the given number of rods removed. These potentially limiting configurations are generated from both the previous limiting configuration and near-limiting configurations. This approach leads to the consideration of several possible configurations to reduce the probability that a more reactive configuration is inadvertently omitted. The increase in k_{eff} caused by removing additional rods approaches zero at the optimum number of removed rods, so no attempt is made to identify the exact optimum number of rods. The k_{eff} of several configurations would also be statistically equivalent near this point. For the purposes of these analyses, the k_{eff} change at this optimum condition has been sufficiently estimated.

3.1.3 Loss of Rod Pitch Control

This configuration is based on failure of one or more of the assembly structural grids, resulting in a loss of fuel rod pitch control. For these analyses, this condition is first modeled as a uniform increase in the fuel rod pitch within the assembly lattice. The rod pitch expansion continues until the outer surface of the fuel rod unit cells in the outer row of the assembly has impacted the storage cell walls. A slight gap of half the fuel rod pitch minus the fuel rod radius remains between the fuel rods and the cell walls. The increased moderation within the assembly lattice causes an increase in reactivity. All fuel assemblies are assumed to undergo a uniform rod pitch expansion to completely fill the internal dimension of the storage cell.

These configurations expand the fuel rod center-to-center spacing in several increments to map the impact on k_{eff} over the full range of expansion. For the BWR fuel, the expansion is performed both with and without the fuel channel present. Two cases are considered with the channel modeled – one where the channel does not deform and restrains the expansion of the fuel rod pitch and the other is a nonphysical assumption that the channel deforms by expanding with a uniform thickness. In this second case, the channel is still present but expands until the storage cell wall restrains the expansion. To maximize the impact on reactivity, the maximum pitch case is considered both with and without cladding present.

After the limiting combination of enrichment and burnup has been established for each fuel type, an additional model is built with the outer row of rods in contact with the fuel storage cell. The small water gap between the rods and the cell walls has been removed in this model. It is used to establish the k_{eff} increase for uniform pitch increase to the limit established by the storage cell walls or assembly channel. The uniform expansion cases with the fuel cladding removed use the same pitch as the cases with cladding intact, so there is no additional pitch expansion caused by cladding removal. The orientation of the cask, vertical of otherwise, is not expected to have any influence on the modeling or analysis of the loss of pitch control configurations.

3.1.3.1 Nonuniform Pitch

Further expansion of the rod pitch for interior rod locations is considered. These models extend further the axially uniform fuel rod pitch expansion discussed above. With the outer row of pins in contact with the storage cell walls, subsequent rows of pins are moved outward until the pins are in contact with the next outermost row. For example, the second row of pins is moved into contact with the first row touching the wall of the storage cell. The process is repeated until additional expansion fails to cause a reactivity increase. Rows containing guide tubes in PWR assemblies are expanded until the guide tubes are in contact with the next row of fuel pins, and the subsequent inner row is moved out until it is in contact with the guide tubes from the inside. These rows have a slightly larger pitch since the outer diameter of the guide tubes is larger than that of the fuel rods.

3.1.3.2 Axial Pitch Variations

One concern associated with the uniform pitch expansion is that it does not account for potential k_{eff} increases caused by axial variations in the pitch distortion. This has been referred to in some instances as "birdcaging." This condition is investigated for the limited uniform expansion case for each cask. The models that are developed are based on the expansion of the assembly until the outer fuel rod unit cell impacts the storage cell wall, not the subsequent case with the rods in contact with the wall. That is, the expanded pitch portion of the assembly maintains a small water gap between the fuel rods and the storage cell walls. The additional pitch in the model that eliminates the water gap is not expected to impact the k_{eff} change of birdcaging relative to a uniform pitch expansion. An axial region adjacent to the elevations of highest reactivity is compressed in an attempt to create a more effective reflector and thus increase k_{eff}.

The length and position of the compressed pitch segment is varied to determine the maximum impact of this effect. For burned fuel, the compressed zone is selected to match one or more axial zones defined by the axial burnup profile modeling. The high-reactivity region is at the top end of the fuel assembly, so the compressed region is varied in position within the top half of the assembly. For fresh fuel, the central region of the fuel is most reactive, so two compressed zones are modeled. One compressed zone is above the midplane of the assembly, and the other is below it. The two zones are always the same length and in symmetric positions.

3.1.4 Loss of Assembly Position Control

The neutron absorber panels in fuel storage and transportation casks are designed to extend beyond the length of the active fuel region within the fuel assembly. In this context, it is important that the active fuel stay in its intended position during and after ES. The cask designs use spacers to ensure that the fuel assemblies are appropriately aligned. If the spacers or assembly end fittings fail, it is possible that the active fuel could shift axially into a region where no neutron absorber separates adjacent assemblies. This would allow for a significant increase in neutronic communication between adjacent assemblies, and a corresponding increase in k_{eff}. The cask orientation is not expected to influence the analysis of the loss of assembly position control configuration, but the orientation would certainly influence the actual fuel motion if such an event occurred.

For these models, the maximum axial translation allowed is determined for the active fuel length neglecting the presence of all fuel assembly hardware above or below the pellet stack and the cask assembly spacers. The models of axial displacement translate all the fuel assemblies uniformly up or down into the lower and upper internal regions of the cask. The assemblies are moved in several relatively small intervals in an effort to map out the response as a function of displacement.

3.1.5 Gross Assembly Failure

Two configurations for the physical form of the failed fuel are considered in these analyses: the first is a homogeneous mixture of fuel, cladding materials, and water, and the second is a dodecahedral array of fuel pellets suspended in water. The homogeneous mixture is likely more representative of the condition of the assembly after significant degradation and reconfiguration. Modeling an ordered array of pellets provides an upper bound of the reactivity of the fuel rubble since low enriched fuel is more reactive lumped as compared to a homogeneous mixture due to resonance self-shielding effects. Each of the modeling techniques is described in more detail here.

The formation of oxidized forms of UO_2 is not considered in this analysis. The expected formation of higher-order oxidative states would require an ample supply of oxygen which would require a breach of the canister while in storage. Because monitoring is in place to detect and repair breaches, this condition is not being evaluated. Also, as the results presented in Section 5 demonstrate, the UNF casks are undermoderated systems, so representing oxidation of internal components would act to effectively displace the moderator, resulting in a less reactive condition.

3.1.5.1 Homogeneous Rubble

Following a gross assembly failure, a large number of intermediate configurations is possible. To evaluate the effects of varying degrees of rubblization, a series of total debris elevations is considered. This approach considers a range of moderation ratios without specifying the cask orientation. The homogeneous rubble configuration considers the entire fuel assembly to have failed; no calculations are performed for rubblizing a portion of a fuel assembly or for rubble collecting within a partial intact assembly or skeleton. The parameter that is varied is the height of the debris bed and thus the amount of moderation within the bed.

The homogeneous rubble configuration is modeled as occupying the internal volume of the fuel storage cell to varying elevations. The exact elevations used vary among the cask designs. All the designs are evaluated with the homogeneous rubble replacing the fuel assembly in its original elevation. Other elevations include 40%, 60%, 80%, and 100% of the inside height of the cask from the base plate. The volume occupied by water varies from about 21% to almost 74% of the homogenized mixture. The water volume is determined by subtracting the fuel and cladding volumes from the cask volume modeled as containing debris. A fully compressed case is also considered in which the fuel assembly debris has compacted to just fuel and cladding material, excluding all water, to complete coverage of the parametric space. A range of heights is also considered from nominal assembly height to fully compressed assuming that the debris is maintained within the neutron absorber elevations. These configurations approximate a debris bed that is made up of non-homogeneous pieces, such as fuel rod segments, that are too large to pass through the assembly end hardware and fuel assembly spacer. Some cask models also have configurations for neutron absorber height and/or basket height. Most of these models contain rubble material above and/or below the neutron absorber panels, which are assumed to remain intact. The debris is not necessarily contained by the cask fuel spacers because they are generally designed to allow water to flow through and out of the fuel storage cells. In the full cask height configurations, the fuel rubble is assumed to remain within the radial extent of the fuel storage cell, even above the storage basket. This is assumed mainly as a modeling convenience, and it likely reduces the k_{eff} of the configuration slightly. For purposes of these analyses, however, the approximations are sufficient to provide a good estimate of the k_{eff} changes associated with gross assembly failure leading to homogeneous rubble within the cask.

All models with homogeneous rubble assume that the cask is maintained in a vertical position. No explicit modeling is performed for horizontal or angled positions which may alter the distribution of rubble within the cask. Given the range of rubble heights considered, it is unlikely that a horizontal or angled configuration would lead to a greater overall k_{eff} increase than the maximum calculated in this work, but the intermediate volumes could be impacted in these alternate orientations.

3.1.5.2 Dodecahedral Array of Pellets

The case of gross assembly failure modeled as an ordered array of bare pellets is considered as a bound to the possible k_{eff} increase resulting from these configurations. An ordered array of lumped low enriched fuel should lead to a greater k_{eff} increase for fuel assembly failure than the homogeneous case described above because of resonance self-shielding of ^{238}U in low enriched fuel. The complete removal of cladding is nonphysical, as discussed above in Section 3.1.1, but is included to bound possible k_{eff} increases.

As with the homogeneous rubble case described above, a range of pellet array heights is considered along with the entire internal area of the storage cell assumed to be filled with the pellet array. The independent parameter for the dodecahedral array is the pitch, so a range of pitches is used in the models to achieve the different heights. Most of the cask models are evaluated with four different pitches/array heights. The minimum pitch in all cases maintains the height of the original fuel assembly, and the maximum pitch fills the inner area of the storage cell for the entire internal height of the cask. Each of the cases is considered with two fuel pellet orientations. The pellets are aligned along the Z axis in one case and along the X axis in the other.

All models with dodecahedral pellet arrays assume that the cask is maintained in a vertical position. No explicit modeling is performed for horizontal or angled positions which may alter the distribution of the pellets within the cask. Given the range of heights considered, it is unlikely that a horizontal or angled configuration would lead to a greater overall k_{eff} increase than the maximum calculated in this work, but the intermediate volumes could be impacted in these alternate orientations.

3.1.6 Neutron Absorber Degradation

In addition to the failed fuel configurations, degradation of the neutron absorbers is investigated. Neutron absorber panels in long-term service in spent fuel pools have generally suffered a range of degradation mechanisms, as discussed in Ref. 33 and other sources. Although the environments within the spent fuel pool and the dry storage casks are significantly different, it is reasonable to assume that some degradation and/or damage of the neutron absorber material may occur in ES. A range of configurations is considered in these analyses to provide some estimates for the potential k_{eff} changes that could be associated with neutron absorber panel damage or degradation. The orientation of the cask is not expected to effect the k_{eff} change caused by neutron absorber degradation, and has no impact on the analysis of the configurations.

3.1.6.1 Limiting Elevation of Neutron Absorber Damage

One aspect that can impact the k_{eff} change caused by neutron absorber damage is the axial elevation of the defect. For these analyses the neutron absorber panel damage was assumed to be 5 cm tall and across the full width and thickness of the panel. The gap in the neutron absorber panel is modeled as void, and not water-filled, to maximize the neutron streaming, and associated neutronic communication, through the gap and the corresponding increase in neutron multiplication in neighboring assemblies. Also, all neutron absorber panels in the cask are assumed to contain the same defect at the same elevation. This approach will result in a conservative estimation of the k_{eff} increase due to panel damage relative to non-aligned damage modeling. The neutron absorber damage may be highly correlated, in which case modeling the gaps at the same elevation is potentially appropriate.

For fresh fuel, the limiting elevation is most likely in the center of the assembly, so a few widely spaced intervals are used. For used fuel, the limiting elevation should shift to a position near the top end of the assembly. For these conditions, a larger number of cases are investigated with finer resolution in the gap positions between calculations. The minimum spacing is slightly in excess of 5 cm, so a more detailed survey is likely to reveal a slight increase in the k_{eff} increase of this neutron absorber degradation. For purposes of these analyses, however, the resolution is sufficient to capture the vast majority of the k_{eff} change.

3.1.6.2 Sensitivity to Extent of Damage

To evaluate the sensitivity of the k_{eff} change to the extent of panel damage, several additional configurations were evaluated using 7.5 and 10 cm gaps centered at the elevation determined to be limiting with the 5 cm gap cases discussed above in Section 3.1.6.1. As before, the larger gaps extend across the entire width and thickness of the neutron absorber panel, and also occur at the same elevation in all panels. The sizes of the larger gaps have been chosen arbitrarily. It is unlikely that the extent of any potential neutron absorber panel damage can be appropriately bounded without significant material testing. The magnitude of the sensitivity results will provide some indication of the importance of neutron absorber material testing.

3.1.6.3 Neutron Absorber Panel Thinning

While uniform thinning of all neutron absorber panels in the cask may be unlikely, it provides a simple basis for examining the potential impact of general degradation. The neutron absorber material is reduced in thickness in a series of steps so that the magnitude of the effect as a function of neutron absorber loss can be determined.

3.2 Varying Number of Reconfigured Assemblies

The k_{eff} change caused by fuel reconfiguration is nonlinear with respect to the number of assemblies that experience reconfiguration, and is not well characterized in the available literature. For these reasons, a series of configurations is considered in each cask by varying the number of assemblies that have been degraded for each of four of the configurations described in Section 3.1. The four degraded configurations considered are single rod failure (Section 3.1.2.1), multiple rod failure (Section 3.1.2.2), uniform fuel pin pitch expansion (Section 3.1.3), and the homogeneous rubble configuration of gross assembly failure (Section 3.1.5.1).

The number of assemblies in the cask experiencing reconfiguration is varied from one to all assemblies. A central cell location is selected as the first assembly to experience reconfiguration, and additional assemblies are added in approximately symmetric groups. An example order in which the failed assemblies are added is presented for each cask along with the results of the calculations in Section 5.

3.3 Multiple Reconfiguration Mechanisms

Many of the configurations described in Section 3.1 are predicated on the degradation of similar materials. The cladding, guide/instrument tubes, water tubes, and most of the structural grids are all fabricated from the same or very similar zirconium alloys. It is therefore assumed that reconfiguration could occur involving more than one of the degradation mechanisms studied separately for each configuration. For example, if the fuel rod cladding is failing and multiple fuel rods have collapsed, then the cladding on the remaining intact fuel rods may have experienced some thinning. A very large number of combinations of such configurations could be generated, but only a small subset is considered here. The primary purpose of this portion of the analysis is to compare the k_{eff} changes of multiple degradation mechanisms with the consequence estimated by simply adding the effects of each separate reconfiguration. To that end, two combinations are considered in both casks: a configuration involving a moderate number of failed fuel rods combined with 50% clad thinning in one study and with a moderate amount of uniform pitch expansion in another. The results for this set of cases are provided in Section 5.

3.4 Credibility of Degraded Configurations

Several of the configurations used in this report are not physically possible. These configurations may be disregarded in assessing the mitigation strategies necessary to provide confidence that UNF can be safely transported following ES. The configurations are still useful as they provide indications as to reconfiguration impacts for various changes in fuel, neutron absorber, or structural materials within the casks during or after ES. The consequences that require mitigation are significantly less severe than the most limiting, non-credible configurations reported in Section 5. A summary of the credibility and relevance of each of the configurations discussed in Section 3.1 is presented in Table 1.

The complete removal of all fuel cladding material is not credible as there is no mechanism to remove the cladding from the fuel matrix. There is also no credible place for the cladding material to go within the cask that will not have an impact on the calculated k_{eff}. Any event that leads to massive cladding failure will also lead to significant rearrangement of the fissile material. Some amount of clad thinning through corrosion and/or radiation-induced growth of the fuel rods is credible and is included in the results. To observe the impacts of clad thinning effects, the maximum thinning considered is chosen to be up to 50% of the nominal thickness.

Significant neutron absorber panel damage at highly correlated locations is not considered credible in extended dry storage. Many fixed absorber materials have experienced degradation in wet storage, as documented in Ref. 33, and this damage is often caused by the effects of radiation, temperature, and environmental insults. These parameters can be highly correlated based on the proximity of neutron absorber panels to the same high temperatures and high radiation fields in the same region of a spent fuel pool. There are currently no known mechanisms applicable to dry storage systems that could cause the local panel defects or generalized thinning examined in this report.

The cask assembly spacers are unlikely to degrade sufficiently for significant axial misalignment to be possible within the cask. The spacers are designed to withstand loads in excess of 60 g, as documented in Ref. 38. These loads are associated with hypothesized accident conditions (HAC), so the cask assembly spacers can be relied upon to maintain assembly position with the neutron absorber elevations in both storage and transportation. Current practice allows small gaps between the spacers and the fuel, but these gaps are typically on the order of a few inches. It is therefore reasonable to assume that significant misalignments cannot occur and will be limited to less than 20 cm.

Simultaneous gross failure of all fuel assemblies in the cask is also not considered credible in normal conditions of transport. The two configurations used to investigate the consequences of gross failure are also extremely conservative. Both configurations examine a range of debris bed sizes to find the largest increase in k_{eff}. Large debris beds, such as those filling the entire inner volume of the fuel cask, are not physically possible. Fuel assembly hardware and fuel spacers would also occupy a significant volume and thus reduce the k_{eff} increase. Some smaller debris beds, consistent with partial assembly failure, are potentially credible. These detailed debris models are not considered in this analysis as the primary focus of the configurations analyzed is to establish bounding conditions of the extent of k_{eff} increases due to total failure. Gross assembly failure may be plausible in some HACs, but is not considered credible in normal conditions of transport.

Table 1. Credibility and relevance summary

Configuration	Credibility and applicability to normal transport analysis
Clad thinning/loss	
Complete cladding loss	Nonphysical condition that is not credible Relevant as potential bound of credible condition
Uniform cladding thinning	Potentially credible as a result of corrosion Relevant to storage and transportation analysis
Rod failures	
Single rod failure	Potentially credible as a result of cladding failure Relevant to storage and transportation analysis
Multiple rod failure	Potentially credible as a result of cladding failure Relevant to storage and transportation analysis
Loss of rod pitch control	
Uniform expansion, constrained by cell or channel	Potentially credible as a result of end load Relevant to storage and transportation analysis
Nonuniform expansion, constrained by cell	Potentially credible as a result of end load Relevant to storage and transportation analysis
Axially variable expansion, constrained by cell	Potentially credible as a result of end load Relevant to storage and transportation analysis
Loss of assembly position control	
Maximum misalignment	Not credible with end fitting and spacers Relevant as potential bound of credible condition
Limited misalignment	Small misalignments credible Relevant to storage and transportation analysis
Gross assembly failure	
Homogeneous rubble of entire assembly with debris beyond neutron absorber elevations	Not credible for normal transport Relevant as potential bound for credible condition
Homogeneous rubble of entire assembly within neutron absorber elevations	Not credible for normal transport Relevant as potential bound for credible condition
Uniform pellet array	Not credible for normal transport Relevant as potential bound for credible condition
Neutron absorber degradation	
5-cm (small) defect in all panels, same elevation	Not credible for intact dry storage system Relevant as potential bound of credible condition
10-cm defect in all panels, same elevation	Not credible for intact dry storage system Relevant as potential bound of credible condition
Uniform thinning of all panels	Not credible for intact dry storage system Relevant as potential bound of credible condition

4. MODELS, CODES, AND METHODS USED

The models, codes, and methods used for these analyses are based on similar work completed previously and documented in Ref. 7. The codes used are part of the SCALE code system, Ref. 34.

4.1 Fuel Assembly Models

Two fuel assembly designs are used in these analyses: one PWR type and one BWR type. The designs chosen are intended to represent a large portion of the current inventory of discharged UNF and/or a significant portion of the fuel currently in use. The PWR design selected is the Westinghouse 17 × 17 Optimized Fuel Assembly (OFA). The Westinghouse 17 × 17 assembly, as modeled, represents over 14% of the total discharged PWR inventory, as documented in Ref. 35. The BWR design selected is based on a General Electric (GE) 10 × 10 design such as the GE14 fuel product. The GE 10 × 10 represents less than 0.5% of the discharged BWR fuel documented in Ref. 35; however, the 10 × 10 fuel design was just being introduced when the data for Ref. 35 were being collected. The array is the most common fuel design in use in domestic BWRs today. Detailed descriptions of the fuel assembly models used in this analysis are provided in Appendix A.

The use of Westinghouse and GE fuel assemblies is a continuance of the work documented in Ref. 7. The use of these fuel types is not an endorsement of any particular fuel design or vendor relative to any others but is used to provide a basis of comparison with the previous work.

4.2 Cask Models

Two cask models were used for the evaluations presented in the main body of this report – the GBC-32 and MPC-68. The MPC-24 cask is also evaluated in Appendix B to complete coverage of the parametric space via the inclusion of fresh 5 weight percent (w/o) PWR fuel. The representative cask models selected are the same as those used in Ref. 7 and are based on the Holtec HI-STAR 100 system, Ref. 36–38. The incorporation of Holtec designs in this work is not an endorsement of any design or vendor relative to any others. The GBC-32 and MPC-68 models are described in more detail in the following subsections.

4.2.1 GBC-32 Cask Model

The GBC-32 model is a generic burnup credit cask benchmark model as defined in Ref. 39. The cask model was designed to be a nonproprietary representation of high-capacity PWR storage and transportation casks used within the nuclear power industry. The dimensions and material specifications of the cask model are described in Section 2.1 of Ref. 39 and are not repeated here. The only notable difference from that description is that the cask lid modeled in these analyses has a thickness of 20 cm instead of 30 cm. This reduced lid thickness has no impact on the analyses presented here because the cavity height is maintained.

The fuel assemblies, cask basket, neutron absorber panels, neutron absorber panel wrappers, cask wall, lid, and base plate are modeled explicitly. The nominal condition for this model is fully flooded with unit density, unborated water. A cross section of the GBC-32 model is shown in Figure 2. The representative assembly design is the Westinghouse 17 × 17 OFA with a range of initial enrichments, burnups, and cooling times considered. For more details about the fuel assembly model, see Appendix A.

A burnup credit loading curve is generated assuming a maximum k_{eff} of 0.94, as shown in Figure 3. The maximum fresh enrichment that can be stored is determined to be 1.92 w/o ^{235}U, and minimum burnups are calculated for 3.5 w/o and 5 w/o initial enrichment fuel with 5 years of post-irradiation cooling time. The minimum burnup for 3.5 w/o fuel is 25.5 GWd/MTU and for 5 w/o is 44.25 GWd/MTU to meet the

0.94 k_{eff} limit. Explicit degraded configuration calculations are performed for fuel from this loading curve. These two enrichments are used because they encompass the majority of the current UNF inventory as of 2002, and the 5-year cooling time is selected as it is a typical minimum required cooling time for fuel to be placed in dry storage. Sensitivity studies are also performed for fuel of higher burnup (70 GWd/MTU) and for a range of cooling times up to 300 years to establish the sensitivity of the change in k_{eff} to these parameters. The results of these sensitivity studies are discussed in Section 5 and in Appendix C.

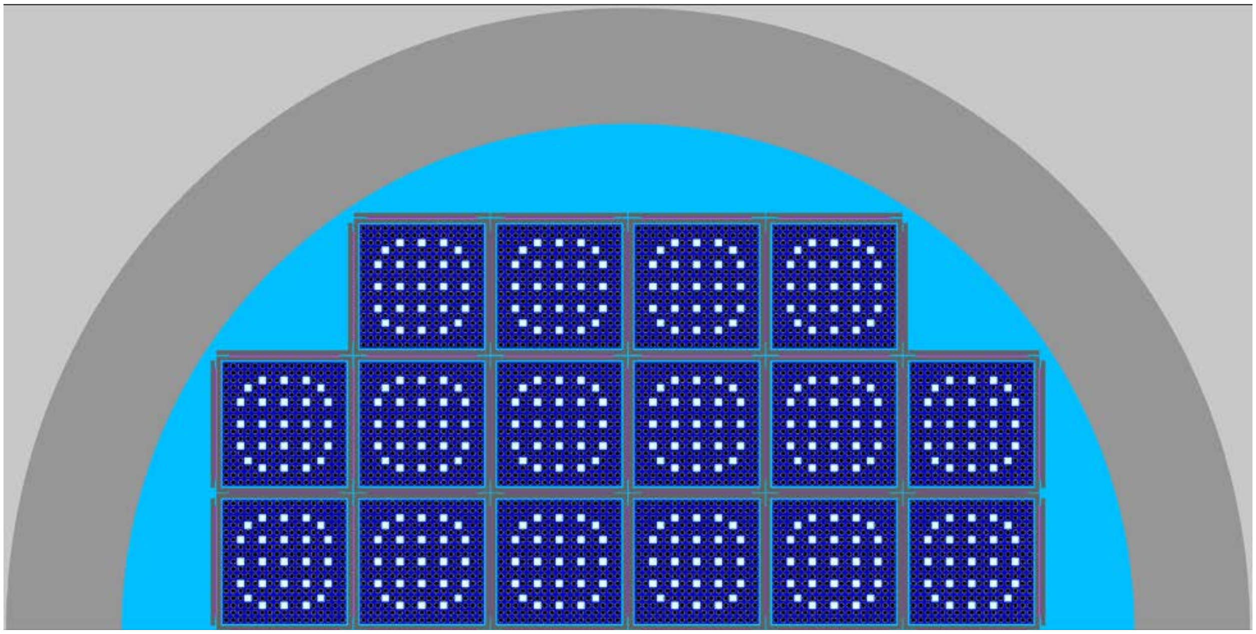

Figure 2. Cross section of GBC-32 half-cask model.

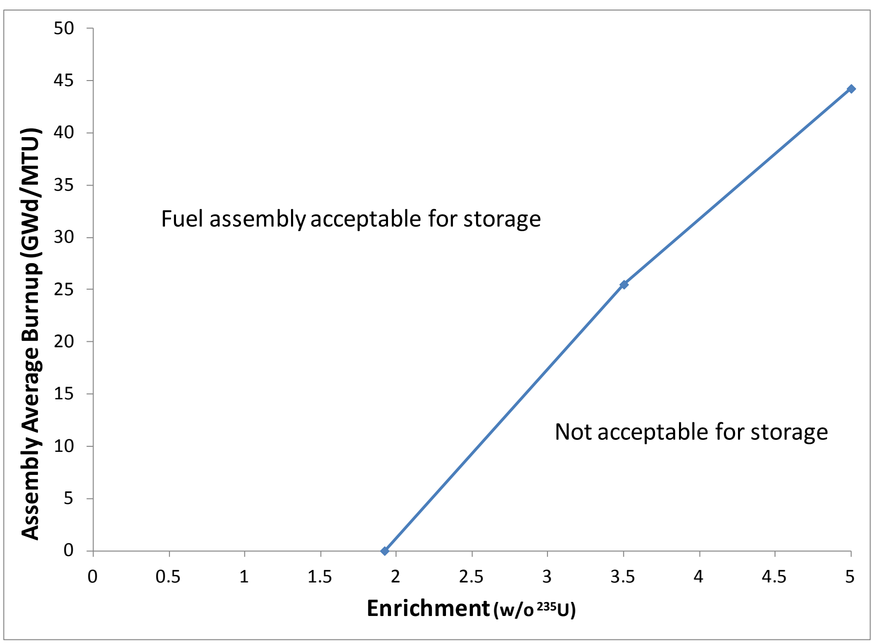

Figure 3. Representative fuel assembly loading curve for GBC-32.

4.2.2 MPC-68 Cask Model

The MPC-68 cask is designed for storage and transportation of up to 68 fresh BWR fuel assemblies but is being used in this analysis for evaluating both fresh and irradiated assemblies. Fresh fuel is considered in these analyses to provide complete coverage of the parametric space; in this case burnup is the parameter of interest. The nominal condition for this model is fully flooded with unit density, unborated water. A cross section of the MPC-68 model is shown in Figure 4. Dimensions and material specifications of the cask model are provided in Appendix D. The fuel assemblies modeled in the MPC-68 are based on a 10 × 10 design similar to the GE14 product. More details about the fuel assembly models are provided in Appendix A.

Fuel assemblies in the MPC-68 models used in these analyses use an initial enrichment of 5 w/o ^{235}U and consider fresh and irradiated conditions. The nominal model k_{eff} value with fresh fuel is in excess of 0.96. A second set of cases considers an assembly average burnup of 35 GWd/MTU and a 5-year cooling time, resulting in a base case k_{eff} of approximately 0.83. Sensitivity studies are also performed for fuel of higher burnup (70 GWd/MTU) and for a range of cooling times up to 300 years to establish the sensitivity of the change in k_{eff} to these parameters. The results of these sensitivity studies are discussed in Section 5 and in Appendix C.

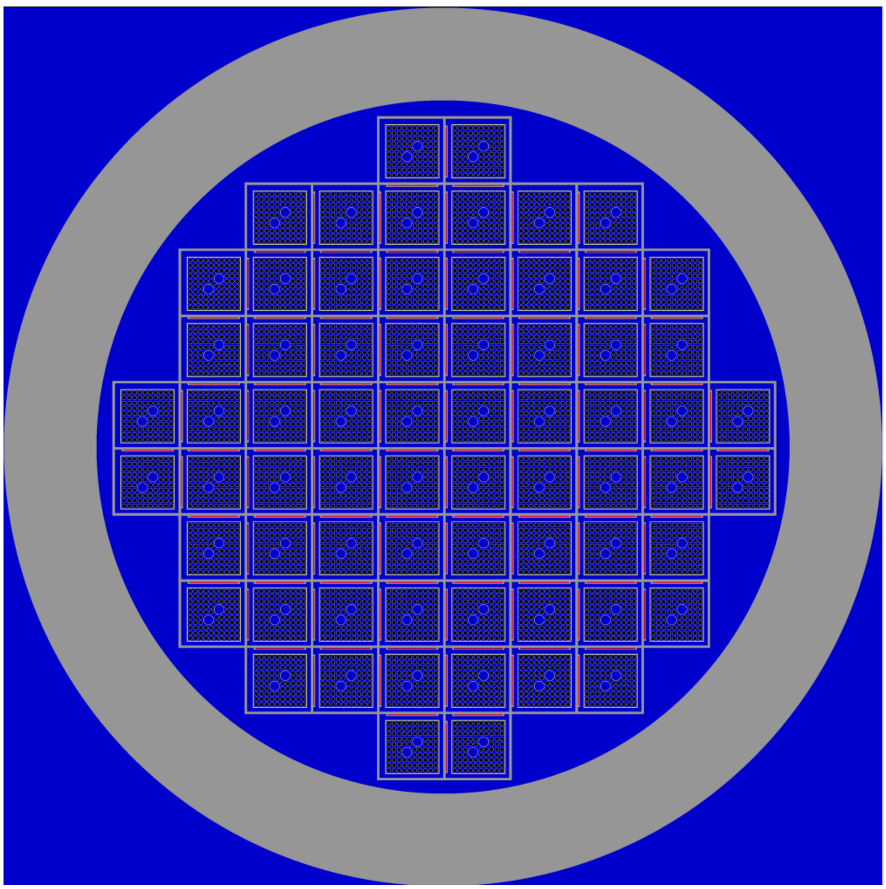

Figure 4. Cross section of MPC-68 model.

4.3 Software Codes

The SCALE code system is used to perform the large number of k_{eff} and depletion calculations necessary for these analyses. All calculations use the 238-group neutron data library based on ENDF/B-VII.0, distributed with the SCALE system. The same library is used in k_{eff} and depletion calculations.

The KENO V.a and KENO-VI Monte Carlo codes are used for k_{eff} calculations within the appropriate CSAS5 and CSAS6 sequences. Both codes use Monte Carlo transport to solve the k_{eff} eigenvalue problem. KENO-VI uses a generalized geometry process and is used for the fuel pellet array configuration and some increased fuel rod pitch configurations. KENO V.a has a more restrictive geometry package but is significantly faster because of the simpler geometry treatment. KENO V.a is used for the majority of configurations considered in this analysis. The KENO codes and CSAS sequences are further described and documented in Ref. 34. The KENO calculations are run with a large number of particles per generation, typically 10,000, and enough generations to reach an uncertainty less than or equal to 0.00010 Δk_{eff}. The number of generations needed to reach the uncertainty target is determined by KENO during each calculation. In most calculations, the first 100 generations are discarded to ensure proper source convergence.

All depleted fuel isotopic compositions were generated with the STARBUCS sequence. The STARBUCS sequence uses the ORIGEN-ARP methodology to generate depleted fuel compositions and uses the compositions in a KENO model to calculate k_{eff}. The TRITON t-depl sequence is used to generate ARP libraries for both PWR and BWR UNF for the depletion conditions described in Section 4.4. The TRITON sequence couples the NEWT discrete-ordinates code with the ORIGEN depletion module. The local fluxes calculated with NEWT are used to perform fuel depletion calculations with ORIGEN. The STARBUCS and TRITON sequences, NEWT and ORIGEN modules, and ORIGEN-ARP methodology are described and documented in Ref. 34.

4.4 Depletion Modeling Parameters

For analyses of irradiated fuel, the depletion modeling parameters that the fuel experiences can have a significant impact on the calculated k_{eff} values. Several key factors can impact the reactivity of discharged fuel in light water reactor (LWR) burnup credit criticality safety analyses. The key parameters include the nuclides represented in the isotopic compositions, parameters used for the depletion analysis, cooling time, axial burnup profiles, and horizontal burnup profiles, as discussed in Ref. 40.

For the analyses in this report, the depletion parameters used are consistent with burnup credit safety analyses and are not representative of nominal core conditions. It is expected that any operating conditions that are not bounded by the depletion conditions used in this report would result in a higher discharged assembly k_{eff}, but the k_{eff} increase caused by fuel reconfiguration is expected to be similar to the results determined here. Generic data is used in the PWR depletion conditions as PWR burnup credit has been studied extensively, including in, for example, Refs. 39, 41, 42, 43, 44, and 45. Additional details on the specific PWR conditions used are provided in Section 4.4.1. Because commensurate studies are not available in the literature for BWR burnup credit, the BWR depletion conditions are based on the operating history of a specific assembly as described in Section 4.4.2 and Appendix E.

The k_{eff} calculations performed for these analyses involving UNF, for both BWR and PWR fuel, consider the same 12 actinide and 16 fission product isotopes listed in Table 2 (Set 2 Table 1 Ref. 44). Although Ref. 44 specifically addresses PWR burnup credit, the major isotopes affecting reactivity of irradiated uranium oxide fuel will be the same in BWR fuel. The k_{eff} impacts caused by the use of this set of isotopes, as compared to actinide-only burnup credit or a more extensive list of fission products, are discussed in Ref. 39.

Different axial burnup profiles are used for PWR fuel than for BWR fuel, though the same uniform horizontal burnup profile is considered for both fuel types. The PWR axial profiles are taken from Table 4-3 of Ref. 45. Profile 2 is used for fuel discharged at 25.5 GWd/MTU and profile 3 is used for discharged at 44.25 GWd/MTU. The development of the profile used for BWR fuel is described in Appendix E.

Table 2. Isotopes included in depleted fuel models

Actinides					
^{234}U	^{235}U	^{236}U	^{238}U	^{238}Pu	^{239}Pu
^{240}Pu	^{241}Pu	^{242}Pu	^{241}Am	^{243}Am	^{237}Np
Fission products					
^{95}Mo	^{99}Tc	^{101}Ru	^{103}Rh	^{109}Ag	^{133}Cs
^{143}Nd	^{145}Nd	^{147}Sm	^{149}Sm	^{150}Sm	^{151}Sm
^{152}Sm	^{151}Eu	^{153}Eu	^{155}Gd		

4.4.1 PWR Depletion Conditions

The depletion parameters that impact discharged fuel reactivity as listed in Ref. 40 are fuel temperature, moderator temperature/density, soluble boron concentration, specific power and operating history, use of fixed burnable poisons, and use of integral burnable poisons. Each of these parameters must be addressed in a burnup credit analysis to demonstrate that conservative depletion parameters have been implemented in the safety basis. These depletion calculations are intended to provide used fuel isotopic compositions that are representative of the compositions generated for a safety analysis and not for nominal core operating conditions. The parameters used in the PWR depletion calculations are listed below in Table 3.

Table 3. PWR depletion parameters

Parameter	Value
Fuel temperature	1100 K
Moderator temperature	610 K
Moderator density	0.63 g/cm^3
Soluble boron concentration	1000 ppm
Specific power and operating history	Constant 60 W/g (MW/MTU)
Fixed burnable absorber	24 Wet Annular Burnable Absorber (WABA)
Integral burnable absorber	None – Bounded by 24 WABA
Control rod insertion	None

4.4.2 BWR Depletion Conditions

The mechanisms whereby depletion conditions influence discharged fuel assembly reactivity are largely similar for BWR and PWR fuel. Data for specific BWR assemblies are gathered and reviewed from the commercial reactor critical (CRC) state points documented in Refs. 46 and 47. The depletion parameters used in this report are summarized in Table 4. The methods used to generate axial burnup and void profiles and the specific power from the CRC information, Refs. 46 and 47, are presented in Appendix E. The BWR depletion calculations are performed with no control blades present. Although it is more conservative to include the control blades during depletion, their absence is not expected to impact the results of this analysis.

Table 4. BWR depletion parameters

Parameter	Value
Fuel temperature	840 K
Moderator temperature	512 K
Moderator density	Varied axially, see Appendix E for details
Specific power and operating history	Constant 30.31 W/g (MW/MTU), see Appendix E for details
Integral burnable absorber	None
Control blade insertion	None

5. RESULTS

This section reports the results of the calculations to determine the k_{eff} changes associated with each of the configurations described above in Section 3. The results are presented in unique subsections for each cask. The conclusions that can be drawn from these results are presented in Section 6.

The reported consequence is the difference in calculated k_{eff} values; the reported changes are not divided by any k_{eff} values and therefore do not represent change in reactivity ($\Delta\rho$). The Δk_{eff} unit indicates that the results presented are the difference in two calculated k_{eff} values. The reported k_{eff} changes are also best-estimate changes; the difference in k_{eff} values is not altered or adjusted to account for the Monte Carlo uncertainties of the calculations. The one standard deviation uncertainty in all calculated Δk_{eff} values is approximately 0.00014 (0.014%) Δk_{eff}, unless otherwise noted.

5.1 GBC-32 Cask Model Results

The k_{eff} change associated with each of the reconfigurations discussed in Section 3 is presented in this section for the GBC-32 cask. The configurations assume a range of loadings of Westinghouse 17 × 17 OFA fuel. The description of the fuel assembly is provided in Appendix A. The enrichments and burnups used are presented in Table 5. The rationale used to select these points is provided in Section 4.2.1. The reference case k_{eff} value for intact fuel for each of these cases is also provided in Table 5.

Table 5. Enrichment, burnup, and cooling time for reference cases considered in GBC-32

Enrichment (w/o ^{235}U)	Burnups (GWd/MTU)	KENO V.a		KENO-VI	
		k_{eff}	σ	k_{eff}	σ
1.92	0	0.94017	0.00010	0.94040	0.00010
3.5	25.5	0.93988	0.00010	0.93976	0.00010
5.0	44.25	0.94000	0.00010	0.93995	0.00010

5.1.1 Reconfiguration of All Assemblies

A summary of the k_{eff} increase associated with each configuration is provided in Table 6. Additional details for each configuration and the results for non-limiting cases are provided in the subsequent subsections.

Table 6. Summary of k_{eff} increases for the GBC-32 cask

Configuration	Increase in k_{eff} (% Δk_{eff})	Limiting case	
		Enrichment (w/o ^{235}U)	Burnup (GWd/MTU)
Clad thinning/loss			
Cladding removal	3.49	5	44.25
Rod Failures			
Single rod removal	0.09	5	44.25
Multiple rod removal	1.86	5	44.25
Loss of rod pitch control			
Uniform rod pitch expansion, clad	2.65	5	44.25
Uniform rod pitch expansion, unclad	5.34	5	44.25
Nonuniform pitch expansion, clad	3.90	5	44.25
Loss of assembly position control			
Axial displacement (maximum)	16.70	5	44.25
Axial displacement (20 cm)	10.82	5	44.25
Gross assembly failure			
Uniform pellet array	21.37	5	44.25
Homogeneous rubble	14.30	5	44.25
Neutron absorber degradation			
Missing neutron absorber (5-cm segment)	1.05	5	44.25
Missing neutron absorber (10-cm segment)	2.33	5	44.25
50% reduction in neutron absorber panel thickness	1.78	1.92	0

5.1.1.1 Clad Thinning/Loss

The clad thinning and loss configurations are modeled as discussed in Section 3.1.1. As shown in Table 6, the limiting k_{eff} increase associated with complete cladding removal is 3.49% Δk_{eff} and occurs for the 44.25 GWd/MTU burnup case with an initial enrichment of 5 w/o ^{235}U. The results for all three cases are summarized in Table 7. For the limiting case of 5 w/o and 44.25 GWd/MTU burnup, the k_{eff} increase as a function of nominal cladding thickness remaining is shown in Table 8 and Figure 5. The trend of increasing k_{eff} with decreasing cladding thickness is similar for the other fuel compositions, and therefore not shown here. The configuration with 50% of the nominal cladding remaining is shown in Figure 6. The results are in good agreement with those presented in Refs. 7 and 15.

Table 7. Increase in k_{eff} for cladding removal in GBC-32

Enrichment (w/o ^{235}U)	Burnup (GWd/MTU)	Increase in k_{eff} (% Δk_{eff})
1.92	0	2.81
3.5	25.5	3.34
5	44.25	3.49

Table 8. Increase in k_{eff} in GBC-32 cask as a function of cladding fraction remaining (5 w/o ^{235}U initial enrichment, 44.25 GWd/MTU burnup)

Fraction of cladding thickness remaining	Increase in k_{eff} (% Δk_{eff})
0.90	0.38
0.75	0.99
0.50	1.94
0.25	2.76
0.00	3.49

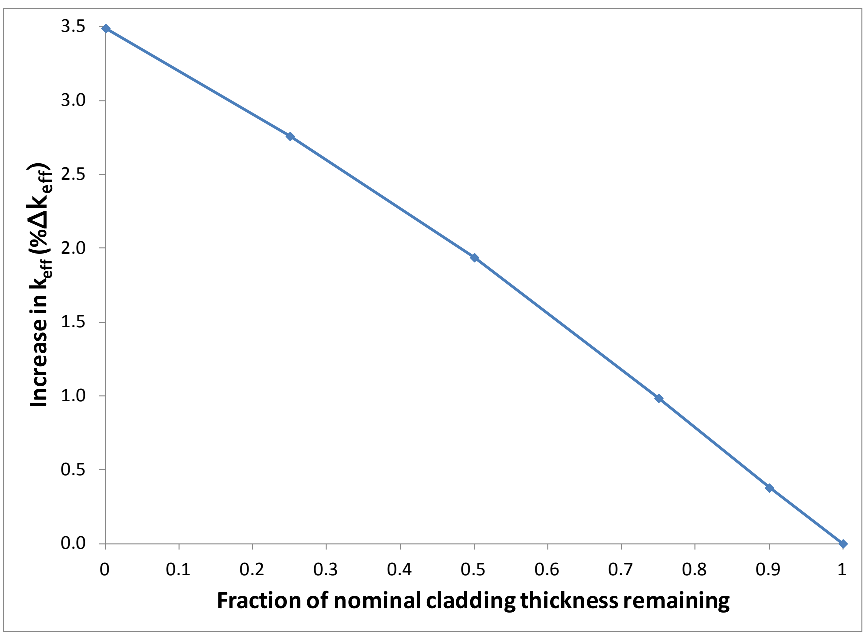

Figure 5. Increase in k_{eff} due to reduced cladding thickness (5 w/o ^{235}U initial enrichment, 44.25 GWd/MTU burnup).

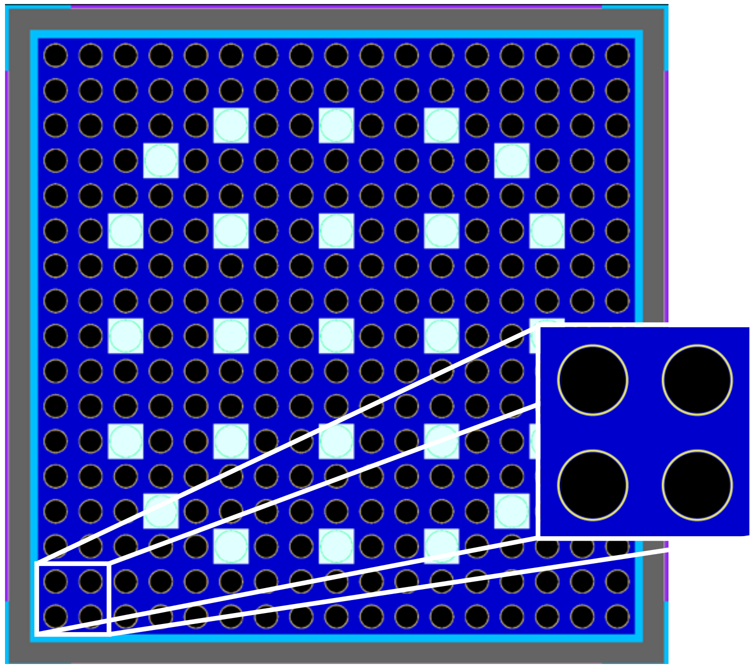

Notes: Fuel shown in black
Cladding is light grey around fuel material
Guide/instrument tubes are larger water-filled tubes
Storage cell is dark grey box
Neutron absorber panel is purple
Water is shown in dark blue, light blue, and white

Figure 6. Configuration with 50% cladding thickness.

5.1.1.2 Rod Failures

Each of the 39 eighth-assembly symmetric rods is removed individually to determine its worth, as discussed in Section 3.1.2.1. Table 9 presents the rod locations and worth of the limiting rod location for each of the three cases. A sketch showing the eighth-assembly symmetry and row and column labels is provided in Figure 7. The maximum k_{eff} change is 0.09% Δk_{eff} and is associated with rod H5 in the 5 w/o, 44.25 GWd/MTU burnup case. The worth of H5 in the GBC-32 cask is. It should be noted that several rods across many of the cases have a reactivity worth that is statistically equivalent to this particular limiting case. The worth is very small relative to the k_{eff} increase of other configurations, so further examination is not necessary.

Multiple rods are also removed in groups, as discussed in Section 3.1.2.2. Groups of 2, 4, 8, 16, 24, 28, 32, 36, 40, 44, and 48 rods are considered. The maximum k_{eff} increase for each of the enrichment and burnup combinations is shown in Table 10. Figure 8 shows the k_{eff} increase as a function of rods removed for the limiting case at 5 w/o and 44.25 GWd/MTU burnup. The limiting lattice is shown in Figure 9. The maximum k_{eff} value occurs for 44 rods removed and corresponds to a k_{eff} increase of 1.86% Δk_{eff}.

Multiple rod removal in the fresh fuel 1.92 w/o case resulted in a decrease in the cask reactivity. Hence, the single rod removal case bounds all multiple rod removal configurations considered.

The k_{eff} increase for both rod removal configurations in the GBC-32 cask is in generally good agreement with Ref. 7. The multiple rod removal k_{eff} increase is somewhat higher, most likely because of the use of a distributed axial burnup profile in this work.

Table 9. Single rod removal results for 17 × 17 OFA in GBC-32

Enrichment (w/o ^{235}U)	Burnup (GWd/MTU)	Location	Maximum increase in k_{eff} (% Δk_{eff})
1.92	0	H8	0.04
3.5	25.5	H7	0.08
5	44.25	H5	0.09

Table 10. Multiple rod removal results for 17 × 17 OFA in GBC-32

Enrichment (w/o ^{235}U)	Burnup (GWd/MTU)	Maximum increase in k_{eff} (% Δk_{eff})
1.92	0	N/A*
3.5	25.5	1.07
5	44.25	1.86

*All multiple removal cases resulted in a decrease in k_{eff}

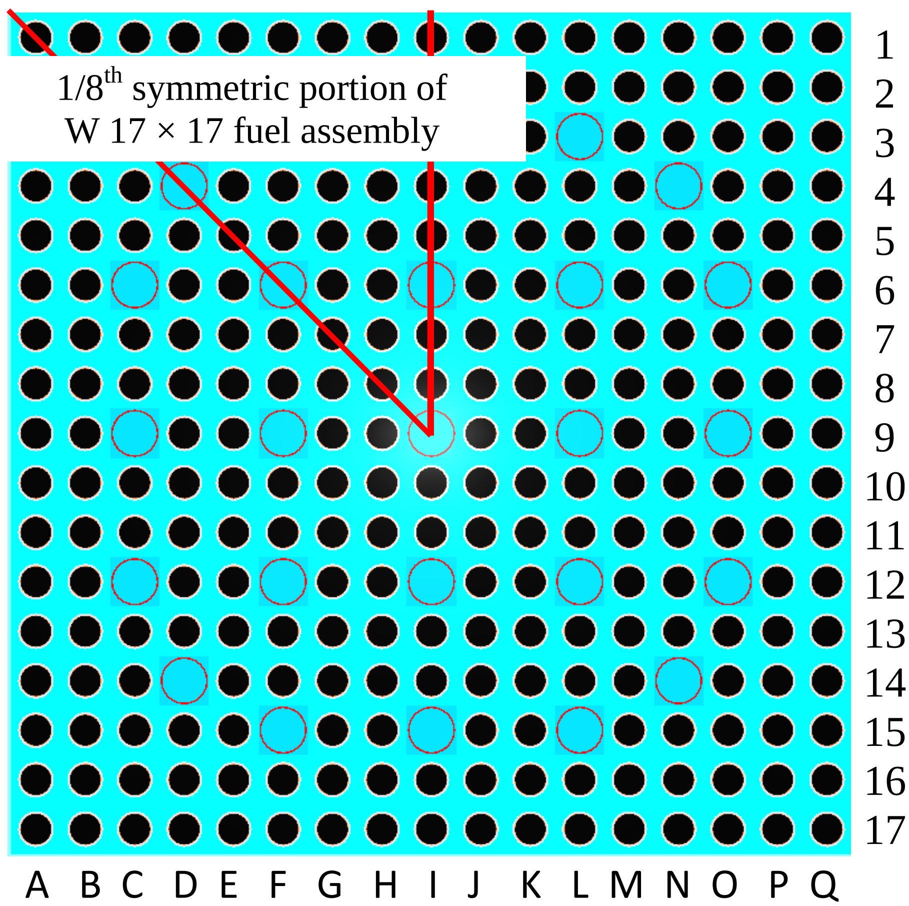

Figure 7. Sketch of symmetry, row, and column labels for W 17 × 17 fuel assembly.

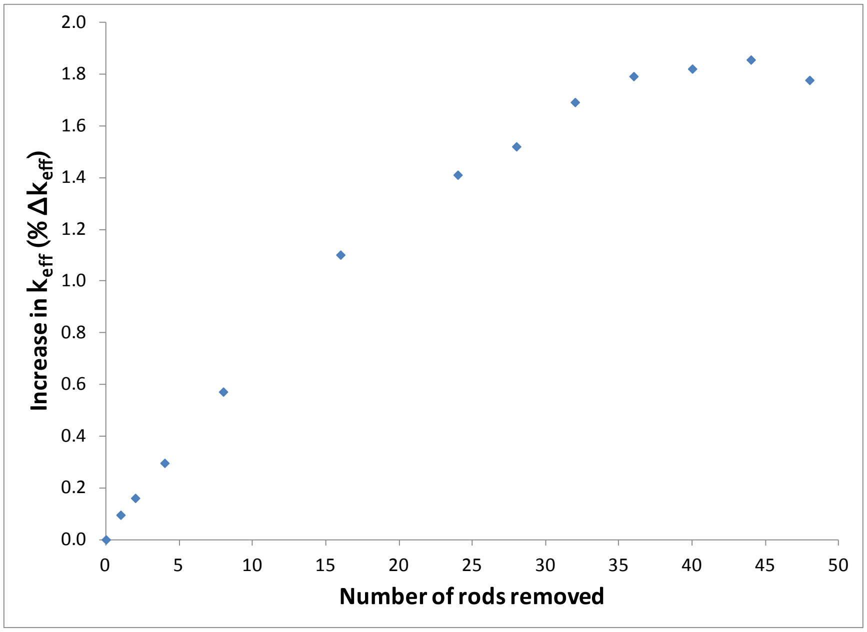

Figure 8. Increase in k_{eff} in GBC-32 cask as a function of number of rods removed (5 w/o ^{235}U initial enrichment, 44.25 GWd/MTU burnup).

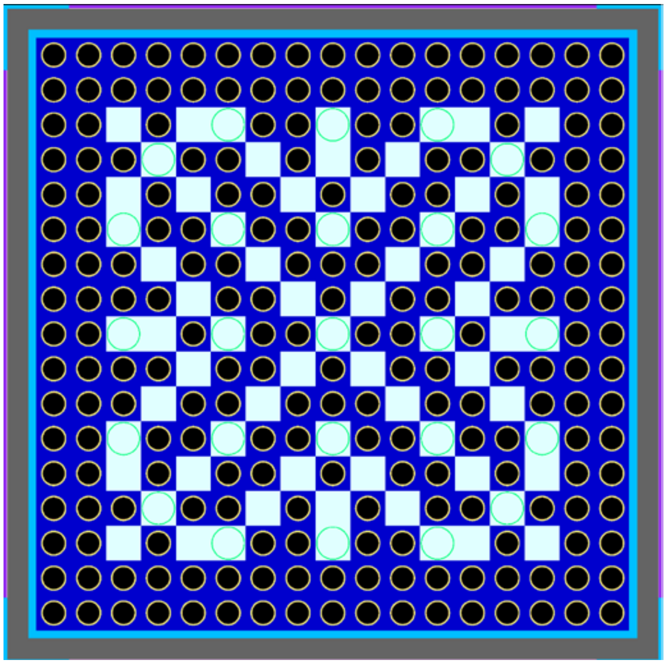

Note: Missing rod locations are shown in white; the same water mixture was used in empty cell locations and guide tube locations

Figure 9. Limiting multiple rod removal lattice (44 rods removed).

5.1.1.3 Loss of Rod Pitch Control

The loss of rod pitch control is modeled first as a uniform increase in fuel assembly pitch, as discussed in Section 3.1.3. The pitch between rods is expanded uniformly until the rod unit cells of the outer row of fuel rods are coincident with the inner surface of the storage cells. The largest expansion is modeled in two configurations – with the clad fully intact and also completely removed. The limiting condition for both cases is for fuel with an initial enrichment of 5 w/o and 44.25 GWd/MTU burnup. The results with the pitch expanded until the outer unit cell boundary contacts the storage cell, both with and without cladding, for all three combinations of initial enrichment and burnup are shown in Table 11.

The limiting configuration, with 44.25 GWd/MTU burnup, is further expanded until the outermost fuel rods are in contact with the storage cell walls as shown in Figure 10. The increase in k_{eff} in this case relative to the nominal configuration is 2.65% Δk_{eff} with cladding intact and 5.34% Δk_{eff} with cladding removed. The unclad fuel rods are modeled in the same locations with the cladding removed; the pitch is not increased further to put the fuel material in contact with the storage basket. The first five points in Figure 11 show the increase in k_{eff} associated with this uniform pitch expansion. These results indicate a k_{eff} increase that is approximately 0.5% Δk_{eff} lower for loss of rod pitch control compared to Refs. 15 or 25.

Fuel rod pitch is further increased in the GBC-32 model to examine the effect of nonuniform pitch, as discussed in Section 3.1.3.1 and References 31 and 32. The inner portion of the assembly continues to expand until the outer rows are in contact with each other; although the fuel rod pitch is still uniform axially, it is nonuniform in the radial direction. An example model is shown in Figure 12. The pitch in each of the outer rows is constant within the row and is equal to the pitch that caused that row to make contact with the previous row or the basket wall. The increase in pitch in inner rows leads to a nonuniform pitch in the lattice. The results of the calculations with increasing pitch are shown in Figure 11 as a function of the pitch of the inner, uniform portion of the assembly. The maximum k_{eff} increase, as shown in Table 6, is 3.90% Δk_{eff}. The first five points represent the uniform pitch expansion. Nonuniform expansion begins when the fuel rod pitch is in excess of approximately 1.32 cm. The additional k_{eff} increase beyond the uniform expansion case reported above is 1.25% Δk_{eff}, thus indicating that further expansion is a significant effect. This is consistent with the results presented in References 31 and 32.

The limiting pitch expansion case corresponds to 5 w/o fuel with 44.25 GWd/MTU burnup, so the most reactive axial section is near the top end. The fuel rod pitch is varied as function of axial position to investigate the potential effect of birdcaging, as discussed in Section 3.1.3.2. The increased and decreased pitch variations are applied over discrete sections of the fuel rods, and not as continuous changes as a function of elevation. The irradiated fuel is represented with segments 20.32 cm in length to capture the axial burnup gradient, as discussed in Appendix A, and these segments are used as the discrete sections for pitch variation. The size of the compressed pitch region is varied from one and four segments, and the expanded pitch section at the top of the assembly ranges from two to eight segments in length in an effort to identify the maximum change in k_{eff} attributable to birdcaging. An example with four segments in the compressed region and four segments in the upper expanded region is shown in Figure 13. Slight reactivity increases are observed in the cases with four or more fuel segments in the expanded pitch zone. The maximum k_{eff} change is 0.05% Δk_{eff} beyond the 2.65% Δk_{eff} resulting from uniform pitch expansion configuration. This additional increase in k_{eff} is negligible.

Table 11. Results for loss of rod pitch control in GBC-32

Enrichment (w/o ^{235}U)	Burnup (GWd/MTU)	Increase in k_{eff} (% Δk_{eff})
Cladding intact		
1.92	0	0.78
3.5	25.5	1.48
5	44.25	1.69
Cladding removed		
1.92	0	3.30
3.5	25.5	4.49
5	44.25	4.89

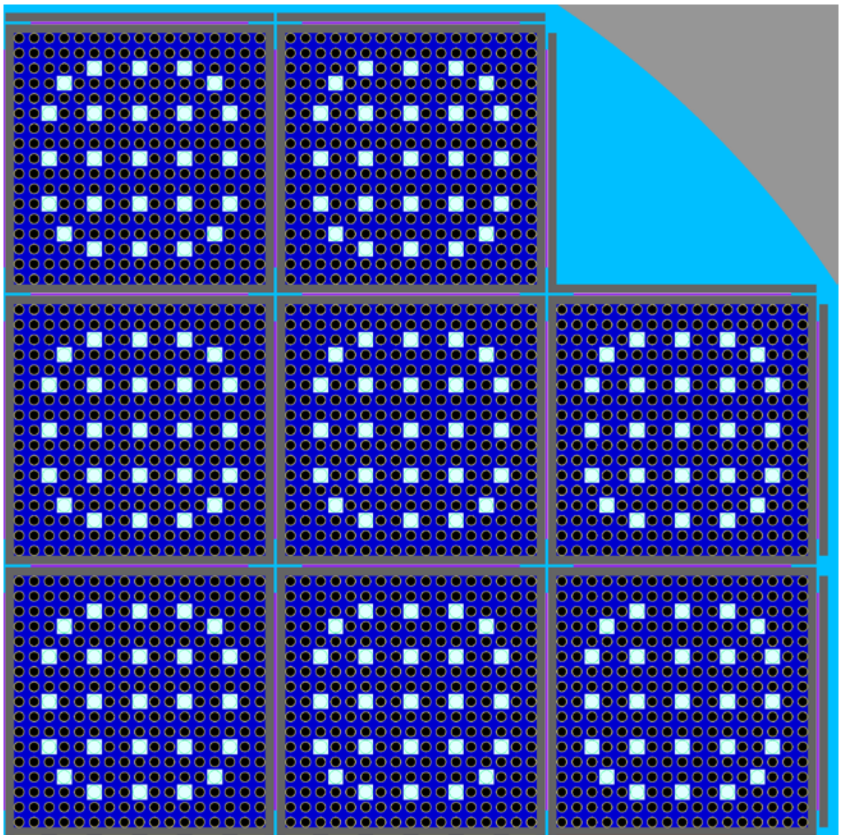

Figure 10. Maximum uniform pitch expansion case.

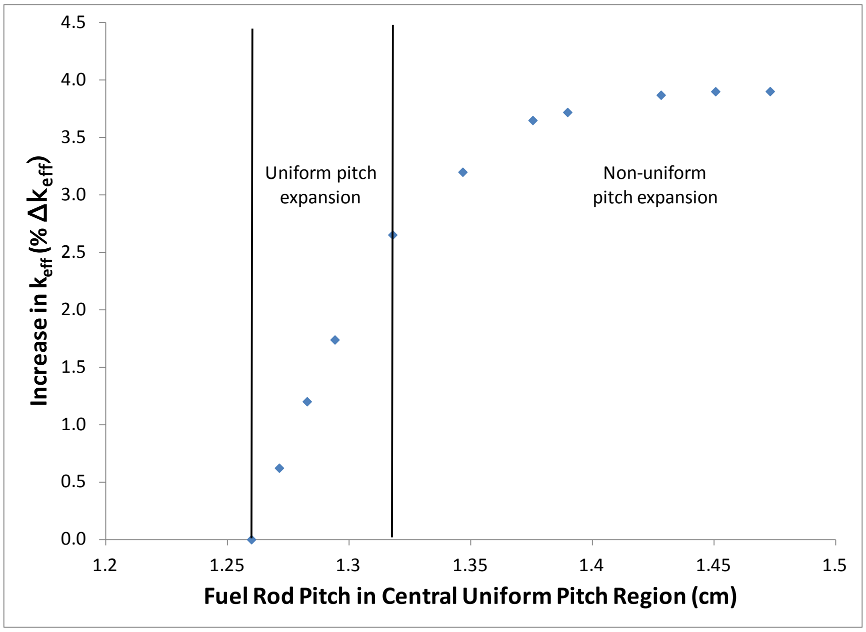

Figure 11. Increase in k_{eff} in GBC-32 cask due to increased fuel rod pitch (5 w/o initial enrichment, 44.25 GWd/MTU burnup).

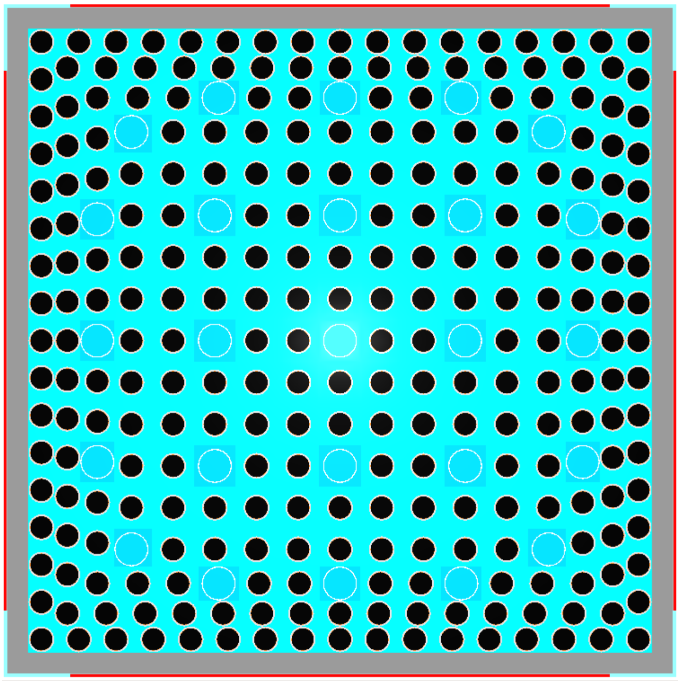

Notes: Both shades of light blue are identical water compositions
Neutron absorber panels are shown in red

Figure 12. Example nonuniform pitch model in GBC-32 storage cell.

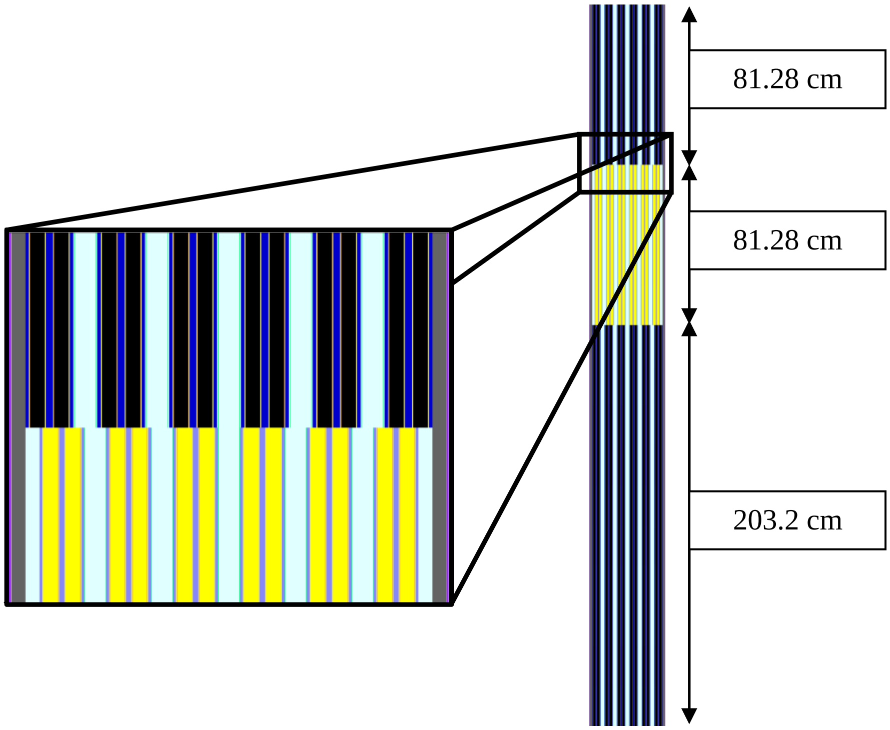

Notes: Fuel in expanded pitch segments is shown as black, regardless of isotopic composition
Fuel in compressed pitch segments is shown in yellow, regardless of isotopic composition
Large gaps between pairs of fuel rods indicate the presence of guide tubes

Figure 13. Assembly with axially varying pitch in the GBC-32.

5.1.1.4 Loss of Assembly Position Control

Loss of assembly position control is calculated over a range of displacements. The consequence of the maximum misalignment for all three burnup and enrichment combinations is shown in Table 12 and is over 16% Δk_{eff} for the limiting condition. A more limited misalignment case (20 cm) is also evaluated as a surrogate for potential degradation of assembly end fittings or the spacers used inside the cask to ensure proper assembly alignment at the time of loading. The consequences of this more limited misalignment, shown in Figure 14 and Table 13, are significantly less, but the increase in k_{eff} is still nearly 11% Δk_{eff}. The limiting condition for misalignment is for fuel with 44.25 GWd/MTU burnup and an initial enrichment of 5 w/o. Misalignment toward the bottom of the cask has significantly less impact because the fuel at the bottom end of the assembly has lower reactivity. The variation of the k_{eff} increase as a function of axial position is shown in Figure 15 for fuel with an initial enrichment of 5 w/o ^{235}U and 44.25 GWd/MTU burnup. The reactivity increase reported here is significantly higher than that reported in Ref. 25. Insufficient detail is available for review in Ref. 25 to propose any likely causes for the differences.

Table 12. Increase in k_{eff} for assembly axial displacement in GBC-32 (30 cm displacement relative to the neutron absorber panel)

Enrichment (w/o ^{235}U)	Burnup (GWd/MTU)	Increase in k_{eff} (% Δk_{eff})
1.92	0	10.38
3.5	25.5	16.37
5	44.25	16.70

Table 13. Increase in k_{eff} for limited (20 cm displacement relative to the neutron absorber panel) assembly axial displacement in GBC-32

Enrichment (w/o ^{235}U)	Burnup (GWd/MTU)	Increase in k_{eff} (% Δk_{eff})
1.92	0	3.85
3.5	25.5	10.22
5	44.25	10.82

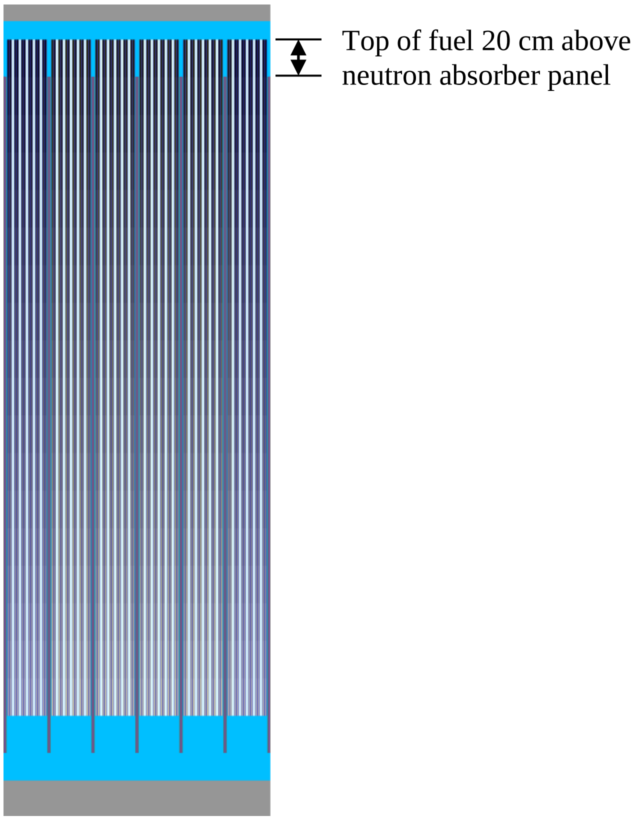

Figure 14. Misalignment of fuel assembly 20 cm toward lid of GBC-32.

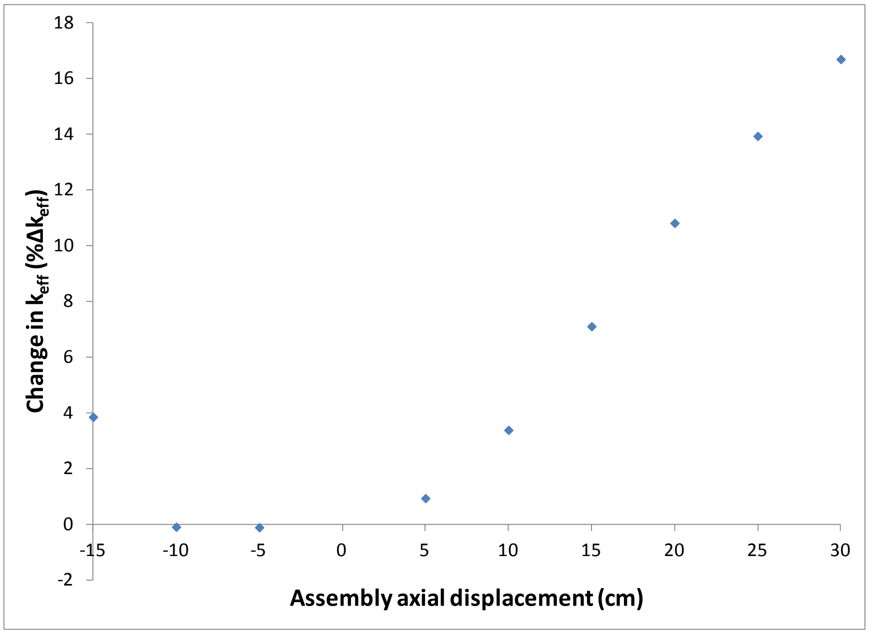

Figure 15. Increase in k_{eff} in GBC-32 as a function of assembly axial displacement (5 w/o initial enrichment and 44.25 GWd/MTU burnup).

5.1.1.5 Gross Fuel Assembly Failure

The two gross assembly failure configurations described in Section 3.1.5 are investigated in the GBC-32 cask. Axial representations are shown in Figure 16 and 17 for the homogeneous rubble and ordered pellet array cases, respectively. In both cases, the limiting case is the non-physical condition in which the fissile material extends from the base plate to the lid. As expected, these configurations have the highest k_{eff} increase, and the ordered pellet array case is more limiting than the homogeneous rubble case. As shown previously in Table 6, the k_{eff} associated increase in the homogeneous rubble case is over 14% Δk_{eff}, and the ordered pellet array case increases k_{eff} by over 21% Δk_{eff}. The limiting case is for the 44.25 GWd/MTU burnup case with 5 w/o initial enrichment for both gross assembly failure configurations. The results for both configurations for all three enrichment and burnup combinations are presented in Table 14 for the maximum increase case. If the fissile material is maintained within the poison panel elevations, the resulting change in k_{eff} is reduced to 4.18% Δk_{eff} for the ordered array of pellets. Results for a range of homogeneous rubble cases within the neutron absorber elevations are provided in Table 15. The results with fissile material restrained in the neutron absorber elevations demonstrate that these cases result in significantly lower k_{eff} increases than the unrestrained material cases.

The results for the pellet array case are significantly higher than those reported previously in Ref. 7. There are two main differences between that analysis and this one, both of which contribute to a sizeable k_{eff} increase in the work presented here. The pellet array case modeled here includes a distributed burnup profile in the pellet array, and the array is allowed to extend beyond the neutron absorber panel elevations. This latter change is the larger of the two effects, but the former change is also important.

Table 14. Increase in k_{eff} in GBC-32 due to gross fuel assembly failure, fissile material outside neutron absorber elevations

Enrichment (w/o ^{235}U)	Burnup (GWd/MTU)	Maximum increase in k_{eff} (% Δk_{eff})
Limiting pellet array		
1.92	0	11.09
3.5	25.5	20.20
5	44.25	21.37
Homogeneous rubble		
1.92	0	6.66
3.5	25.5	13.95
5	44.25	14.30

Table 15. Increase in k_{eff} in GBC-32 due to homogeneous rubble, debris within absorber elevations (5 w/o initial enrichment, 44.25 GWd/MTU burnup)

Fraction of nominal assembly height	Increase in k_{eff} (% Δk_{eff})
1.0	-4.64
0.9	-7.05
0.8	-10.16
0.7	-14.36
0.6	-20.16
0.5	-28.34
0.4	-39.10
0.36 (Fully compressed rubble)	-45.50

Figure 16. Limiting homogeneous rubble configuration for GBC-32.

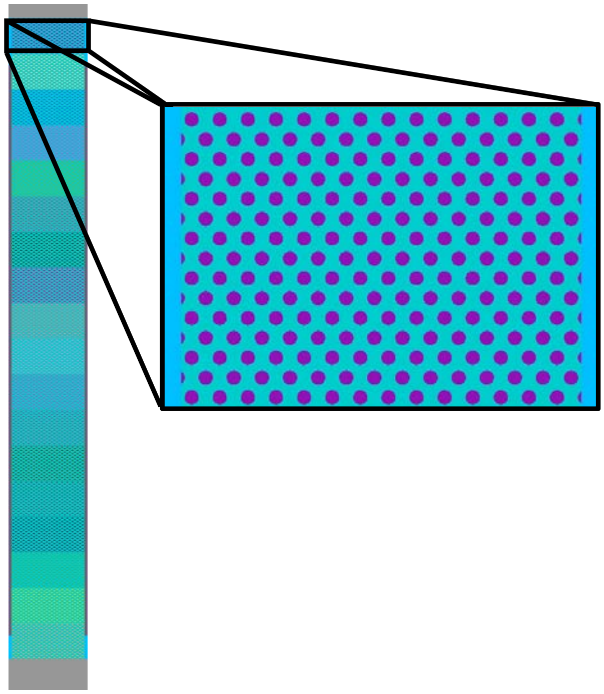

Figure 17. Limiting ordered pellet array configuration for GBC-32.

5.1.1.6 Neutron Absorber Degradation

The results of the calculations, described in Section 3.1.6.1, considering a 5-cm neutron absorber defect at varying elevations for all three enrichment and burnup combinations are presented in Table 16. The limiting condition is for fuel with an initial enrichment of 5 w/o and 44.25 GWd/MTU burnup. As expected, the limiting elevation is near the top of the active fuel height, as shown in Figure 18. The results for the full range of elevations considered in the limiting fuel condition are presented in Table 17. As expected, the limiting elevation for the fresh 1.92 w/o fuel is located at the centerline. The largest k_{eff} increase observed for the 5-cm defect is 1.05% Δk_{eff} and increases to 2.33% Δk_{eff} if the defect size is increased to 10 cm. As discussed in Section 3, these defects are assumed to be present at the same elevation in all neutron absorber panels within the cask and the sizes of the defects are chosen arbitrarily.

The consequences of uniform neutron absorber panel thinning as discussed in Section 3.1.6.3 are shown in Table 18 and Figure 19 for fresh 1.92 w/o fuel. The panel thinning results shown in Appendix C confirm that the fresh fuel case is most limiting. As shown in Table 6, a 50% reduction in absorber panel thickness increases k_{eff} by 1.78% Δk_{eff}. Complete removal of the panels causes a k_{eff} increase of 9.5%, but the increase is not in excess of 3% until nearly 70% of the neutron absorber panel is removed. The consequence of complete absorber panel removal is less severe than the axial displacement cases discussed in Section 5.1.1.4 because the steel fuel storage basket walls reduce neutronic communication between assemblies.

Table 16. Maximum k_{eff} increase caused by a 5-cm neutron absorber defect in GBC-32

Enrichment (w/o ^{235}U)	Burnup (GWd/MTU)	Defect center elevation (cm)	Maximum increase in k_{eff} (% Δk_{eff})
1.92	0	182.88	0.29
3.5	25.5	342.09	0.94
5	44.25	348.86	1.05

Table 17. Increase in k_{eff} caused by a 5-cm neutron absorber defect at various elevations in GBC-32 (5 w/o initial enrichment, 44.25 GWd/MTU burnup)

Defect center elevation (cm)	Increase in k_{eff} (% Δk_{eff})
321.77	0.44
328.54	0.67
335.31	0.84
342.09	1.00
348.86	1.05
355.64	0.82

Table 18. Increase in k_{eff} caused by uniform neutron absorber panel thinning (fresh 1.92 w/o enrichment)

Fraction of neutron absorber panel thickness remaining	Increase in k_{eff} (%Δk_{eff})
0.9	0.29
0.8	0.59
0.7	0.92
0.6	1.32
0.5	1.78
0.4	2.39
0.3	3.15
0.2	4.20
0.1	5.86
0.0	9.51

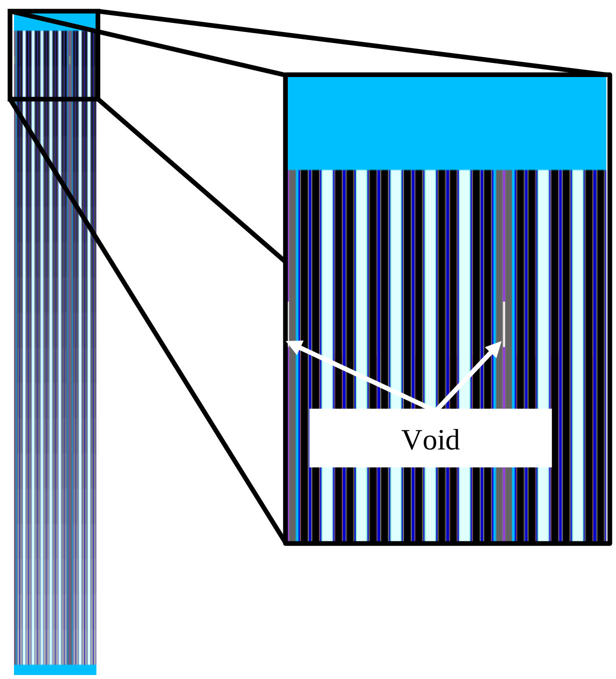

Figure 18. Limiting location of 5-cm neutron absorber panel defect in GBC-32.

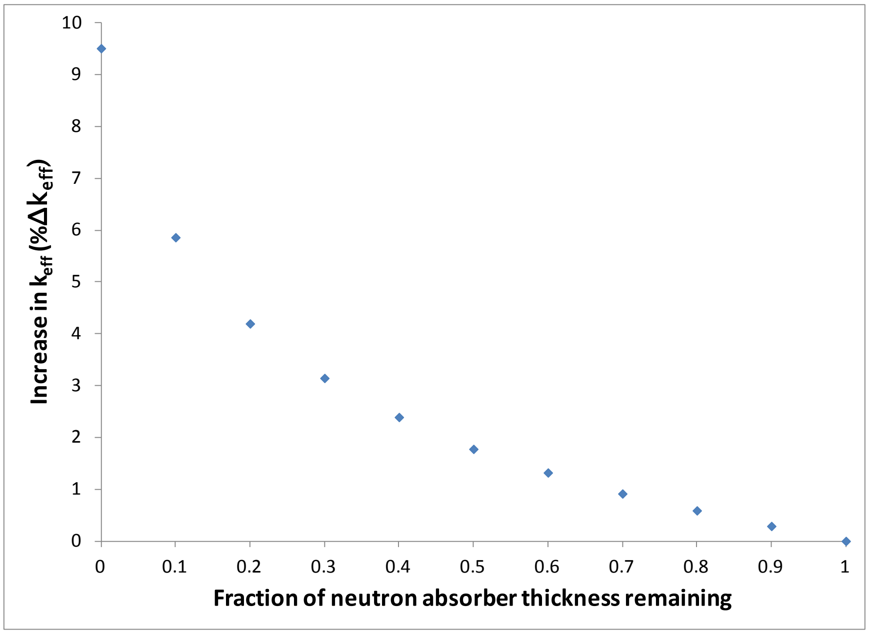

Figure 19. Increase in k_{eff} as a function of remaining neutron absorber panel thickness for fresh 1.92 w/o fuel.

5.1.1.7 Burnup and Cooling Time Sensitivities

The results of the sensitivity studies relating to additional burnup and cooling time are presented in Appendix C (Section C.1). Each configuration discussed in the previous six subsections is considered explicitly. The results of the calculations for additional burnup and cooling time conditions indicate that the increase in k_{eff} reported for each configuration encompasses the changes that may result for additional burnups and cooling times. That is, the differences in the change in k_{eff} are smaller than the changes in the base case k_{eff} caused by the additional burnup and/or cooling time considered.

5.1.2 Varying Number of Reconfigured Assemblies

The results presented in Section 5.1.1 and Table 6 assume that all 32 fuel assemblies in the GBC-32 cask experience the same fuel or neutron absorber reconfiguration within the respective configuration of interest. As discussed in Section 3.2, a series of calculations is performed to establish the k_{eff} increase as a function of the number of reconfigured assemblies within the cask. The four configurations considered are the limiting conditions for single rod failure, multiple rod failure, uniform rod pitch increase, and homogeneous rubble resulting from gross assembly failure.

The first fuel assembly to experience the reconfiguration being examined is selected in an attempt to maximize the k_{eff} increase, and is therefore one near the center of the cask. Additional assemblies are added in mostly symmetric groups of equal distance from the first reconfigured assembly. For some low numbers of reconfigured assemblies, multiple combinations of assemblies are considered. Eight combinations of reconfigured assemblies are considered in the GBC-32. One order in which the assemblies experience reconfiguration is shown in Figure 20. Results are presented in the following subsections.

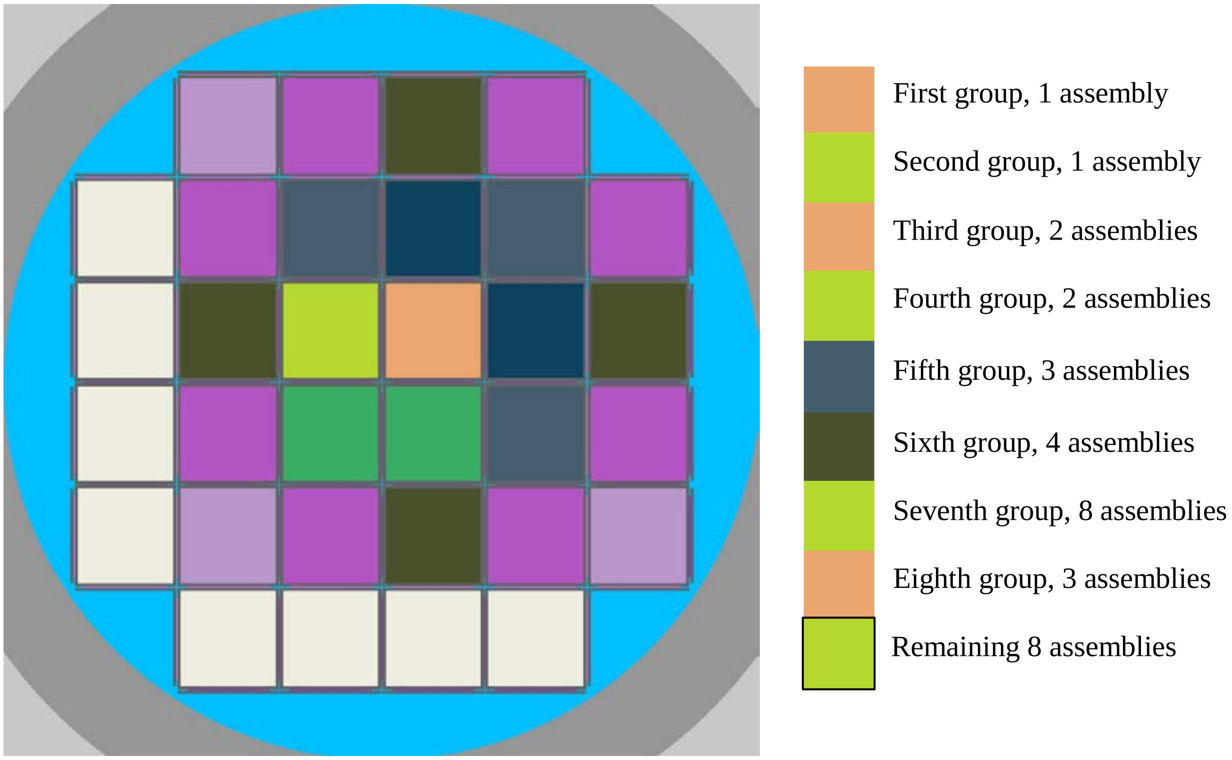

Figure 20. One order of assembly reconfiguration in GBC-32 partial degradation configurations.

5.1.2.1 Rod Failures

The single and multiple rod failure configurations that result in the largest increase in k_{eff}, as discussed in Section 5.1.1.2, are used to study the impact of some assemblies suffering reconfiguration while others in the cask remain intact. All assemblies, reconfigured or intact, use the isotopic number densities representing 5 w/o ^{235}U fuel depleted to 44.25 GWd/MTU and cooled for 5 years.

The results for single rod failure are shown below in Table 19 and Figure 21. The results for multiple rod failure are shown below in Table 20 and Figure 22. The portion of the k_{eff} impact introduced by each group of assemblies for the single rod failure configurations shows more than 50% of the reactivity change coming after only four assemblies experience reconfiguration and more than 75% of the reactivity change caused by the first nine assembly reconfigurations. The Monte Carlo uncertainty is relatively large compared to the k_{eff} changes being examined in this series of calculations because of the relative insensitivity of the cask k_{eff} to single rod failures. The resulting k_{eff} increase is therefore not a smooth function.

The multiple rod failure results are similar, with fewer than nine assemblies causing 50% of the increase in k_{eff} and 13 assemblies causing almost 75% of the change. The results indicate that a reduced number of reconfigured assemblies will not significantly reduce the k_{eff} increase associated with fuel reconfiguration if the degraded assemblies are in close proximity, and particularly if they are in the center region of the cask.

Table 19. Increase in k_{eff} in GBC-32, single rod failure (5 w/o initial enrichment, 44.25 GWd/MTU burnup)

Number of degraded assemblies	Increase in k_{eff} (% Δk_{eff})
1	0.01
2	0.01
2	0.01
4	0.06
5	0.04
5	0.05
9	0.07
13	0.07
21	0.07
24	0.07
32	0.09

Table 20. Increase in k_{eff} in GBC-32, multiple rod failure (5 w/o initial enrichment, 44.25 GWd/MTU burnup)

Number of degraded assemblies	Increase in k_{eff} (% Δk_{eff})
1	0.20
2	0.37
2	0.36
4	0.71
5	0.79
5	0.82
9	1.16
13	1.38
21	1.70
24	1.74
32	1.86

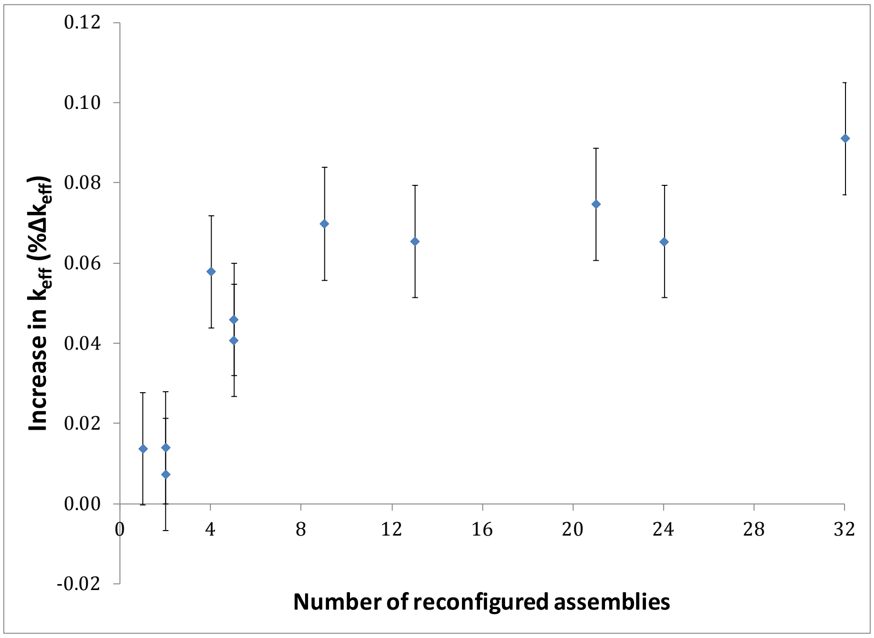

Figure 21. Increase in k_{eff} in GBC-32 as a function of number of reconfigured assemblies, single rod failure (5 w/o initial enrichment, 44.25 GWd/MTU burnup).

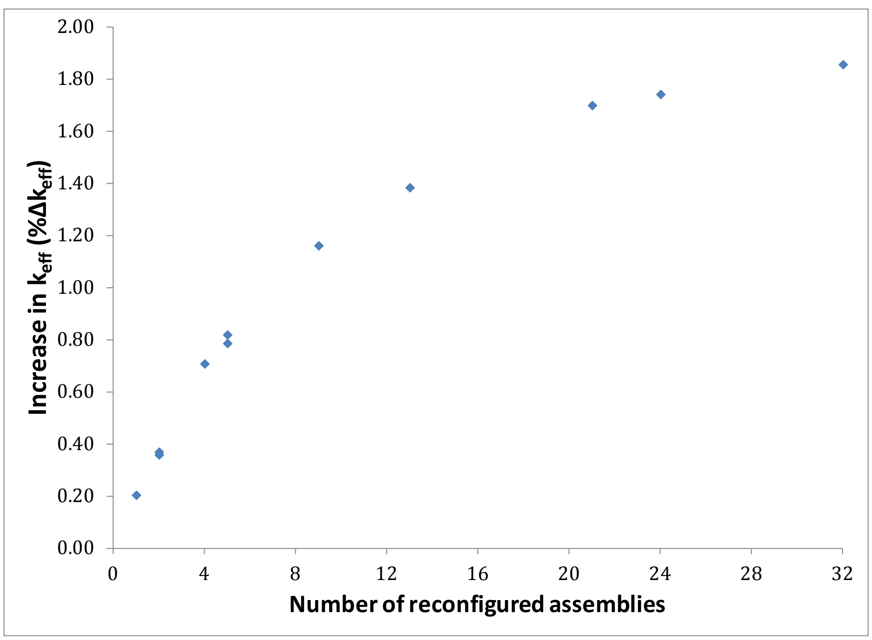

Figure 22. Increase in k_{eff} in GBC-32 as a function of number of reconfigured assemblies, multiple rod failure (5 w/o initial enrichment, 44.25 GWd/MTU burnup).

5.1.2.2 Loss of Rod Pitch Control, Uniform Pitch Increase

The maximum uniform pitch increase case is used to examine the k_{eff} impact of varying the number of assemblies that have experienced reconfiguration. The assembly configuration used for this study models

the outer row of fuel rods in contact with the inner wall of the fuel storage basket in each cell. The fuel composition used for all assemblies corresponds to 5 w/o fuel with 44.25 GWd/MTU burnup and 5 years of cooling time. The increase in k_{eff} for each number of reconfigured assemblies is provided in Table 21 as well as Figure 23. The first 50% of the total increase in k_{eff} has occurred with about seven reconfigured assemblies. Almost 75% of the increase in k_{eff} is caused by the first 13 reconfigured assemblies. The shape of the increase in k_{eff} as a function of reconfigured assemblies is similar to that seen for rod failure configurations in Section 5.1.2.1. The results indicate that a reduced number of reconfigured assemblies will not significantly reduce the k_{eff} increase associated with fuel reconfiguration if the degraded assemblies are in close proximity, and particularly if they are in the center region of the cask.

Table 21. Increase in k_{eff} in GBC-32, uniform pitch increase (5 w/o initial enrichment, 44.25 GWd/MTU burnup)

Number of degraded assemblies	Increase in k_{eff} (% Δk_{eff})
1	0.27
2	0.51
2	0.49
4	1.00
5	1.14
5	1.08
9	1.66
13	1.96
21	2.41
24	2.49
32	2.66

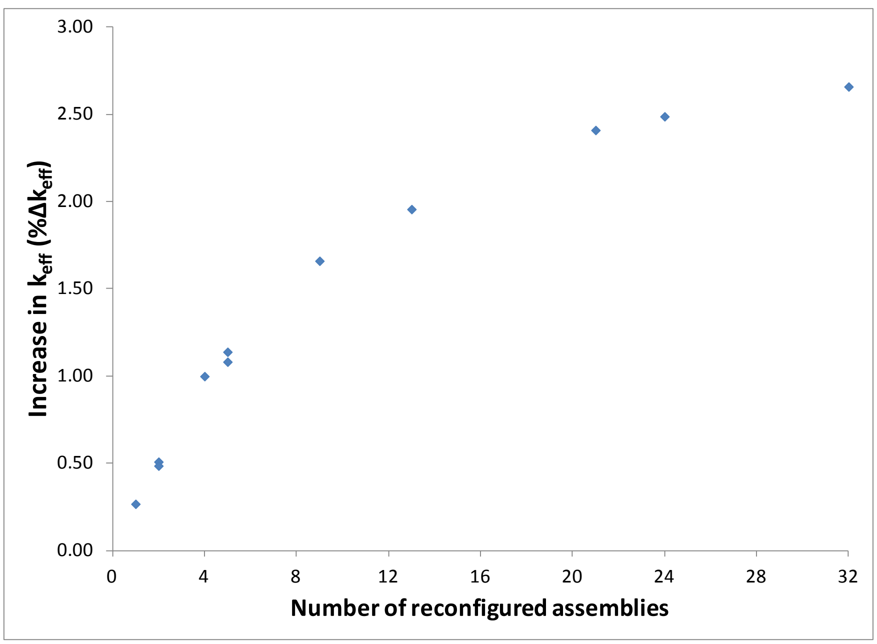

Figure 23. Increase in k_{eff} in GBC-32 as a function of number of reconfigured assemblies, uniform pitch increase (5 w/o initial enrichment, 44.25 GWd/MTU burnup).

5.1.2.3 Gross Assembly Failure, Homogeneous Rubble

The homogeneous rubble modeling of the gross assembly failure configuration is the final configuration used to examine the k_{eff} impact of varying the number of assemblies that have experienced reconfiguration. The configuration used for this study fills the entire inside volume of the storage cell with homogeneous rubble, as described in Section 3.1.5.1. Each axial zone of rubble is approximately 23 cm tall; thus, the 18 zones fill the cask from the base plate to the lid and retain the axial burnup profile of the intact assembly. The fuel composition is based on fuel with an initial enrichment of 5 w/o and 44.25 GWd/MTU burnup. This configuration resulted in the largest k_{eff} increase of the homogeneous rubble configurations used in Section 5.1.1.5. The increase in k_{eff} for each number of reconfigured assemblies is provided in Table 22 as well as Figure 24. The general trend in the k_{eff} change for the uniform pitch increase cases is different from that for single and multiple rod failure and uniform pitch expansion configurations presented in Sections 5.1.2.1 and 5.1.2.2. The first two reconfigured assemblies lower the cask k_{eff} because of the effects of homogenization and fissile material relocation. An increase in k_{eff} is noted for four or more reconfigured assemblies after a sufficient number of assemblies are reconfigured to relocate the most reactive portion of the cask to the top of the homogeneous rubble. More than 60% of the increase in k_{eff} is caused by the first nine reconfigured assemblies, and more than 70% of the total k_{eff} increase results from the reconfiguration of 13 assemblies.

Table 22. Increase in k_{eff} in GBC-32, homogeneous rubble configuration of gross assembly failure (5 w/o initial enrichment, 44.25 GWd/MTU burnup)

Number of degraded assemblies	Increase in k_{eff} (% Δk_{eff})
1	-0.53
2	-0.87
2	-1.07
4	1.93
5	2.91
5	1.70
9	8.59
13	10.07
21	12.94
24	13.37
32	14.30

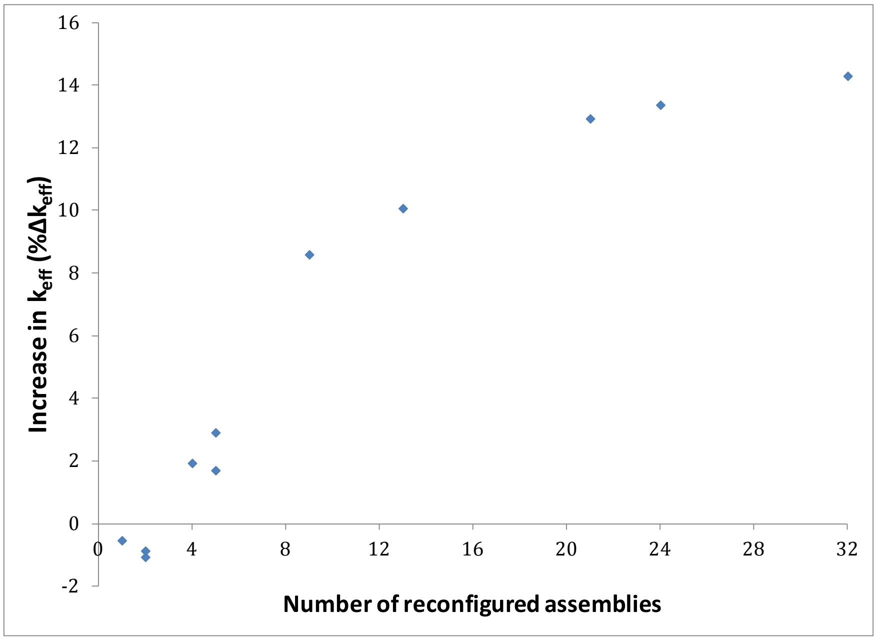

Figure 24. Increase in k_{eff} as a function of number of reconfigured assemblies, gross assembly failure.

5.1.3 Combined Configurations

As discussed in Section 3.3, some of the mechanisms that could result in fuel reconfigurations could result in a combination of configurations. Therefore, selected combined configurations are evaluated, including: 16 failed rods with 50% clad thinning and 16 failed rods with a uniform pitch expansion of 0.011 cm. These combinations of configurations are selected as they both pertain to failure of zirconium alloy components of the fuel assembly. The combined degradation cases consider fuel with an initial enrichment of 5 w/o ^{235}U depleted to 44.25 GWd/MTU and 5 years of cooling time.

The multiple rod failure results presented in Section 5.1.1.2 indicate that the failure of 16 fuel rods results in an increase in k_{eff} of 1.1% Δk_{eff}. This is approximately half the maximum increase for multiple failed rod configurations and is therefore selected as an intermediate configuration. The cladding thickness on all intact rods in both combined configurations is represented with 50% of the nominal thickness. The pitch increase of 0.011 cm, based on the results presented in Figure 11, is approximately 0.6% Δk_{eff}. This represents about 15% of the increase in maximum k_{eff} associated with the nonuniform pitch expansion.

The results of the two combined configurations considered in the GBC-32 cask are presented in Table 23. For comparison, the k_{eff} increase resulting from each degraded configuration separately as well as the sum of the two is provided. The increase in k_{eff} associated with explicit modeling of the combined configurations is less than the estimated increase based on summing the individual increases. The conservatism of adding the separate effects is less than 0.4% Δk_{eff}. It appears that the linear combination of the k_{eff} increases is conservative, but more combined configurations would need to be investigated prior to drawing general conclusions. If it is confirmed, the k_{eff} increase caused by combinations of degradations could be conservatively bounded by adding the increase associated with individual configurations where applicable.

Table 23. Increase in k_{eff} for combined configurations in GBC-32

Case	Increase in k_{eff} (% Δk_{eff})
Multiple failed rods and clad thinning (44.25 GWd/MTU; 5-y cooling time)	
16 failed rods	1.10
50% clad thinning	1.94
Sum of k_{eff} increases	3.04
Combined configuration model	2.67
Overestimation of k_{eff} increase by summing individual effects	0.37
Multiple failed rods and 0.011-cm increase in fuel rod pitch (44.25 GWd/MTU; 5-y cooling time)	
16 failed rods	1.10
Uniform pitch increase	0.62
Sum of k_{eff} increases	1.72
Combined configuration model	1.63
Overestimation of k_{eff} increase by summing individual effects	0.09

5.2 MPC-68 Cask Model Results

The k_{eff} change associated with each of the reconfigurations discussed in Section 3 is presented here for the MPC-68 cask. The configurations assume a range of loadings of 10 × 10 fuel. The description of the fuel assembly modeling is provided in Appendix A. All fuel is modeled with a uniform initial enrichment of 5 w/o. The burnups and cooling times used are presented in Table 24. The basis for selecting these points is provided in Section 4.2.2. All configurations, with the exception of the uniform array of pellets model of gross fuel assembly failure, also consider the fuel both with and without the channel present. The reference case k_{eff} results for both fresh and used fuel in both the channeled and unchanneled conditions are provided in Table 24.

Table 24. Nominal k_{eff} results for enrichment, burnup, and cooling time cases considered in MPC-68, channeled and unchanneled fuel

Channel present	Burnup (GWd/MTU)	Cooling time (years)	KENO V.a		KENO-VI	
			k_{eff}	σ	k_{eff}	σ
Yes	0	0	0.96800	0.00010	0.96828	0.00010
	35.0	5	0.83269	0.00010	0.83258	0.00010
No	0	0	0.96768	0.00010	0.96763	0.00010
	35.0	5	0.83434	0.00010	0.83420	0.00010

5.2.1 Reconfiguration of All Assemblies

A summary of the increases in k_{eff} caused by each configuration is provided in Table 25. Additional details for each configuration and the results for non-limiting cases are provided in the subsequent subsections.

Comparing the results of these analyses to those presented in Ref. 7 is more difficult for the MPC-68 cask than for the GBC-32 cask. The difficulty is primarily a result of the analyses in Ref. 7 using a 9 × 9 fuel assembly.

Table 25. Summary of k_{eff} increases for the MPC-68 cask

Configuration	Increase in k_{eff} (% Δk_{eff})	Limiting case		
		Burnup (GWd/MTU)	Cooling time (years)	Channel present
Clad thinning/loss				
Cladding removal	4.98	0	0	Yes
Rod failures				
Single rod removal	0.29	0	0	Yes
Multiple rod removal	2.40	35	5	Yes
Loss of rod pitch control				
Uniform rod pitch expansion, clad	13.16	0	0	No
Uniform rod pitch expansion, unclad	15.32	0	0	No
Channel constrained uniform expansion, clad	2.09	0	0	Yes
Nonuniform rod pitch expansion, clad	13.31	0	0	No
Loss of assembly position control				
Axial displacement (maximum)	19.40	35	5	Yes
Axial displacement (20 cm)	6.29	35	5	Yes
Gross assembly failure				
Uniform pellet array	34.40	35	5	No
Homogeneous rubble	29.36	35	5	No
Neutron absorber degradation				
Missing neutron absorber (5-cm segment)	2.49	35	5	Yes
Missing neutron absorber (10-cm segment)	5.62	35	5	Yes
50% reduction of neutron absorber panel thickness	3.67	0	0	Yes

5.2.1.1 Clad Thinning/Loss

The loss of cladding configuration is modeled as discussed in Section 3.1.1. As shown in Table 25, the limiting k_{eff} increase associated with complete cladding removal is 4.98% Δk_{eff} and occurs with fresh fuel. The results for both fuel burnups, both with and without the fuel channel, are summarized in Table 26. For the limiting case, fresh fuel, the increase in k_{eff} as a function of the fraction of nominal cladding thickness remaining is shown in Table 27 and Figure 25. The trend of increasing k_{eff} with decreasing cladding thickness is the same for depleted fuel, so these results are not presented here. The configuration with 25% of the nominal cladding remaining is shown in Figure 26. The results are in good agreement with those presented in Ref. 7.

Table 26. Increase in k_{eff} for cladding removal in MPC-68

Burnup (GWd/MTU)	Cooling time (years)	Channel	Increase in k_{eff} (% Δk_{eff})
0	0	Yes	4.98
35	5		4.82
0	0	No	4.71
35	5		4.59

Table 27. Increase in k_{eff} in MPC-68 as a function of fraction of intact cladding, fresh 5 w/o fuel

Fraction of intact cladding	Increase in k_{eff} – Channeled (%Δk_{eff})	Increase in k_{eff} – Unchanneled (%Δk_{eff})
0.90	0.59	0.51
0.75	1.40	1.31
0.50	2.69	2.55
0.25	3.84	3.68
0	4.98	4.71

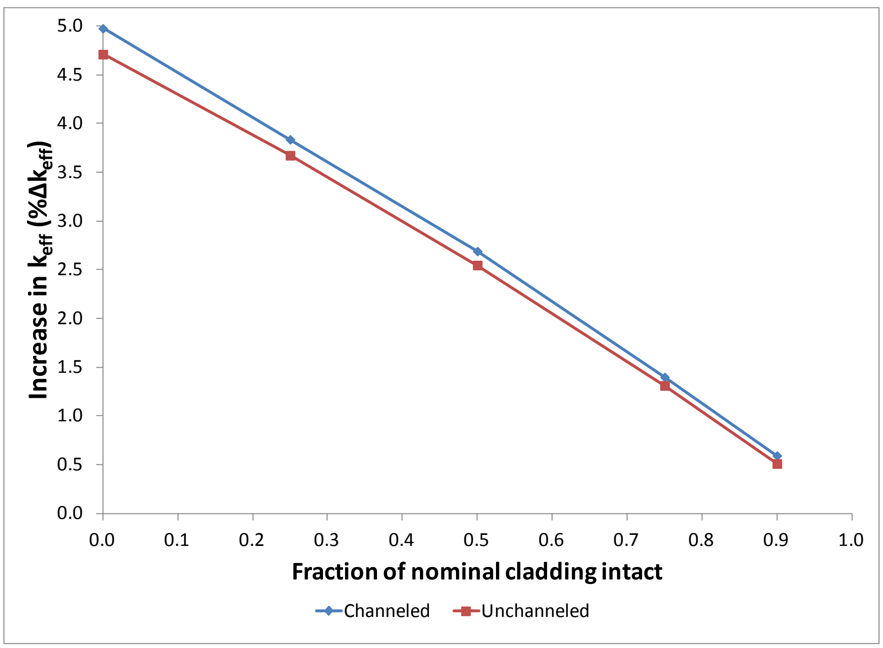

Figure 25. Increase in k_{eff} as a function of fraction of intact cladding, fresh 5 w/o fuel.

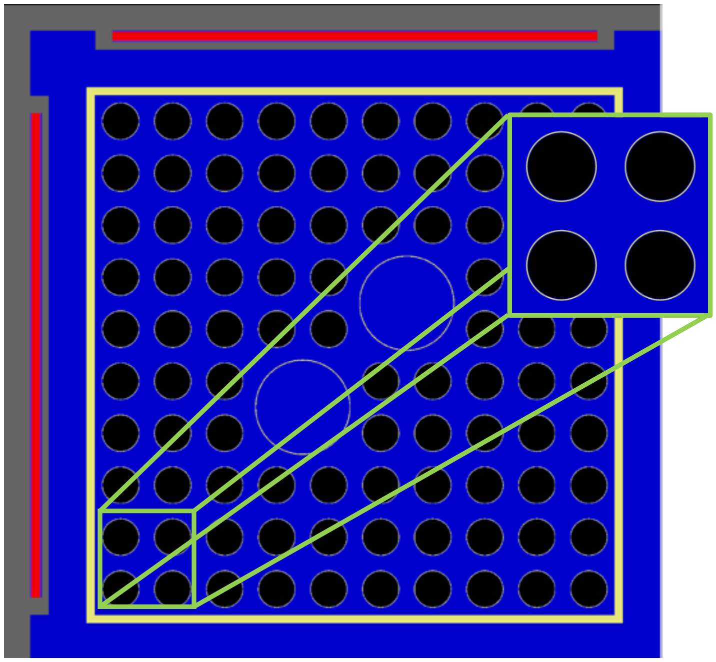

Notes: Fuel shown in black
Cladding is light grey around fuel material
Water tubes are larger, water-filled tubes
Storage cell wall and neutron absorber panel wrappers are dark grey
Neutron absorber panel is red
Fuel assembly channel yellow box around fuel rods
Water is shown in dark blue

Figure 26. Configuration with 25% nominal cladding thickness.

5.2.1.2 Rod Failures

Each of the 51 unique half-assembly symmetric rods is removed individually to determine its worth, as discussed in Section 3.1.2.1. Table 28 presents the rod locations and worth of the limiting rod location for each of the four cases. For both fuel burnups, the k_{eff} increase for the channeled fuel assembly is greater than for the unchanneled assembly. This is likely caused by the slightly harder initial spectrum when the channel is present. The increase in moderation caused by the removal of the fuel rods has a greater impact on the harder initial spectrum.

A sketch showing the half-assembly symmetry and row and column labels is provided in Figure 27. The columns in the assembly are designated with a letter, from A to J, and the rows are designated with numbers, from 1 to 10. The maximum worth is 0.29% Δkeff and is associated with rod H7 with fresh 5 w/o fuel. It should be noted that some rods have a worth that is statistically equivalent to the limiting case presented in Table 28. The worth is very small relative to the k_{eff} increases of other configurations, so further examination is not necessary.

The magnitude of the k_{eff} change caused by rod failure is somewhat less for these analyses than for the previous work documented in Ref. 7. The primary cause of the reduction is the difference in the size of the fuel rods. The fuel rods in the 10 × 10 fuel assembly have smaller diameters, so the increase in moderation is smaller for a single rod removal.

Multiple rods are removed in groups, as discussed in Section 3.1.2.2. Groups of 2, 4, 8, 12, 16, 18, and 20 rods are considered. The increase in k_{eff} is shown for each of the four cases in Table 29. Figure 28 shows the k_{eff} change as a function of rods removed for the limiting case at 35 GWd/MTU burnup and 5 years of cooling time with the fuel assembly channel. The limiting lattice is shown in Figure 29. The maximum k_{eff} value occurs for 18 rods removed and corresponds to a k_{eff} increase of 2.40% Δk_{eff}. The limiting lattice is determined with the fuel channel intact and then rerun with the fuel channel removed. In each case, the k_{eff} increase is higher with the channel intact.

The k_{eff} increase for multiple rod removal in the MPC-68 cask is about twice that reported in Ref. **7**. This is most likely due to the difference in the fuel assembly modeled in the analysis. The result for fresh fuel shown in Table 29 demonstrates that the effect of depleted fuel instead of fresh fuel is small.

Table 28. Single rod removal results for GE 10 × 10 fuel in MPC-68

Burnup (GWd/MTU)	Cooling time (years)	Channel	Location	Maximum increase in k_{eff} (% Δk_{eff})
0	0	Yes	H7	0.29
35	5		G7	0.26
0	0	No	H7	0.25
35	5		D3	0.26

Table 29. Multiple rod removal results for GE 10 × 10 fuel in MPC-68

Burnup (GWd/MTU)	Cooling time (years)	Channel	Maximum increase in k_{eff} (% Δk_{eff})
0	0	Yes	2.24
35	5		2.40
0	0	No	2.11
35	5		2.30

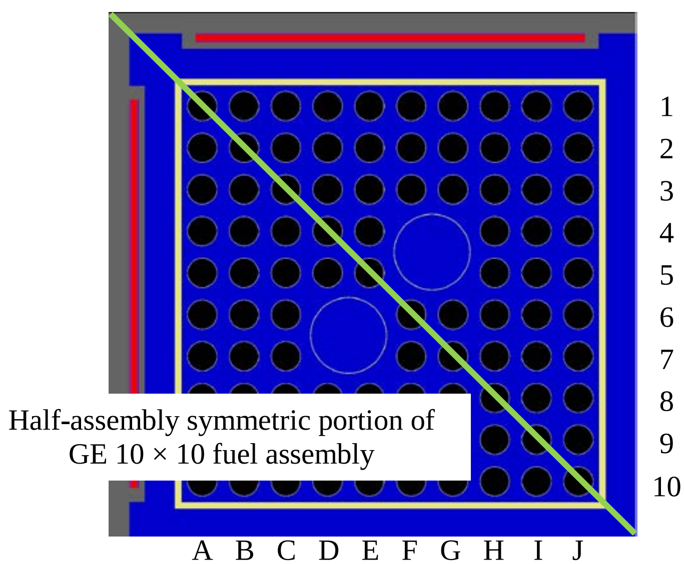

Figure 27. Sketch of symmetry, row, and column labels for GE 10 × 10 fuel assembly.

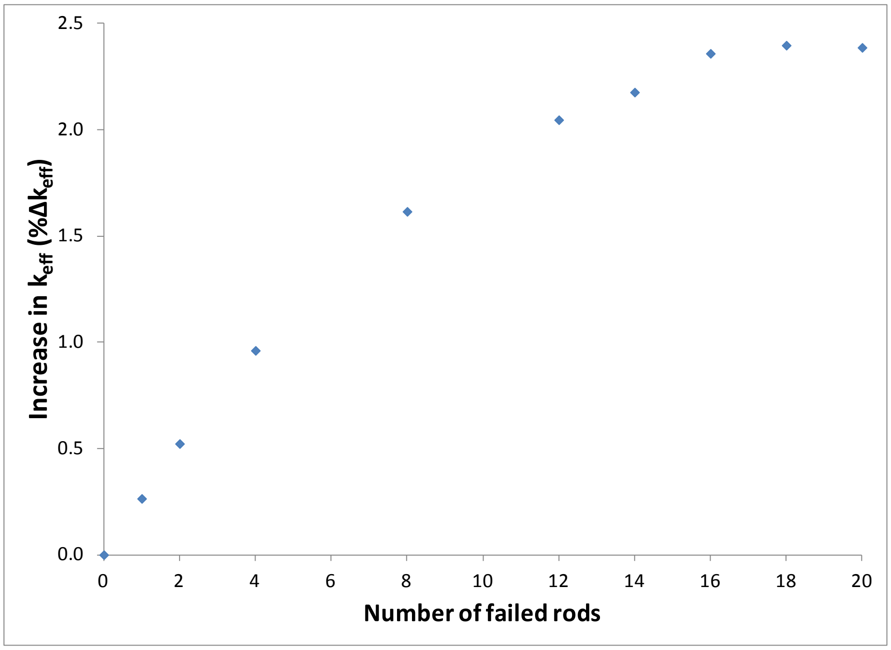

Figure 28. Increase in k_{eff} in MPC-68 as a function of number of rods removed (35 GWd/MTU burnup and 5-year cooling time).

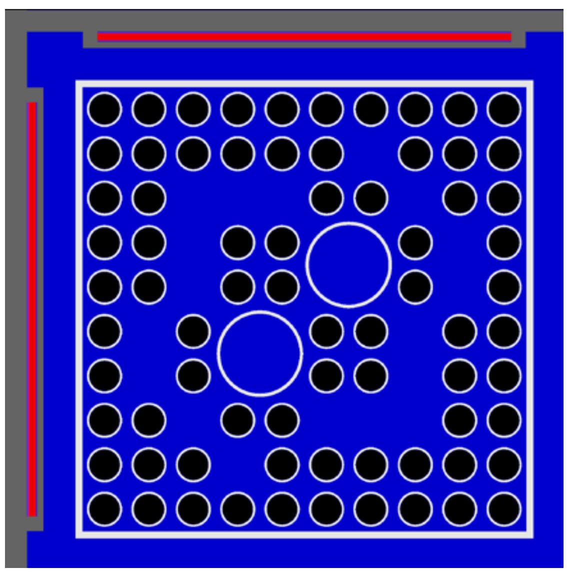

Figure 29. Limiting multiple rod removal lattice (18 rods removed).

5.2.1.3 Loss of Rod Pitch Control

The loss of rod pitch control is modeled first as a uniform increase in fuel assembly pitch, as discussed in Section 3.1.3. Two different assumptions are made about the condition of an intact fuel assembly channel. In one case, the fuel channel is assumed to expand with uniform thickness along with the fuel bundle. In this nonphysical model, the presence of the channel acts only to limit the uniform pitch increase by the thickness of the channel wall on both sides. The expansion is constrained by the contact of the assembly channel with the neutron absorber wrappers on one side and the storage cell walls on the other. The second assumption is that the fuel channel does not deform, and thus constrains the expansion of the fuel rod pitch.

The assembly is also considered with no channel present. In this condition, the constraint is provided by fuel rod contact with neutron absorber wrappers. For the unchanneled cases, the modeled expansion ends when the unit cell containing the outermost fuel rods contacts the neutron absorber wrappers and storage cell walls.

The results with and without cladding, with and without the fuel channel, are shown in Table 30. As shown in Table 25, the limiting condition is with fresh fuel. The k_{eff} increase for clad fuel restrained by an intact fuel assembly channel is 2.09% Δk_{eff}.

The limiting condition, with fresh fuel and no assembly channel, is further expanded until the outermost fuel rods are in contact with the neutron absorber wrappers and basket walls, as shown in Figure 30. This pitch is maintained even in cells with fewer than two neutron absorber panels. The resulting increase in k_{eff}, is more than 13% Δk_{eff} with cladding intact and 15.32% Δk_{eff} with cladding removed.

Fuel rod pitch is further increased in the MPC-68 model to examine the effect of nonuniform pitch, as discussed in Section 3.1.3.1 and Refs. 31 and 32. The inner portion of the assembly continues to expand until the outer rows are in contact with each other; although the fuel rod pitch is still uniform axially, it is nonuniform in the radial direction. An example model is shown in Figure 31. In the model with the largest pitch, the outermost fuel is in contact with the walls of the storage cell and the neutron absorber wrappers. The second set of fuel rods is in contact with the outermost rods. The pitch of the outermost fuel is constant within the row and is equal to the pitch that caused the pins to make contact with the basket wall. The increase in pitch in the inner portion of the assembly leads to a nonuniform pitch. The results of the calculations with increasing pitch are shown in Figure 32 as a function of the pitch of the inner, uniform portion of the assembly. The maximum total k_{eff} increase is 13.31% Δk_{eff}. The first six points represent the uniform pitch expansion. Nonuniform expansion begins when the fuel rod pitch is in excess of approximately 1.58 cm. The additional k_{eff} increase beyond the uniform expansion case is 0.15% Δk_{eff}, indicating that further expansion is a minor effect. The additional k_{eff} impact caused by nonuniform expansion is consistent with Refs. 31 and 32.

The limiting case for the MPC-68 cask contains fresh fuel, so the most reactive axial portion of the assembly is the center. For that reason, the birdcaging analysis, described in Section 3.1.3.2, includes two compressed pitch sections, each 30.48 cm in length, symmetrically positioned above and below the mid-plane of the assembly. A range of center section lengths is considered, but no k_{eff} increase is observed in any case containing the compressed pitch sections. One birdcaging configuration is shown in Figure 33. Birdcaging does not cause any additional k_{eff} increase beyond 13.16% k_{eff} associated with the uniform pitch expansion configuration for fresh fuel in the MPC-68 cask.

The results presented here show a larger increase in k_{eff} than that reported in Ref. 7. This is probably a result of the different fuel assembly lattice. Figure 21 in Ref. 7 indicates that the reactivity consequence of uniform pitch expansion increases with the array size. The effects of the different fuel rod and water rod diameters in the 10 × 10 fuel are not accounted for in Ref. 7, however, so it is possible that these factors also influence the difference between the two analyses.

Table 30. Results for loss of rod pitch control in MPC-68, no channel restraint

Burnup (GWd/MTU)	Cooling time (years)	Channel	Maximum increase in k_{eff} (% Δk_{eff})
Cladding intact			
0	0	Yes	11.00
35	5		9.55
0	0	No	12.07
35	5		10.56
Cladding removed			
0	0	Yes	14.05
35	5		12.74
0	0	No	14.70
35	5		13.30

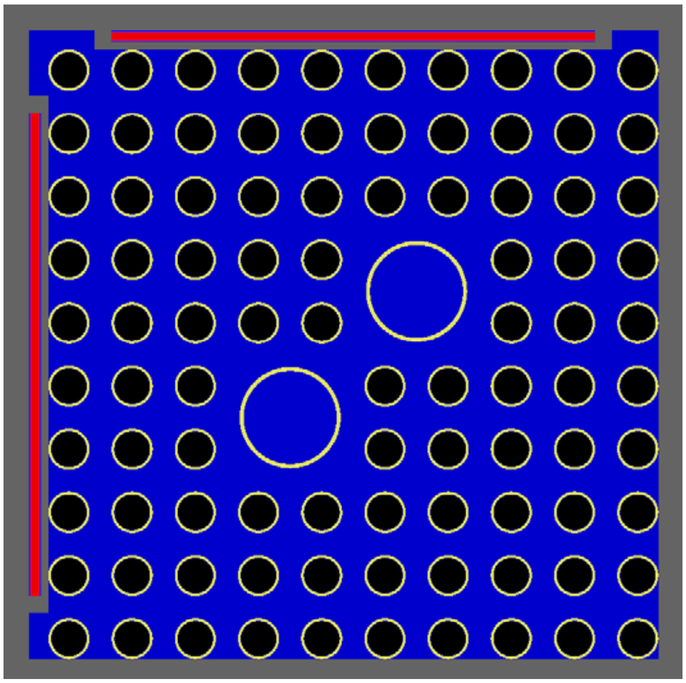

Figure 30. Maximum uniform pitch expansion configuration in MPC-68.

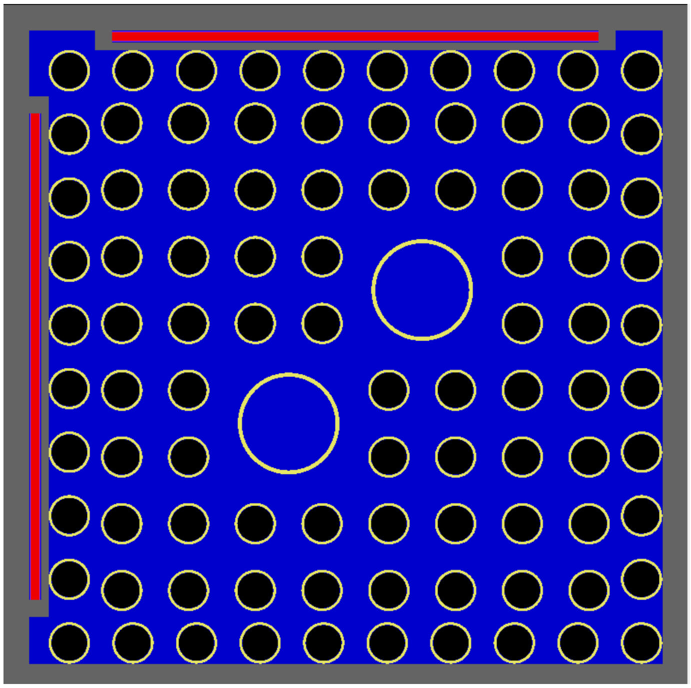

Figure 31. Example nonuniform pitch model for MPC-68.

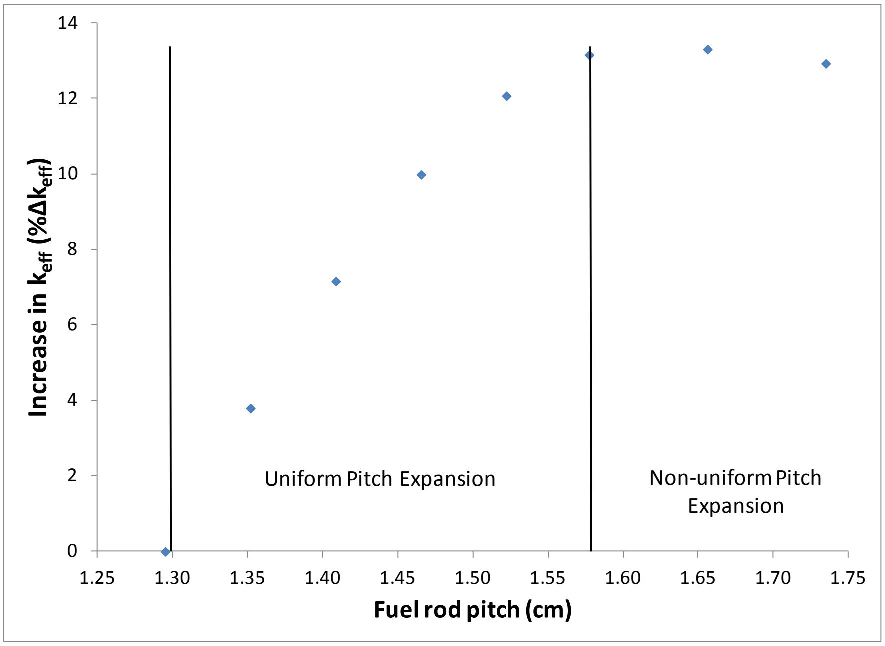

Figure 32. Increase in k_{eff} in MPC-68 as a function of fuel rod pitch, fresh 5 w/o fuel.

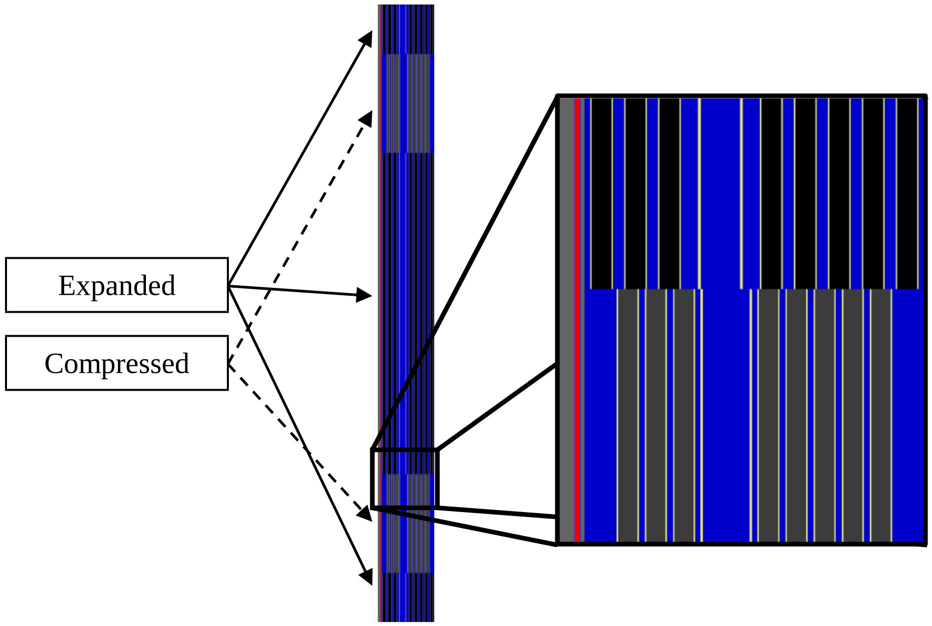

Notes: Expanded section fuel is shown in black
Compressed section fuel is shown in grey
All fuel has the same isotopic composition
The gaps just to the left of the center of the zoomed portion are water tubes

Figure 33. A fresh fuel birdcaging configuration for MPC-68.

5.2.1.4 Loss of Assembly Position Control

The loss of assembly position control configuration is calculated over a range of displacements. The consequence of the maximum misalignment for both fresh and irradiated fuel, both with and without the assembly channel, is shown in Table 31 and is almost 20% Δk_{eff} for the limiting condition. A more limited misalignment case (20 cm) is also evaluated as a surrogate for potential degradation of assembly end fittings or the spacers used inside the cask to ensure proper assembly alignment. The consequences of this more limited misalignment, shown in Figure 34 and Table 31, are significantly less, but the k_{eff} increase is still over 6% Δk_{eff}. The limiting condition for both the maximum and limited misalignment is for fuel with 35 GWd/MTU burnup and 5 years of cooling time. The limited misalignment case is illustrated in Figure 34. Misalignment toward the bottom of the cask causes a significantly smaller k_{eff} increase because the fuel at the bottom end of the assembly has lower reactivity. The misalignment toward the cask base plate also differs for the MPC-68 compared to the GBC-32. The MPC-68 model has more distance below the fuel, so larger misalignments are possible. The neutron absorber in the MPC-68 extends below the bottom of the fuel; this difference acts to increase the displacement distance for which no significant change in k_{eff} occurs. The variation of the k_{eff} changes as a function of axial position is shown in Figure 35 for fuel with 35 GWd/MTU burnup and 5 years of cooling time.

Table 31. Increase in k_{eff} caused by loss of assembly position control in MPC-68

Burnup (GWd/MTU)	Cooling time (years)	Channel	Increase in k_{eff} (% Δk_{eff})
Maximum displacement (33.78 cm displacement relative to basket)			
0	0	Yes	8.18
35	5		19.40
0	0	No	7.79
35	5		18.65
Limited displacement (20 cm displacement relative to basket)			
0	0	Yes	0.33
35	5		6.29
0	0	No	0.27
35	5		6.07

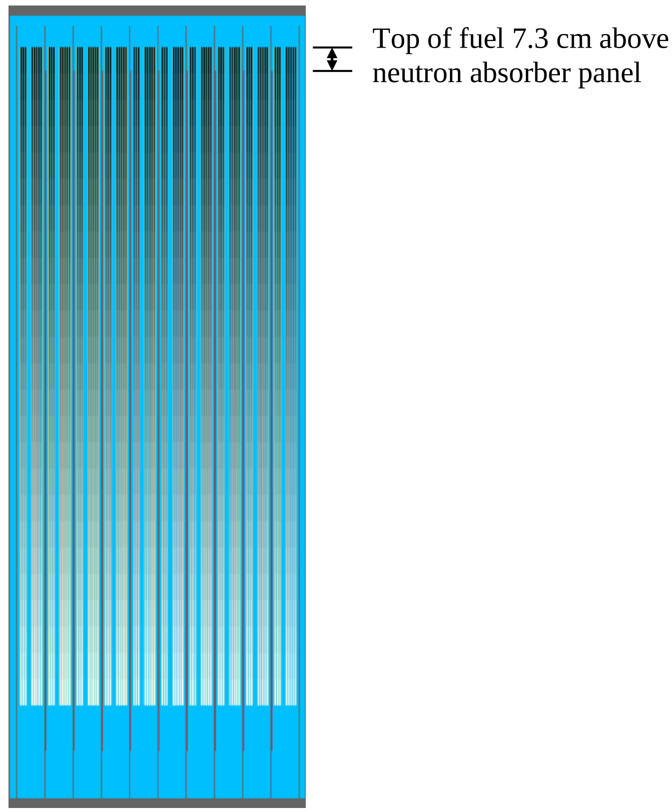

Figure 34. Limited axial misalignment of 20 cm toward cask lid.

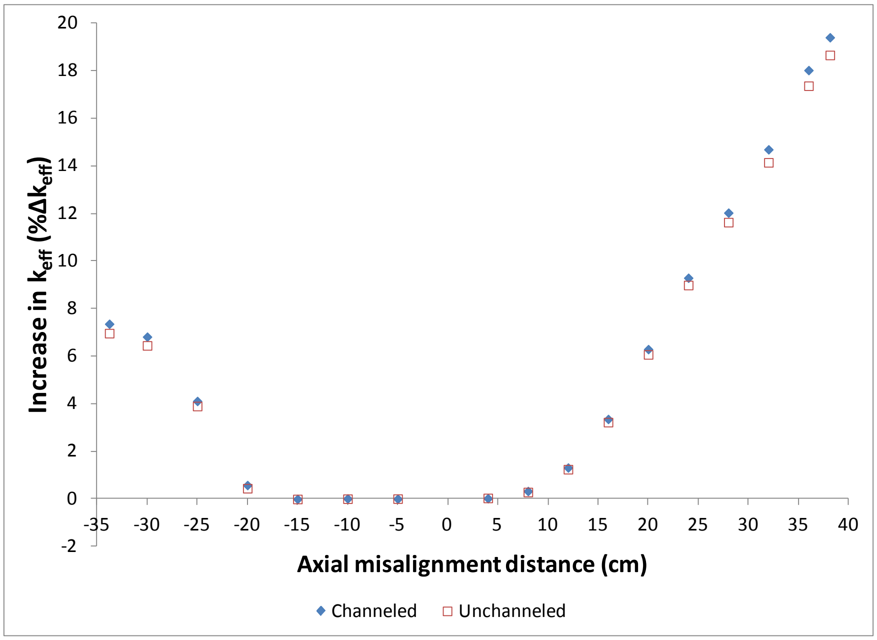

Figure 35. Increase in k_{eff} in MPC-68 as a function of assembly axial displacement (35 GWd/MTU burnup and 5-year cooling time).

5.2.1.5 Gross Assembly Failure

The two gross assembly failure configurations described in Section 3.1.5 are investigated in the MPC-68 cask. Axial representations of the most reactive homogeneous rubble and ordered pellet array configurations are shown in Figure 36 and , respectively. In both cases, the limiting case is the non-physical condition in which the fissile material extends from the base plate to the lid. As expected, this configuration has the highest k_{eff} increase, with the ordered pellet array configuration being more limiting than the homogeneous rubble case. As shown previously in Table 25, the k_{eff} increase in the homogeneous rubble case is almost 30% Δk_{eff}, and the pellet array case increases k_{eff} by over 34% Δk_{eff} for the maximum increase case. The limiting case for both configurations is with fuel at 35 GWd/MTU burnup and a 5-year cooling time. The results for the maximum k_{eff} increase homogeneous configuration for both fuel burnups with and without the fuel channel are presented in Table 32 and for the pellet array case for both fuel burnups in Table 33. The pellet array case was only considered without the fuel assembly channel. If the fissile material is maintained within the poison panel elevations, the resulting change in k_{eff} is reduced to 17.21% Δk_{eff} for the ordered array of pellets. Results for a range of homogeneous rubble cases within the neutron absorber elevations are provided in Table 34. The largest increase in k_{eff} for this configuration corresponds to fresh 5 w/o fuel. The results with fissile material restrained in the neutron absorber elevations demonstrate that these cases result in significantly lower k_{eff} increases than the unrestrained material cases.

The results for the pellet array case are significantly higher than those reported previously in Ref. 7. There are two differences between that analysis and this one, both of which contribute to the increased magnitude of the k_{eff} increase in the work presented here. The pellet array case modeled here includes a distributed burnup profile in the pellet array, and the array is allowed to extend beyond the neutron absorber panel elevations. This latter change is the larger of the two effects, but the former change is also important. The homogeneous rubble case is not included in Ref. 7.

Table 32. Increase in k_{eff} for homogeneous rubble configuration of gross fuel assembly failure in MPC-68

Burnup (GWd/MTU)	Cooling time (years)	Channel	Maximum increase in k_{eff} (% Δk_{eff})
0	0	Yes	21.68
35	5		28.58
0	0	No	22.90
35	5		29.36

Table 33. Increase in k_{eff} for pellet array configuration of gross fuel assembly failure in MPC-68

Burnup (GWd/MTU)	Cooling time (years)	Maximum increase in k_{eff} (% Δk_{eff})
Channel removed		
0	0	28.12
35	5	34.40

Table 34. Increase in k_{eff} in MPC-68 due to homogeneous rubble, debris within absorber Elevations, fresh 5 w/o fuel

Fraction of nominal assembly height	Increase in k_{eff} (% Δk_{eff})	
	Channeled	**Unchanneled**
1.0	7.40	9.49
0.9	6.65	9.12
0.8	5.06	8.10
0.7	2.30	6.16
0.6	-2.57	2.66
0.5	-11.07	-3.62
0.4	-25.64	-15.10
Fully compressed rubble*	-34.23	-31.44

*The fraction of nominal assembly height varies for fully compressed rubble with and without the channel. With the channel it is approximately 0.36 with the channel and 0.32 without it.

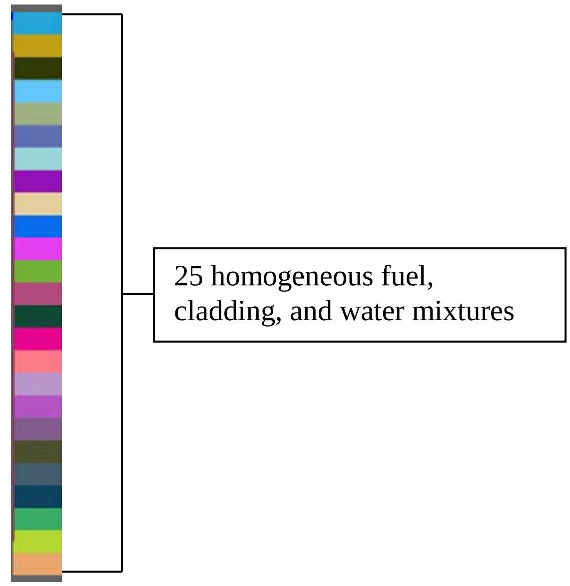

Figure 36. Limiting homogeneous rubble configuration in MPC-68.

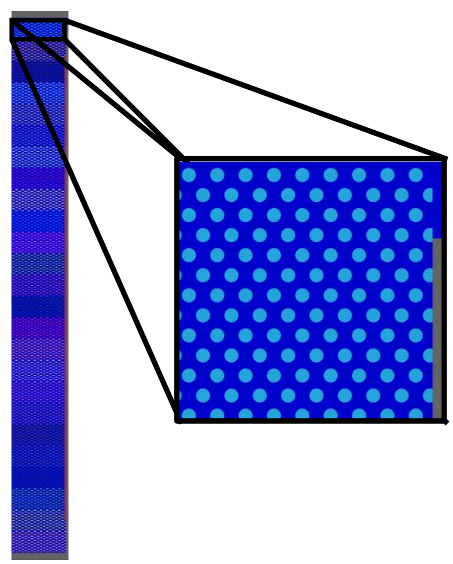

Figure 37. Limiting ordered pellet array configuration for MPC-68.

5.2.1.6 Neutron Absorber Degradation

The results of the calculations, described in Section 3.1.6.1, considering a 5-cm neutron absorber defect at varying elevations for both fuel burnups, both with and without the fuel channel, are presented in Table 35. The limiting condition is for fuel with 35 GWd/MTU burnup and 5 years of cooling time, with the fuel channel intact. As expected, the limiting elevation is near the top of the active fuel height, as shown in Figure 38. The results for the full range of elevations considered in the limiting fuel condition are presented in Table 36 for cases with the fuel channel intact. As expected, the limiting elevation for the fresh 5 w/o fuel is located at the centerline. The largest k_{eff} increase observed for this configuration is 2.49% Δk_{eff} and increases to 5.62% Δk_{eff} if the defect size is increased to 10 cm. As discussed in

Section 3, these defects are assumed to be present at the same elevation in all neutron absorber panels within the cask.

The increase in k_{eff} associated with uniform neutron absorber panel thinning as discussed in Section 3.1.6.3 is shown in Table 37 and Figure 39 with fresh 5 w/o fuel modeled in the MPC-68 cask. The absorber thinning results shown in Appendix C confirm that the fresh fuel case is most limiting. As shown previously in Table 25, a 50% reduction in thickness results in a 3.67% Δk_{eff} increase. Complete neutron absorber panel removal increases k_{eff} by almost 22% Δk_{eff}, but more than 40% of the thickness must be removed before an increase of more than 3% Δk_{eff} is realized.

The complete removal of the neutron absorber panels causes a larger increase in k_{eff} than the maximum axial displacement case discussed in Section 5.2.1.4, a result which differs from that observed for the GBC-32 cask presented in Section 5.1. The MPC-68 cask has a smaller distance between the top of the fuel storage basket and the cask lid, allowing for only a shorter portion of the assembly to be above the basket walls. The MPC-68 also has a higher nominal neutron absorber loading, resulting in a larger increase in k_{eff} when all the absorber is removed. These two differences in cask design cause the relative consequence of the two configurations to be different for the MPC-68 compared to the GBC-32.

Table 35. Maximum k_{eff} increase caused by a 5-cm neutron absorber defect in MPC-68

Burnup (GWd/MTU)	Cooling time (years)	Defect center elevation (cm)	Channel	Maximum increase in k_{eff} (% Δk_{eff})
0	0	190.50	Yes	0.83
35	5	365.13		2.49
0	0	190.50	No	0.77
35	5	365.13		2.41

Table 36. Increase in k_{eff} caused by a 5-cm neutron absorber defect at various elevations in MPC-68 (35 GWd/MTU burnup and 5-year cooling time)

Defect center elevation (cm)	Increase in k_{eff} (% Δk_{eff})
0.00	-0.02
95.25	-0.01
190.50	0.00
285.75	0.01
317.50	0.21
333.38	0.52
349.25	1.43
354.54	1.83
359.83	2.29
365.13	2.49
370.42	2.39
375.71	2.00
381.00	0.69

Table 37. Increase in k_{eff} in MPC-68 caused by uniform neutron absorber panel thinning, fresh 5 w/o fuel

Fraction of neutron absorber panel thickness remaining	Increase in k_{eff} (%Δk_{eff})
0.9	0.59
0.8	1.21
0.7	1.91
0.6	2.72
0.5	3.67
0.4	4.87
0.3	6.35
0.2	8.49
0.1	11.93
0.0	21.84

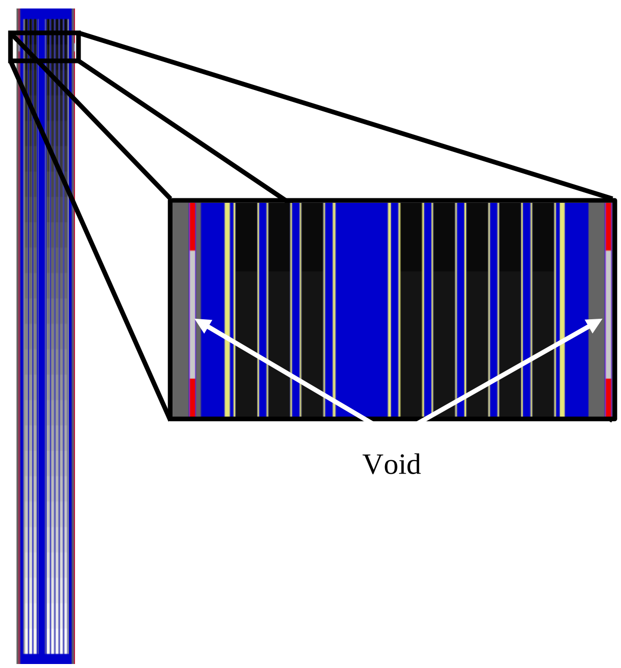

Figure 38. Limiting neutron absorber defect configuration in MPC-68.

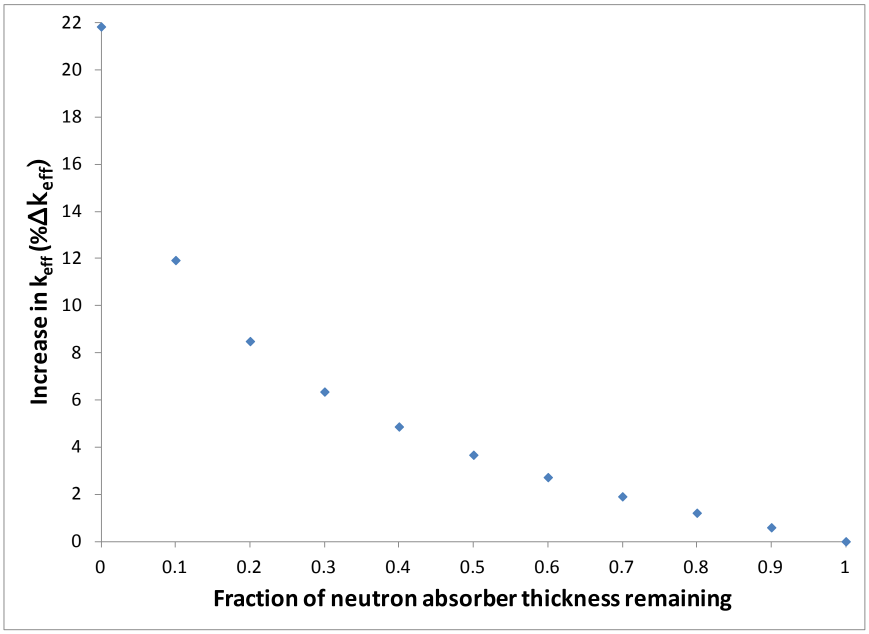

Figure 39. Increase in k_{eff} in MPC-68 as a function of remaining neutron absorber panel thickness for fresh 5 w/o fuel.

5.2.1.7 Burnup and Cooling Time Sensitivities

The results of sensitivity studies relating to addition burnup and cooling time are presented in Appendix C (Section C.2). Each configuration discussed in the previous six subsections is considered explicitly. The results of the calculations for additional burnup and cooling time conditions indicate that the increase in k_{eff} reported for each configuration encompass changes that may result for additional burnups and cooling times. That is, the differences in the change in k_{eff} are smaller than the changes in the base case k_{eff} caused by the additional burnup and/or cooling time considered. For the axial displacement configuration, a high-burnup and cooling time condition causes a larger increase in k_{eff}, but that case is significantly subcritical and therefore can be excluded from the results considered here.

5.2.2 Varying Number of Reconfigured Assemblies

The results presented in Section 5.2.1 and Table 25 assume that all 68 fuel assemblies in the MPC-68 cask experience the same fuel or neutron absorber reconfiguration within the respective configuration of interest. As discussed in Section 3.2, a series of calculations is performed to establish the k_{eff} increase as a function of the number of reconfigured assemblies within the cask. The four configurations considered are the limiting conditions for single rod failure, multiple rod failure, uniform rod pitch increase, and homogeneous rubble resulting from gross assembly failure.

The first fuel assembly to experience the reconfiguration being examined is selected in an attempt to maximize the k_{eff} increase, and is therefore one near the center of the cask. Additional assemblies are added in mostly symmetric groups of equal distance from the first reconfigured assembly. For some low numbers of reconfigured assemblies, multiple combinations of assemblies are considered. Sixteen combinations of reconfigured assemblies are considered in the MPC-68. One order in which the assemblies experience reconfiguration is shown in Figure 40. Results are presented in the following subsections.

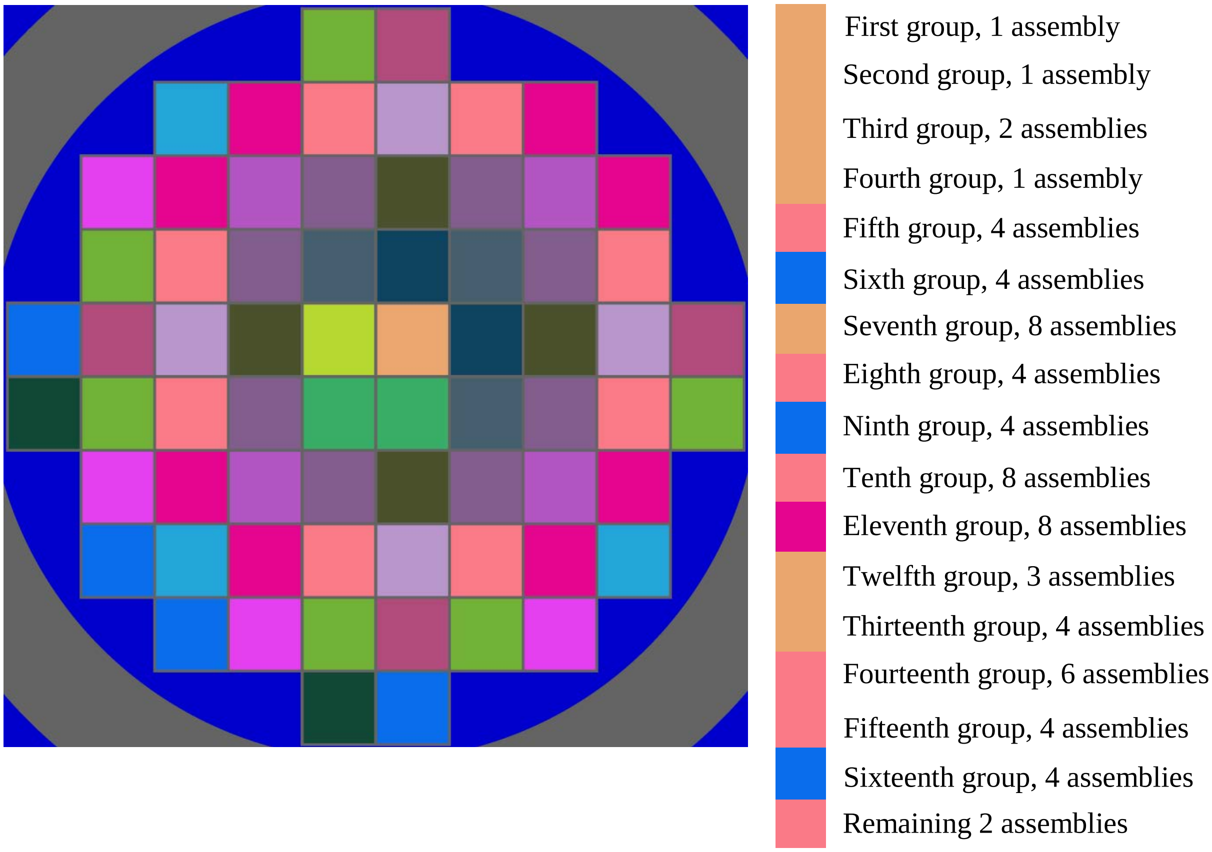

Figure 40. One order of assembly reconfiguration in MPC-68 partial degradation configurations.

5.2.2.1 Rod Failures

The single and multiple rod failure configurations that result in the largest increase in k_{eff}, as discussed in Section 5.2.1.2, are used to study the impact of some assemblies suffering reconfiguration while others in the cask remain intact. The single rod failure configurations are based on fresh 5 w/o fuel, while the multiple rod failure configurations are based on fuel depleted to 35 GWd/MTU and 5 years of cooling time. The fuel channel is modeled as intact for both rod failure configurations. The results for single rod failure are shown below in Table 38 and Figure 41. The results for multiple rod failure are shown below in Table 39 and Figure 42. The portion of the k_{eff} impact introduced by each group of assemblies for both rod failure configurations show nearly 50% or more of the k_{eff} change coming after 13 assemblies experience reconfiguration and approximately 75% to 80% of the k_{eff} change caused by the first 29 assembly reconfigurations. The Monte Carlo uncertainty is relatively large compared to the k_{eff} changes being examined in this series of calculations because of the relative insensitivity of the cask k_{eff} to single rod failures. The resulting k_{eff} increase is therefore not a smooth function. The single rod failure results are generally similar to the GBC-32 results presented in Section 5.1.2.1. The rate of increase in k_{eff} seems to be slightly slower for the MPC-68, but this is a relatively small difference in the trend and may be related to the relatively large uncertainties in the results compared to the k_{eff} changes being examined. The multiple rod failure results for the MPC-68 are very similar to the GBC-32 results. The results indicate that a reduced number of reconfigured assemblies will not significantly reduce the k_{eff} increase associated with fuel reconfiguration if the degraded assemblies are in close proximity, and particularly if they are in the center region of the cask.

Table 38. Increase in k_{eff} in MPC-68, single rod failure fresh 5 w/o fuel

Number of degraded assemblies	Increase in k_{eff} (% Δk_{eff})
1	0.02
2	0.04
2	0.05
4	0.06
5	0.07
9	0.10
13	0.15
21	0.20
25	0.19
29	0.21
37	0.23
45	0.27
48	0.25
52	0.27
58	0.27
62	0.27
66	0.28
68	0.29

Table 39. Increase in k_{eff} in MPC-68, multiple rod failure (5 w/o initial enrichment, 35 GWd/MTU burnup)

Number of degraded assemblies	Increase in k_{eff} (% Δk_{eff})
1	0.11
2	0.21
2	0.23
4	0.45
5	0.56
5	0.55
9	0.93
13	1.19
21	1.62
25	1.79
29	1.89
37	2.10
45	2.22
48	2.26
52	2.28
58	2.33
62	2.36
66	2.37
68	2.40

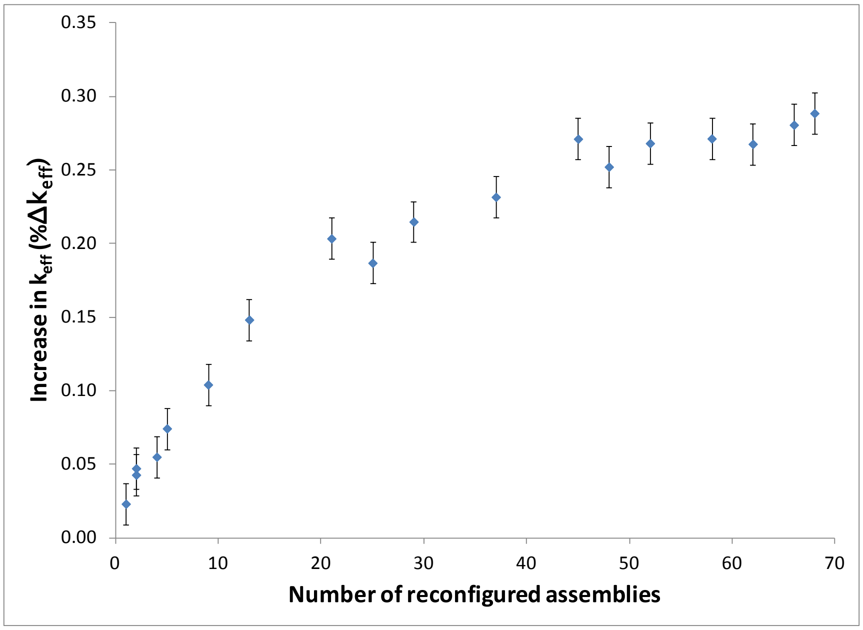

Figure 41. Increase in k_{eff} in MPC-68 as a function of number of reconfigured assemblies, single rod failure for fresh 5 w/o fuel.

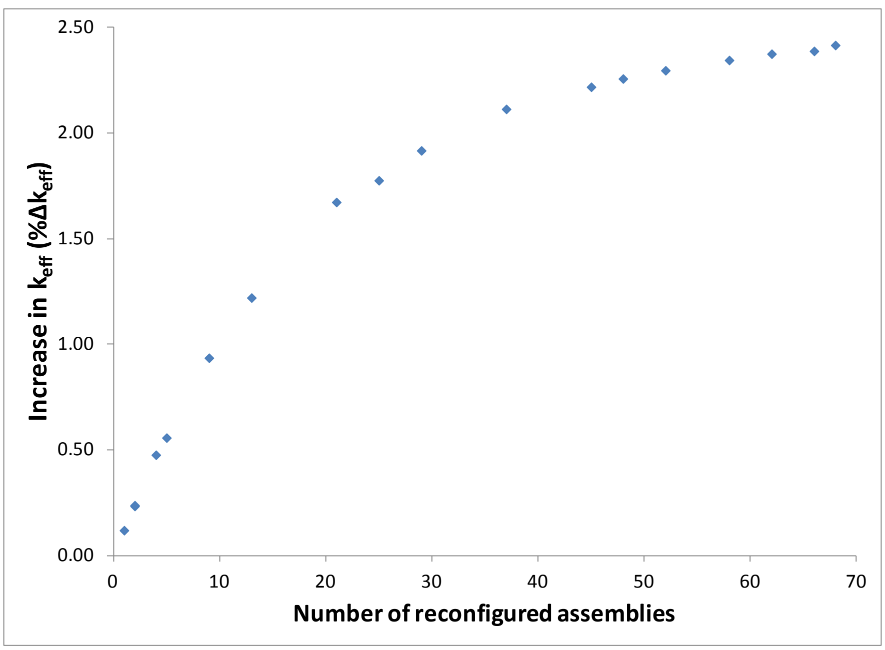

Figure 42. Increase in k_{eff} in MPC-68 as a function of number of reconfigured assemblies, multiple rod failure (35 GWd/MTU burnup and 5-year cooling time).

5.2.2.2 Loss of Rod Pitch Control, Uniform Pitch Increase

The maximum uniform pitch increase case is used to examine the k_{eff} impact of varying the number of assemblies that have experienced reconfiguration. The assembly configuration used for this study models

the outer row of fuel rods in contact with the inner wall of the fuel storage basket in each cell. The fresh 5 w/o fuel composition is used for all assemblies. The increase in k_{eff} for each number of reconfigured assemblies is provided in Table 40 as well as Figure 43. More than 75% of the increase in k_{eff} is caused by the first 21 reconfigured assemblies. The general trend in the k_{eff} change for the uniform pitch increase cases is similar to that for single and multiple rod failure configurations presented in Section 5.2.2.1. More than 50% of the total increase in k_{eff} has occurred with 13 reconfigured assemblies. The shape of the increase in k_{eff} as a function of reconfigured assemblies is similar to that seen for the uniform pitch increase configurations in the GBC-32 cask, as discussed in Section 5.1.2.2. The fraction of the k_{eff} increase introduced for a given fraction of reconfigured assemblies is slightly higher for the MPC-68 than for GBC-32 between about 10% and 70% of the assemblies experiencing reconfiguration. The results indicate that a reduced number of reconfigured assemblies will not significantly reduce the k_{eff} increase associated with fuel reconfiguration if the degraded assemblies are in close proximity, and particularly if they are in the center region of the cask.

Table 40. Increase in k_{eff} in MPC-68, uniform pitch increase fresh 5 w/o fuel

Number of degraded assemblies	Increase in k_{eff} (% Δk_{eff})
1	0.64
2	1.46
2	1.37
4	3.29
5	3.93
5	3.85
9	6.45
13	7.85
21	10.05
25	10.59
29	11.02
37	11.85
45	12.36
48	12.46
52	12.61
58	12.87
62	13.03
66	13.13
68	13.16

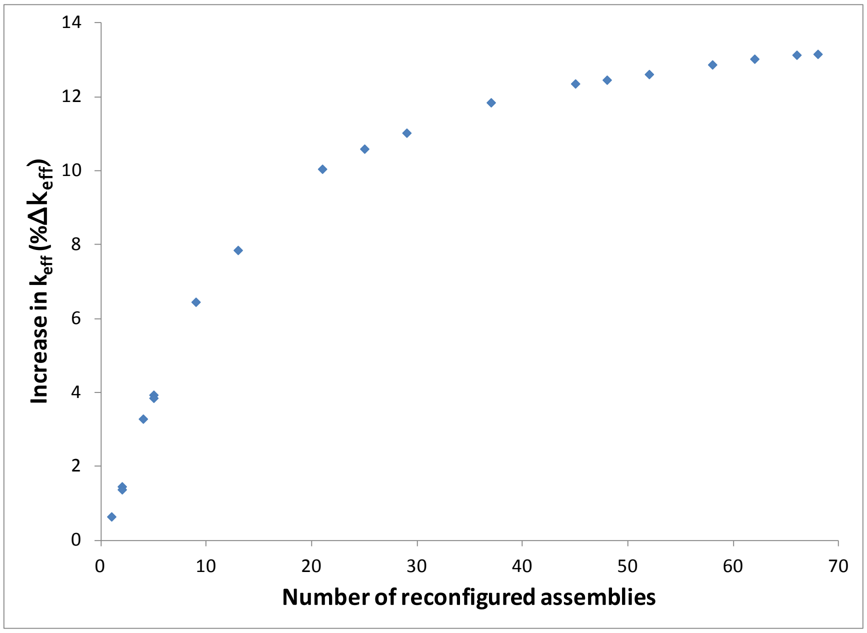

Figure 43. Increase in k_{eff} in MPC-68 as a function of number of reconfigured assemblies, uniform pitch increase fresh 5 w/o fuel.

5.2.2.3 Gross Assembly Failure, Homogeneous Rubble

The homogeneous rubble modeling of the gross assembly failure configuration is the final configuration used to examine the k_{eff} impact of varying the number of assemblies that have experienced reconfiguration. The configuration used for this study fills the entire inside volume of the storage cell with homogeneous rubble, as described in Section 3.1.5.1. Each zone is approximately 18 cm tall; thus, the 25 zones fill the cask from the base plate to the lid. The fuel composition corresponds to 5 w/o fuel depleted to 35 GWd/MTU. This configuration resulted in the largest k_{eff} increase of the homogeneous rubble configurations used in Section 5.2.1.5. The increase in k_{eff} for each number of reconfigured assemblies is provided in Table 41 as well as Figure 44. The first two reconfigured assemblies cause a smaller increase in k_{eff} than the other configurations. A more significant increase in k_{eff} is noted for four or more reconfigured assemblies. More than 50% of the increase is caused by the first nine reconfigured assemblies, and more than 80% of the total k_{eff} increase results from the reconfiguration of 21 assemblies. The results indicate that a reduced number of reconfigured assemblies will not significantly reduce the k_{eff} increase associated with fuel reconfiguration if the degraded assemblies are in close proximity, and particularly if they are in the center region of the cask.

Table 41. Increase in k_{eff}, homogeneous rubble configuration of gross assembly failure

Number of degraded assemblies	Increase in k_{eff} (% Δk_{eff})
1	0.03
2	0.10
4	4.48
5	5.04
9	15.67
13	18.60
21	23.73
25	24.78
29	25.42
37	27.05
45	27.97
48	28.14
52	28.35
58	28.82
62	29.10
66	29.26
68	29.36

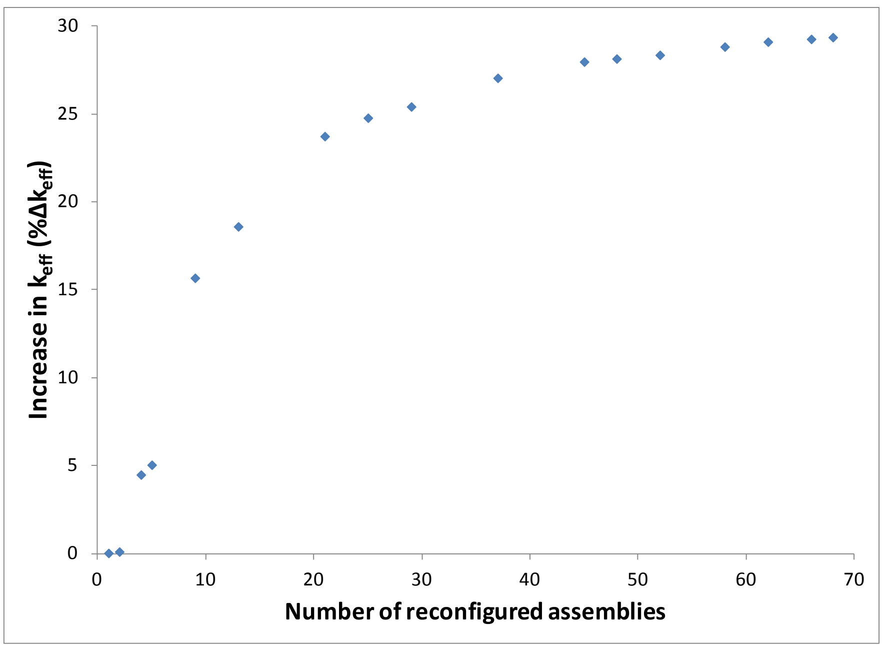

Figure 44. Increase in k_{eff} as a function of number of reconfigured assemblies, gross assembly failure (35 GWd/MTU burnup and 5-year cooling time).

Random Assembly Reconfiguration

A series of 25 calculations is performed in which four assemblies are randomly selected to experience reconfiguration into the limiting homogeneous rubble configuration. These calculations use fuel compositions for fuel with a burnup of 70 GWd/MTU and 300-year cooling time. These compositions are used in the sensitivity studies for higher burnup and cooling times and lead to the largest increase in k_{eff} for all burnup and cooling time combinations considered. The increase in k_{eff} for four reconfigured assemblies in the center of the cask is 6.95% Δk_{eff}. The use of four assemblies is somewhat arbitrary but is selected because the increase in k_{eff} is significant. The increase in k_{eff} for each randomly generated case is provided in Table 42. A histogram of the results with a superimposed normal distribution is shown in Figure 45. While some deviations from the ideal normal distribution are evident, the set of k_{eff} increases tests as normal with a 10 bin chi-squared normality test.

The average change in k_{eff} is a reduction of about 0.20% Δk_{eff}, and the standard deviation is approximately 0.25% Δk_{eff}. The largest increase in k_{eff} is 0.14 Δk_{eff}. The one-sided tolerance factor for 95% probability of a 95% confidence interval assuming a normal distribution of 25 samples is 2.292, from Ref. 49. The 95/95 upper bound for the reactivity increase for four random assemblies is 0.37%. This represents a significant reduction in the k_{eff} impact compared to the bounding condition of four reconfigured assemblies in the center of the cask. These results are based on only a cursory examination of the effects of random assembly selection, but the results indicate a significant reduction in the k_{eff} if the reconfigured assemblies are randomly distributed in the cask.

Random sampling of degraded assemblies will not be valid if assembly degradation is not random. Factors such as environment during ES, assembly burnup and fluence, or other relevant parameters could be highly correlated, invalidating a random sampling approach. The difference between random sampling and deterministic selection of assembly locations will be reduced with a larger number of reconfigured assemblies. More study is needed to examine the validity of random sampling as an alternative to deterministic selection to reduce the impact of fuel reconfiguration on k_{eff}.

Table 42. Increase in k_{eff} for 25 realizations of four randomly selected reconfigured assemblies

Increase in k_{eff} (%Δk_{eff})				
-0.02	0.14	-0.04	0.13	-0.33
-0.19	0.09	-0.29	-0.13	-0.19
0.04	-0.75	-0.47	-0.66	-0.38
-0.06	-0.23	-0.19	-0.02	-0.22
-0.01	-0.03	-0.73	-0.13	-0.37

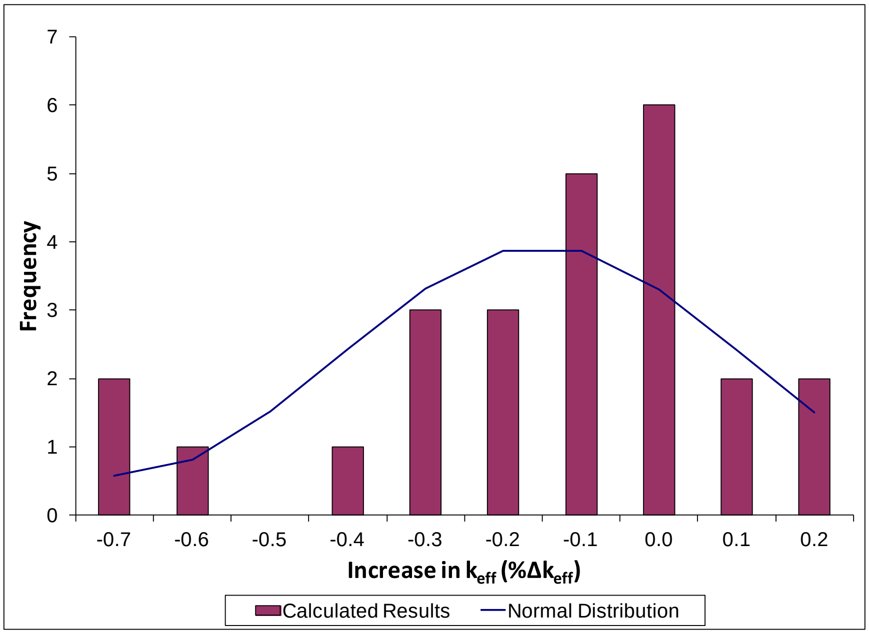

Figure 45. Histogram of increases in k_{eff} for 25 random samples of four reconfigured assemblies.

5.2.3 Combined Configurations

As discussed in Section 3.3, some of the mechanisms that could result in fuel reconfigurations could result in a combination of configurations. Therefore, selected combined configurations are evaluated, including: four failed rods with 50% clad thinning and four failed rods with a uniform pitch increase of 0.062-cm. These combinations of configurations are selected as they both pertain to failure of zirconium alloy components of the fuel assembly. Both combined configurations assume fresh 5 w/o fuel and an intact fuel assembly channel.

The multiple rod failure results presented in Section 5.2.1.2 indicate that the failure of four fuel rods results in an increase in k_{eff} of just under 1% Δk_{eff}. This is approximately 40% of the maximum increase for multiple failed rod configurations and is therefore selected as an intermediate configuration. The cladding thickness on all intact rods in both combined configurations is represented with 50% of the nominal thickness. The pitch increase of 0.062 cm is approximately 4.3% Δk_{eff}. This represents about one-third of the maximum k_{eff} increase associated with the uniform pitch expansion.

The results of the two combined configurations considered in the MPC-68 cask are presented in Table 43. For comparison, the k_{eff} increases assuming each degraded configuration separately and the sum of the two is provided. The increase in k_{eff} associated with explicit modeling of the combined configuration is less than the estimated increase based on summing the individual increases. The conservatism of adding the separate effects is 0.25% Δk_{eff} or less. It appears that the linear combination of the k_{eff} increases is conservative, but more combined configurations would need to be investigated prior to drawing general conclusions. If it is confirmed, the k_{eff} increase caused by combinations of degradations could be conservatively bounded by adding the increase associated with individual configurations where applicable.

Table 43. Increase in k_{eff} in combined configurations in MPC-68

Case	Increase in k_{eff} (% Δk_{eff})
Multiple failed rods and clad thinning	
Four failed rods	0.98
50% clad thinning	2.69
Sum of k_{eff} increases	3.67
Combined configuration model	3.75
Overestimation of k_{eff} increase by summing individual effects	0.08
Multiple failed rods and 0.062-cm increase in fuel rod pitch	
Four failed rods	0.98
Uniform pitch increase	4.35
Sum of k_{eff} increases	5.33
Combined configuration model	5.08
Overestimation of k_{eff} increase by summing individual effects	0.25

5.2.4 Part-Length Fuel

Part-length rods are common in BWR assembly designs, including the GE14 design, making an investigation of the impact of part-length rods prudent as a part of these analyses. A total of 14 of the 92 rods are modeled as part-length, and more details of the modeling are provided in Appendix A. Only fresh 5 w/o fuel is considered for the part-length rod studies because no axial burnup profiles are available for fuel assemblies with part-length rods. The removal of some of the fuel in the upper portion of the assembly might cause a more bottom-skewed power shape, but the remaining sparser lattice will likely be more reactive. The axial power shape could therefore also be about the same or even more top-skewed than that developed in Appendix E. Given the unknown relative impact of these effects, depleted fuel is not considered in this study.

Most of the degraded fuel and neutron absorber panel configurations are considered for part-length fuel, though not all. The multiple rod failure study is shortened with the results compared to the full-length results presented in Section 5.2.1.2, and the pellet array configuration of gross assembly failure is not considered at all. Other calculations, such as the axial misalignment configuration, are reduced to the conditions shown to be limiting for full-length fuel in Section 5.2.1. The results of the nominal cases without reconfiguration are shown in Table 44. It should be noted that the base case k_{eff} values for the fuel with part-length rods are approximately 0.7% Δk_{eff} higher than the full-length rod base case. The additional moderation introduced in the upper portion of the assembly by the removal of the upper sections of the part-length rods is responsible for this increase in k_{eff}, and this in itself is a significant result. Only assemblies with full-length fuel rods were used in the analysis documented in Ref. 7. The use of part-length rods is thus another area of expansion over the previous work.

A summary of the k_{eff} impact of the configurations modeled with fresh fuel with part-length rods is shown in Table 45. These results can be compared with those shown in Table 25 to demonstrate the relative impact of reconfiguration for assemblies with part-length rods. In general, it appears that the part-length rods reduce the impact of reconfiguration. This result makes sense as the removal of some fissile material will move the moderator-to-fuel ratio closer to optimum in the base configuration. The neutron absorber defect and limited axial misalignment cases are the only configurations that cause a larger increase in k_{eff} than the full-length assembly. Additional details of the modeling of each configuration using assemblies with part-length fuel rods are included in the following subsections. No calculations are performed for a varying number of reconfigured assemblies, multiple configurations, or combinations of full-length and part-length assemblies.

Table 44. Nominal k_{eff} results for fresh 5 w/o fuel assemblies with part-length rods in MPC-68

Channel present	Burnup (GWd/MTU)	Cooling time (years)	KENO V.a		KENO-VI	
			k_{eff}	σ	k_{eff}	σ
Yes	0	0	0.97497	0.00010	0.97482	0.00019
No	0	0	0.97391	0.00010	0.97396	0.00010

Table 45. Summary of k_{eff} impact for fresh 5 w/o fuel with part-length rods in MPC-68

Configuration	Reactivity consequence (% Δk_{eff})	Channel present
Clad thinning/loss		
Cladding removal	4.16	Yes
Rod failures		
Single rod removal	0.18	Yes
Multiple rod removal (2 rods removed)	0.32	Yes
Loss of rod pitch control		
Uniform rod pitch expansion, clad	12.28	No
Uniform rod pitch expansion, unclad	N/C*	N/A
Non-uniform pitch expansion, clad	N/C*	N/A
Channel constrained uniform expansion, clad	N/C*	N/A
Loss of assembly position control		
Axial displacement (30 cm)	6.17	Yes
Axial displacement (20 cm)	0.56	Yes
Gross assembly failure		
Uniform pellet array	N/C*	N/A
Homogeneous rubble	21.96	No
Neutron absorber degradation		
Missing neutron absorber (5-cm segment)	1.01	Yes
Missing neutron absorber (10-cm segment)	2.92	Yes
50% reduction of neutron absorber panel thickness	3.49	Yes

*Not calculated

5.2.4.1 Clad Thinning/Loss

The loss of cladding configuration is modeled as discussed above in Section 3.1.1. As shown in Table 46, the limiting k_{eff} increase associated with complete cladding removal is 4.16% Δk_{eff} and occurs with channeled fuel. The increase in k_{eff} as a function of the fraction of nominal cladding thickness remaining is also shown in Table 46 as well as in Figure 46. The results are consistently smaller increases in k_{eff} than those presented in Section 5.2.1.1. The increase in k_{eff} caused by the complete loss of cladding for full-length fuel is larger than the difference in the base case k_{eff} values presented in Table 24 and Table 44. The actual k_{eff} value is therefore larger in the case of full-length fuel with reconfiguration than for part-length fuel.

Table 46. Increase in k_{eff} in MPC-68 caused by cladding loss for assemblies with part-length fuel rods, fresh 5 w/o fuel

Cladding fraction remaining	Increase in k_{eff} (% Δk_{eff})
Channel Intact	
0.9	0.43
0.75	1.09
0.5	2.10
0.25	3.12
0.0	4.16
Channel Removed	
0.9	0.42
0.75	1.03
0.5	2.05
0.25	3.04
0.0	3.98

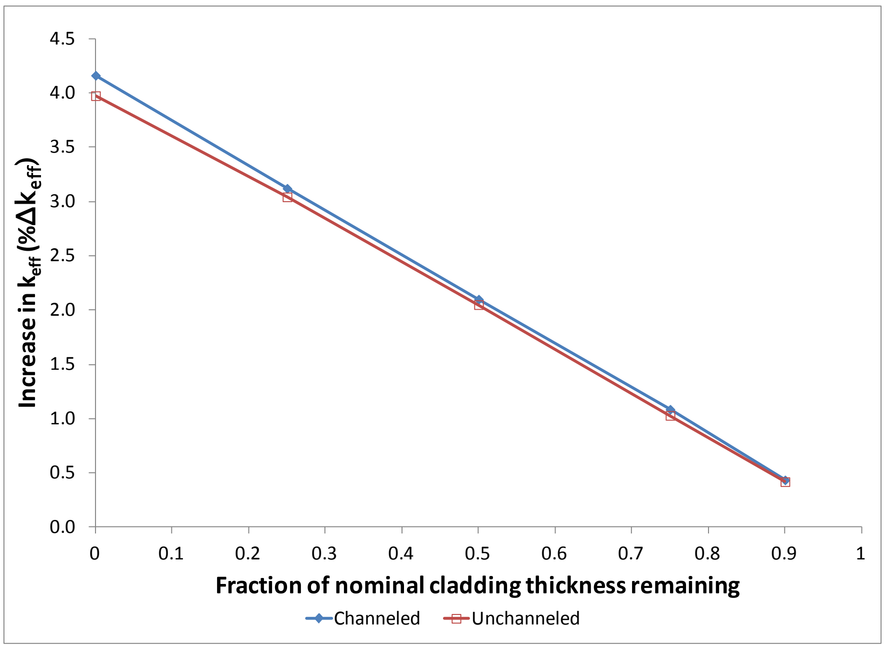

Figure 46. Increase in k_{eff} in MPC-68 as a function of fraction of intact cladding (Fresh 5 w/o fuel with part-length fuel rods).

5.2.4.2 Rod Failures

Each of the 51 unique half-assembly symmetric rods is removed individually to determine its worth, as discussed in Section 3.1.2.1. Table 47 presents the rod locations and worth of the limiting rod location and the three additional locations that are within approximately two standard deviations of the limiting k_{eff} increase. Only channeled fuel is considered since it is shown to be limiting in Section 5.2.1.2. The increase in k_{eff} is 0.18% Δk_{eff}, which is less than the 0.29% Δk_{eff} increase for fuel with full-length rods. The maximum increase in k_{eff} is associated with the removal of rod E3. The location of the limiting rod appears to have shifted from the location identified in Section 5.2.1.2. More precise calculations could be performed to confirm that the shift is real and not a statistical fluctuation.

The magnitude of the k_{eff} change caused by rod failure is somewhat less for fuel with part-length rods than for the full-length fuel used in Section 5.2.1.2. The likely cause of this reduced impact is that the removal of some of the rods in the upper section of the assembly creates a more thermal flux, and reduces the ability of a removed rod to increase thermalization. This is analogous to the reason that the channeled assemblies experience larger k_{eff} increases than unchanneled assemblies.

Two rods are removed in several pairs, as discussed in Section 3.1.2.2. The largest k_{eff} increase is 0.32% Δk_{eff}, which is less than the 0.52% Δk_{eff} increase caused by removing two rods from an assembly with full-length rods. The difference in k_{eff} increase is larger for two failed rods than for a single failed rod. This is an expected result since the impact of single rod failure is less for assemblies with part-length fuel than for assemblies with full-length fuel. No calculations are performed for larger numbers of failed rods as the result is likely to be progressively smaller increases in k_{eff} when compared with the results for full-length assemblies.

It should be noted that even though the increase in k_{eff} is larger for assemblies with full-length fuel, the actual k_{eff} for the cask is still higher in the part-length fuel rod case for the single and double rod failure configurations considered for fresh fuel. It is probable that the k_{eff} increase is large enough for higher numbers of failed rods that the full-length fuel becomes more limiting.

Table 47. Increase in k_{eff} in MPC-68 caused by single rod failure in fresh 5 w/o assemblies with part-length rods

Rod location	Increase in k_{eff} (% Δk_{eff})
E3	0.18
D4	0.16
D3	0.15
H6	0.14

5.2.4.3 Loss of Rod Pitch Control

The loss of rod pitch control is modeled largely as described in Section 3.1.3, except that only unchanneled fuel is modeled. That larger pitch expansion resulting from the removal of the channel leads to a larger k_{eff} increase, as documented in Section 5.2.1.3. As shown in Table 45, the increase in k_{eff} for uniform pitch expansion with part-length rods is 12.28% Δk_{eff}. This is significantly less than the 13.16% for fuel assemblies with full-length rods. As with the rod failure results discussed in Section 5.2.1.3, the lower impact of loss of array control is most likely due to a more thermal neutron spectrum in the base case and the corresponding reduction in additional thermalization caused by the fuel reconfiguration. In this case, the larger increase in k_{eff} is sufficient to result in a larger reconfigured k_{eff} for full-length fuel assemblies.

5.2.4.4 Loss of Assembly Position Control

Assembly axial displacements are calculated for a range of upward displacements up to 30 cm, all with channeled fuel since it is shown to be more reactive than unchanneled fuel in Section 5.2.1.4. As shown in Table 45, the increases in k_{eff} caused by 30-cm and 20-cm displacements are 6.17% Δk_{eff} and 0.56% Δk_{eff}, respectively. The increase in k_{eff} associated with the 30-cm misalignment is smaller than that for fresh fuel with full-length fuel rods, but the increase for a 20-cm misalignment is larger for part-length fuel. Both of these increases are significantly non-limiting compared to the cases included in the results shown in Section 5.2.1.4. The impact of axial displacement is strongly influenced by the burnup profile in UNF, so this configuration with part-length rods and an appropriate axial burnup profile should be examined.

5.2.4.5 Gross Assembly Failure

Only the homogeneous rubble configuration of gross assembly failure is modeled for fuel with part-length fuel rods. Only unchanneled fuel is considered because it is shown to be limiting in Section 5.2.1.5. The limiting configuration for gross assembly failure, as with results presented in Sections 5.1.1.5 and 5.2.1.5, is with the entire cask cavity volume filled with rubble. As shown in Table 45, the resulting k_{eff} increase is nearly 22% Δk_{eff}. The overall limiting increase in k_{eff} for the homogeneous rubble configuration occurs for UNF and is slightly less than 30% Δk_{eff}, as shown in Table 25. For fresh fuel, as shown in Table 32, the k_{eff} increase associated with the homogeneous rubble configuration is nearly 23% Δk_{eff}.

A second calculation with the entire cavity filled with rubble is performed to investigate the effect of separate homogenization for the upper portion of the assembly, with reduced fuel loading, and the lower portion of the assembly, with the entire assembly lattice containing fuel rods. The result of this calculation is a slightly smaller increase in k_{eff} of approximately 21.2% Δk_{eff}. The upper portion of the rubble bed, with reduced fuel loading, has a significantly higher volume fraction of water and is likely overmoderated.

5.2.4.6 Neutron Absorber Degradation

The results of the calculations, described in Section 3.1.6.1, considering a 5-cm neutron absorber defect at varying elevations for fuel assemblies with part-length rods and an intact fuel channel are presented in Table 48 and Figure 47. The limiting condition is for the gap centered at an elevation of 270 cm above the bottom of the fuel. The removal of the upper portion of the part-length rods shifts the limiting elevation up relative to the mid-plane location which is limiting for full-length fresh fuel. As mentioned previously, the increased moderation within the assembly lattice results in the upper portion of the assembly being more reactive than the lower portion. This relative reactivity difference is the cause of the shift in the limiting neutron absorber gap location.

The largest k_{eff} increase observed for this configuration is 1.01% Δk_{eff} and increases to 2.92% Δk_{eff} if the defect size is increased to 10 cm. These results represent a larger increase in k_{eff} than for full-length fresh fuel but a smaller increase in k_{eff} than the limiting condition involving UNF discussed in Section 5.2.1.6. As discussed in Section 3, these defects are assumed to be present at the same elevation in all neutron absorber panels within the cask.

The increase in k_{eff} associated with uniform neutron absorber panel thinning as discussed in Section 3.1.6.3 is shown in Table 49 and Figure 48 with fresh 5 w/o fuel modeled in the MPC-68 cask. As shown in Table 45, a 50% reduction in panel thickness results in a 3.49% increase in k_{eff}. Complete neutron absorber panel removal increases k_{eff} by more than 21% Δk_{eff}, but more than 40% of the absorber must be removed before an increase of more than 3% is realized. These results are similar to those presented in Section 5.2.1.6, but the increases in k_{eff} are slightly smaller. The full-length fuel does not experience a great enough increase in k_{eff} for the resulting cask k_{eff} to exceed that for part-length fuel. This configuration is another example of the part-length fuel leading to a higher k_{eff} after reconfiguration despite having a smaller k_{eff} change because of the higher initial neutron multiplication.

Table 48. Increase in k_{eff} in MPC-68 caused by a 5-cm neutron absorber panel defect, fresh 5 w/o fuel with part-length fuel rods

Elevation of centerline of defect (cm above bottom of fuel)	Increase in k_{eff} (% Δk_{eff})
2.50	-0.01
95.25	0.15
190.50	0.46
222.50	0.77
253.50	0.97
270.00	1.01
285.75	1.00
301.00	0.96
340.00	0.58
378.50	0.00

Table 49. Increase in k_{eff} in MPC-68 caused by uniform neutron absorber panel thinning, fresh 5 w/o fuel with part-length fuel rods

Fraction of neutron absorber panel thickness remaining	Increase in k_{eff} (% Δk_{eff})
0.9	0.53
0.8	1.13
0.7	1.79
0.6	2.57
0.5	3.49
0.4	4.64
0.3	6.08
0.2	8.14
0.1	11.50
0.0	21.33

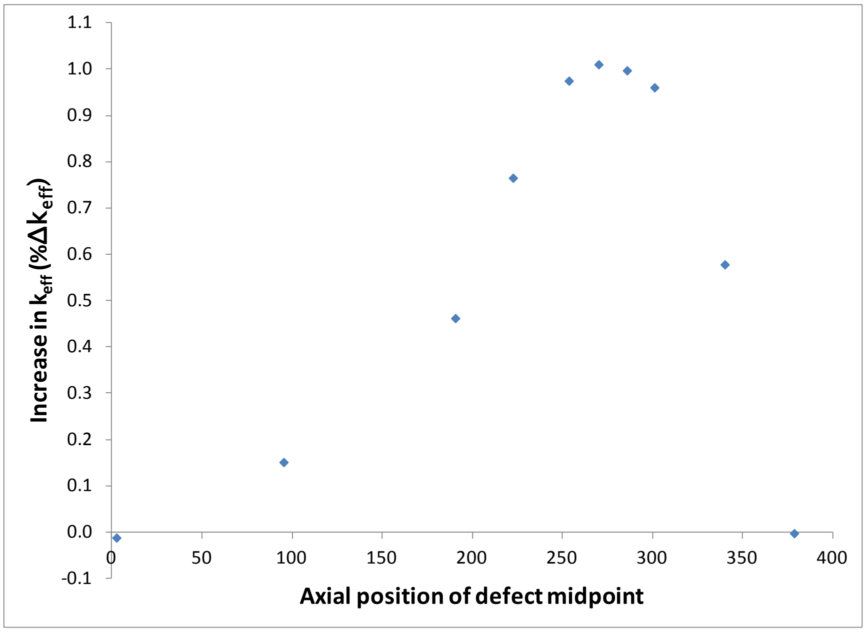

Figure 47. Increase in k_{eff} in MPC-68 as a function of neutron absorber defect axial position, fresh 5 w/o fuel with part-length fuel rods.

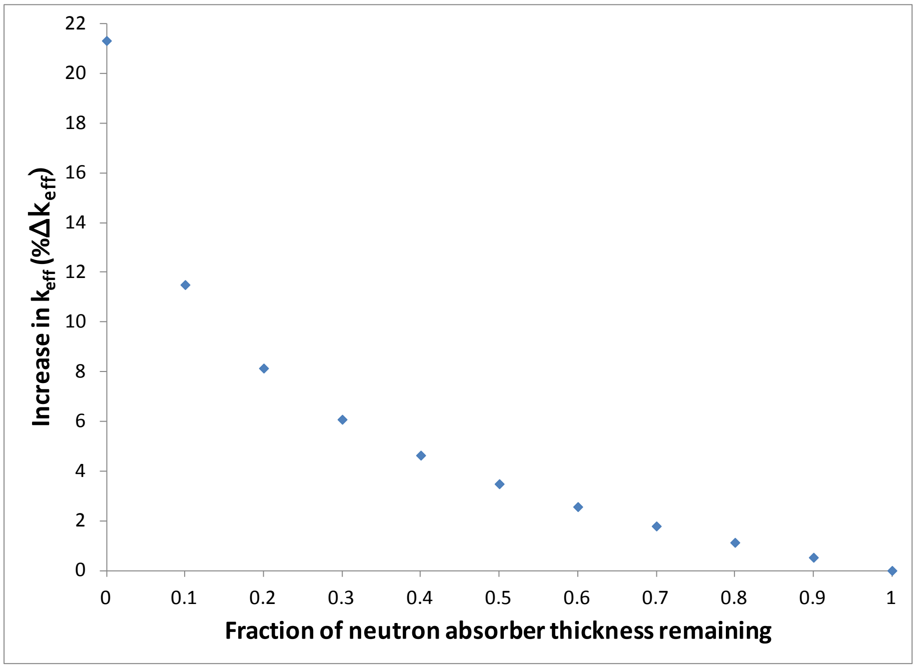

Figure 48. Increase in k_{eff} in MPC-68 as a function of remaining neutron absorber panel thickness, Fresh 5 w/o fuel with part-length fuel rods.

6. SUMMARY AND CONCLUSIONS

This report documents work performed for the DOE-NE Fuel Cycle Technologies Used Fuel Disposition Campaign to assess the consequences of potential fuel failure on the criticality safety of UNF in storage and transportation casks. This work was motivated by concerns related to the potential for fuel degradation during ES periods and transportation following ES, but has relevance to other potential causes of fuel reconfiguration.

Because many of the fuel degradation mechanisms are not well understood, a number of postulated configurations were modeled to calculate the corresponding k_{eff} values and the associated consequences of those configurations relative to the reference intact configuration. The consequence of a given configuration was defined as the difference in the calculated k_{eff} values for the given configuration and the reference intact configuration, with a positive value indicating an increase in k_{eff} as compared to the reference configuration. Because a wide range of configurations was analyzed, the calculated consequences varied widely. Several of the configurations are not considered credible but are included in the analyses for completeness (e.g., to fully understand trends and worst-case situations). Pending improved understanding of the various material degradation phenomena, and subsequent determination and justification for what configurations are and are not credible, the assessment of the credibility of configurations provided herein is based on engineering judgment. The credibility of configurations and the impact of the configurations on criticality safety are dependent on many factors, including storage and transportation conditions, the fuel assembly characteristics, and the storage and/or transportation system characteristics. Therefore, the assessment and analysis of credible configurations for a specific cask system would need to be performed as part of the safety analysis for licensing that system.

6.1 Summary of Analyses

The detailed results for each configuration considered in the PWR cask system (GBC-32) are provided in Section 5.1 and summarized in Table 6. For all the credible and non-credible configurations analyzed, the consequence on k_{eff} varied from a decrease of several percent (safer condition) to an increase of more than 20% Δk_{eff}. For configurations judged to be potentially credible, i.e., configurations for which the authors felt additional information was needed to determine credibility, the maximum increase in k_{eff} was 3.90% Δk_{eff}, corresponding to nonuniform fuel rod pitch expansion in all assemblies within the cask. It is important to emphasize that this result is contingent on the authors' judgment relative to the potential credibility of configurations, which includes not only whether a configuration category is credible but also whether the resulting configurations within a given category are credible for a specific cask system. For example, for the GBC-32 cask system, axial assembly displacement such that assemblies extended more than 7.5 cm above or below the neutron absorber panel was not considered credible because of the presence of fuel assembly hardware and cask assembly spacers. If it were determined that such a configuration is credible, then that configuration and its specific characteristics may be limiting.

The detailed results for each configuration considered in the BWR cask system (MPC-68) are provided in Section 5.2 and summarized in Table 25 and Table 45 for fuel assemblies with full- and part-length rods, respectively. For all the credible and non-credible configurations analyzed, the consequence on k_{eff} varied from a decrease of several percent (safer condition) to an increase of almost 36% Δk_{eff}. In most cases, the k_{eff} increases for BWR UNF in the MPC-68 were larger than for PWR UNF in the GBC-32. For configurations judged to be potentially credible, the maximum increase in k_{eff} was 2.4% Δk_{eff}, corresponding to a configuration with multiple rod failures for fuel with an initial enrichment of 5 w/o and 35 GWd/MTU of burnup. As emphasized above, it is important to recognize that these results are contingent on the authors' judgment relative to the potential credibility of configurations. For example, for this BWR cask system, the fuel assembly channel is assumed to be present and capable of constraining fuel rod pitch expansion. If this assumption is not valid for a specific cask loading, then another configuration and its specific characteristics may be limiting.

The maximum increase for a potentially credible configuration in the BWR cask system (2.4% Δk_{eff}) corresponds to a reference case k_{eff} of approximately 0.833. The reconfigured k_{eff} is therefore only approximately 0.857 and still significantly less than the recommended 0.95 k_{eff} limit. The large subcritical margin is due to the fact that the MPC-68 was designed and licensed to accommodate unburned fuel, whereas the analyses considered fuel irradiated to 35 GWd/MTU (a relatively low discharge burnup for fuel with initial enrichment of 5 w/o). The largest k_{eff} increase associated with fresh fuel is 2.09% Δk_{eff} and is a result of uniform pitch expansion constrained by the fuel assembly channel. Many of the potential issues associated with crediting the constraint provided by the channel are negated in this case since it is fresh fuel. Results presented for the fuel assemblies with part-length fuel rods in Section 5.2.4 demonstrate the potential importance of this design feature. The reference case k_{eff} for fresh assemblies with part-length rods is nearly 0.7% Δk_{eff} higher than for fresh assemblies with only full-length rods. The k_{eff} increase associated with fuel reconfiguration is usually lower for the part-length fuel, but often the difference in the k_{eff} change is less than the difference in the reference cases. The absolute k_{eff} is therefore higher for many configurations involving fresh assemblies with part-length fuel even though the k_{eff} *increase* is smaller. The effect of varying depletion conditions for assemblies with part-length rods was not considered in this report.

In addition to representative conditions for fuel burnup and post-irradiation decay time, the effects of higher burnup and longer cooling times were also investigated in both PWR and BWR cask systems and found to be smaller than the reduction in k_{eff} associated with the higher burnup or cooling time. In addition to the analyses that assume all of the assemblies within the cask have the same degradation condition, analyses were performed to evaluate the consequences of degradation to limited numbers of assemblies. Although the results are configuration dependent, they indicate that the majority of the total potential increase in k_{eff} (observed for a cask fully loaded with degraded fuel) is associated with a relatively small fraction of the assemblies having the degraded condition, provided that the reconfigured assemblies are located in close proximity and in the worst-case location in the cask (generally the center region). A limited study performed with the MPC-68 demonstrated that the increase in k_{eff} is considerably smaller if the reconfigured assemblies are randomly distributed. A limited set of analyses was also performed to investigate the consequences of combinations of degradation, e.g., a number of failed rods and fuel rod pitch expansion. In the cases analyzed, the sum of the k_{eff} increases associated with modeling each configuration separately was determined to be slightly larger than the increase determined from explicitly modeling the combined configurations.

6.2 Observations and Conclusions

Similar to previous works, a key conclusion is that the consequences of fuel failure to criticality safety are directly dependent on the configurations that may form as a result of fuel failure. The magnitude of the potential increases in k_{eff} and the sensitivity of the potential increases in k_{eff} to the determination of the credibility of configurations highlight the importance of being able to determine and justify which configurations are credible under a given set of conditions for a given cask system. It is anticipated, at least in the near term, that these determinations will be done on a case-by-case basis for each cask system and associated licensing conditions.

Analyses of additional large-capacity cask designs and/or additional fuel types are expected to yield k_{eff} changes that are similar in magnitude, as compared to those predicted herein, and the limiting configurations are likely to be the same or similar. Large differences in cask design features could cause significant differences in reconfiguration consequences in specific casks, if such large design differences exist. This conclusion is supported by the similarities in the important effects between PWR and BWR fuel considered in this report. The differences between BWR and PWR fuel designs are more significant than the differences among assembly types within the PWR or BWR fuel classes. The importance of any particular configuration may vary from one cask design to another, but the most limiting configurations will be associated with gross assembly failure and large axial misalignment and are relatively insensitive to assembly design.

The results presented in Section 5 and the cask-specific conclusions presented above indicate larger k_{eff} increases for BWR fuel, as compared to PWR fuel. However, current BWR casks, including the MPC-68 considered in this analysis, are designed and licensed to accommodate unburned fuel. Therefore, these casks generally have in excess of 10% Δk_{eff} margin (as compared to the recommended k_{eff} limit of 0.95) when loaded with fuel with typical discharge burnup values.

Specific, realistic configuration development is likely to provide significant margin compared to the bounding configurations considered here. For both casks, the maximum increases in k_{eff} are based on analyses that assume all of the assemblies within the cask have the same degradation condition. Analyses that consider limited numbers of reconfigured assemblies, either randomly located within the cask or located together, predict smaller increases in k_{eff}. Hence, unless all or most of the assemblies within a cask are expected to the have same or a similar degree of reconfiguration, the cited maximum increases in k_{eff} are conservative estimates; the extent of the conservatism depends on the number and location of the reconfigured assemblies, as well as the configuration.

Given the establishment of a set of credible failed fuel configurations for a given cask system and assuming that one or more of the configurations result in an increase in k_{eff} (above the regulatory limit of 0.95), the consequence of this potential increase in k_{eff} must be addressed. There are a number of potential options, the viability of which depends on the magnitude of the increase in k_{eff}. For BWR fuel, credit for fuel burnup could be used to offset the potential increase in k_{eff} due to fuel failure. Although it is recognized that burnup credit for BWR fuel in storage and transportation casks is not recommended in current regulatory guidance documents, the reactivity reduction associated with burnup is likely sufficient to offset reactivity increases associated with potentially credible BWR failed fuel configurations.

Other potential mitigation options, for either PWR or BWR casks, include 1) separate loading curves for fuel and/or conditions for which fuel integrity cannot be assured, 2) a higher k_{eff} limit for such fuel, e.g., 0.98, 3) increased credit for cooling time, 4) credit for the actual, as-loaded conditions in existing casks, and 5) moderator exclusion. For the first option listed above, a cask design and/or fuel assembly loading conditions could be modified to ensure that the current recommended k_{eff} limit of 0.95 is satisfied for all credible failed fuel configurations. Separate assembly loading curves based on a reduced k_{eff} limit could be developed for fuel assemblies that may have questionable integrity. In the context of high-burnup fuel or ES durations, a separate loading curve based on a lower k_{eff} limit could be developed and applied to fuel assemblies with burnup greater than 45 GWd/MTU and/or with a post-irradiation storage period beyond some specified value. Alternatively, depending on the probability of fuel reconfiguration, the second option listed above, i.e., the use of a higher limit, could be established to allow margin for the increased reactivity effect associated with fuel reconfiguration. This option would be similar to the higher limit (i.e., 0.98) allowed for the unlikely optimum moderation condition in dry storage of fresh fuel under 10 CFR 50.68. In this case, the customary k_{eff} limit would still apply to all conditions involving intact fuel. The third option above refers to crediting the reduction in reactivity between the minimum time for loading, e.g., 5 years, and some time prior to which fuel reconfiguration is postulated to occur, e.g., 50 years. Because the reactivity of UNF reaches a minimum at approximately 100 years and then begins to increase, the total duration for cask storage and transportation is an important consideration in determining how much reactivity reduction can be credited. For fuel that is already loaded in casks, the fourth option above refers to crediting the specific cask conditions – to the extent needed, the specific assembly burnup values, cooling times and locations in the cask may be considered to demonstrate sufficient reactivity margin to offset the potential increase in k_{eff} due to fuel failure. Finally, moderator exclusion could potentially be used to offset criticality safety concerns related to fuel failure, as is currently allowed for HACs in Ref. 51.

Although the results indicate that the potential impacts on subcriticality can be significant for certain configurations, it can be concluded that the consequences of credible fuel failure configurations from ES or transportation following ES are manageable. Some examples for how to address the potential increases in k_{eff} in a criticality safety evaluation were provided. Future work to further inform decision-making relative to which configurations are credible, and therefore need to be considered in a safety evaluation, is recommended.

7. RECOMMENDATIONS FOR FUTURE WORK

Future work to extend these analyses could consider additional fuel assembly types, depletion conditions, and cask designs. As noted in Section 6.2, this is not expected to result in significantly different conclusions. It may be beneficial to investigate more accurate modeling of the fuel assemblies to include such features as axial blankets or radial enrichment zoning and different axial burnup and void histories. These details could give more realistic estimates of their impacts on k_{eff} but are unlikely to change the salient conclusions regarding the relevance of key configurations.

An expanded study of debris configurations is warranted. The homogeneous debris models used in this analysis do not consider partial assembly failure or any intact assembly structure or hardware. Some of these types of configurations, including debris collecting in structural or flow mixing grids, are potentially more credible than the configurations included in this report. Rubble models including rod segments or fragments may also be relevant. Consideration should be given to a range of final cask orientations if the final debris bed does not fill the entire inner volume of the storage cells. A more complete study of degraded fuel forms is also potentially worth investigating. Many degraded fuel forms would include oxidation to other urania compounds of lower densities, effectively displacing moderator. These changes may not result in any increases in estimated k_{eff} but may be worth investigating.

Investigating different enrichments and burnups could be considered. It is unlikely that the relative importance of configurations would be impacted by these changes, but the overall magnitude may be affected. A more complete mapping of the burnup/enrichment space would also allow a quantification of potential conservatisms, especially for BWR fuel, with reduced k_{eff} values for reference case conditions.

Future work should investigate the potential impact of loading fuel assemblies with a range of burnups and irradiation histories in storage casks for ES. These configurations are more realistic since each assembly experiences different conditions during irradiation and will have different discharge burnups and cooling times.

It is advisable to consider more combinations of the configurations used here. A very limited number of calculations have been documented in Sections 5.1.3 and 5.2.3, and the results indicate that explicit modeling of combined configurations generates a slightly smaller increase in k_{eff} than the sum of the two separate effects. A review of other combined effects could generate additional limiting configurations or provide greater evidence that the effects of combined configurations can be adequately accounted for with separate single configuration models.

Finally, it may be advisable to consider the effect of basket or cask degradation if such events are considered credible. Degradation to these cask components is beyond the scope of these analyses.

REFERENCES

1. *Gap Analysis to Support Extended Storage of Used Nuclear Fuel*, U.S. Department of Energy, FCRD-USED-2011-000136, REV 0, January 2012.

2. *UFD Storage and Transportation Working Group Report*, U.S. Department of Energy, FCRD-USED-2011-000323, August 2011.

3. *Identification and Prioritization of the Technical Information Needs Affecting Potential Regulation of Extended Storage and Transportation of Spent Nuclear Fuel*, U.S. Nuclear Regulatory Commission, Draft Report for Comment, May 2012, http://pbadupws.nrc.gov/docs/ML1205/ML120580143.pdf.

4. *Extended Storage Collaboration Program (ESCP) Progress Report and Review of Gap Analysis*, Electric Power Research Institute, Palo Alto, CA (2011), 1022914.

5. *Evaluation of the Technical Basis for Extended Dry Storage and Transportation of Used Nuclear Fuel – Executive Summary*, U.S. Nuclear Waste Technical Review Board, December 2010, http://www.nwtrb.gov/reports/eds_execsumm.pdf.

6. *Used Nuclear Fuel Storage and Transportation Research, Development, and Demonstration Plan,* FCRD-FCT-2012-000053, REV 0, April 2012.

7. K. R. Elam, J. C. Wagner, and C. V. Parks, *Effects of Fuel Failure on Criticality Safety and Radiation Dose for Spent Fuel Casks*, NUREG/CR-6835 (ORNL/TM-2002/255), prepared for the U.S. Nuclear Regulatory Commission by Oak Ridge National Laboratory, Oak Ridge, TN, September 2003.

8. Title 10, *Code of Federal Regulations,* Part 72, 73 FR 63572, October 24, 2008.

9. Title 10, *Code of Federal Regulations,* Part 71, 73 FR 63572, October 24, 2008.

10. *Standard Review Plan for Spent Fuel Dry Storage Systems at a General License Facility* , NUREG-1536, Revision 1, Office of Nuclear Material Safety and Safeguards, July 2010.

11. *Standard Review Plan for Spent Fuel Dry Storage Facilities*, NUREG-1567, Office of Nuclear Material Safety and Safeguards, March 2000.

12. *Standard Review Plan for Transportation Packages for Spent Nuclear Fuel*, NUREG-1617, Office of Nuclear Material Safety and Safeguards, March 2000.

13. Title 10, *Code of Federal Regulations,* Part 50.68, 71 FR 66648, November 16, 2006.

14. *Fuel Reconfiguration – Implications to Criticality and Radiation Safety*, 2011 SFST Technical Exchange, November 1, 2011, David Tang and Zhian Li, U.S. Nuclear Regulatory Commission (ADAMS Accession #ML113120530).

15. A. Machiels and A. H. Wells, *Fuel Relocation Effects for Transportation Packages*, EPRI Report 1015050, Palo Alto, CA, 2007.

16. J. L. Sprung et al., *Reexamination of Spent Fuel Shipment Risk Estimates*, NUREG/CR-6672 (SAND2000-0234), prepared for the U.S. Nuclear Regulatory Commission by Sandia National Laboratories, Albuquerque, NM, March 2000.

17. L. E. Fischer et al., *Shipping Container Response to Severe Highway and Railway Accident Conditions*, NUREG/CR-4829 (UCID-20733), prepared for the U.S. Nuclear Regulatory Commission by Lawrence Livermore National Laboratory, Livermore, CA, February 1987.

18. *Final Environmental Impact Statement on the Transportation of Radioactive Material by Air and Other Modes*, NUREG-0170, U.S. Nuclear Regulatory Commission, Rockville, MD, December 1977.

19. A. Machiels et al., *Transportation of Commercial Spent Nuclear Fuel: Regulatory Issues Resolution*, EPRI Report 1016637, Palo Alto, CA, 2010.

20. A. Machiels and A. Dykes, *Criticality Risks during Transportation of Spent Nuclear Fuel: Revision 1*, EPRI Report 1016635, Palo Alto, CA, 2008.

21. *Interfaces Between Storage and Transportation Casks – Panel on High Burnup Fuel – Industry's View on Spent Fuel Reconfiguration*, 2011 SFST Technical Exchange, November 1, 2011, Albert Machiels, EPRI (ADAMS Accession #ML113120509).

22. D. Nagasawa et al., "Accelerated Corrosion Testing of Aluminum Carbide Metal Matrix Composite in Simulated PWR Spent Fuel Pool Solution," *Proceedings of 16th International Symposium on the Packaging and Transportation of Radioactive Materials* (PATRAM 2010), London, UK, 2010.

23. M. Dallongeville et al., "Description of Fuel Integrity Project Methodology Principles," *Proceedings of 16th International Symposium on the Packaging and Transportation of Radioactive Materials* (PATRAM 2010), London, UK, 2010.

24. P. Purcell, "Method to Evaluate Limits of Lattice Expansion in Light Water Reactor Fuel from an Axial Impact Accident During Transport," *Proceedings of 15th International Symposium on the Packaging and Transportation of Radioactive Materials* (PATRAM 2007), Miami, FL, 2007.

25. I. Reiche, "Influence of the Accident Behaviour of Spent Fuel Elements on Criticality Safety of Transport Packages – Some Basic Considerations," *Proceedings of 15th International Symposium on the Packaging and Transportation of Radioactive Materials* (PATRAM 2007), Miami, FL, 2007.

26. F. Hilbert, "Criticality Assessment of Fuel Assemblies With Missing Fuel Rods – An Intractable Problem?" *Proceedings of 14th International Symposium on the Packaging and Transportation of Radioactive Materials* (PATRAM 2004), Berlin, Germany, 2004.

27. P. J. Vescovi and N. A. Kent, "Nuclear Criticality Safety Analysis for the Traveler PWR Fuel Shipping Package," *Proceedings of 14th International Symposium on the Packaging and Transportation of Radioactive Materials* (PATRAM 2004), Berlin, Germany, 2004.

28. L. Farrington, "Harmonisation of Criticality Assessments of Packages for the Transport of Fissile Nuclear Fuel Cycle Materials," *Proceedings of 14th International Symposium on the Packaging and Transportation of Radioactive Materials* (PATRAM 2004), Berlin, Germany, 2004.

29. B. Gogolin et al., "Drop Tests with the RA-3D Shipping Container for the Transport of Fresh BWR Fuel Assemblies," *Proceedings of 13th International Symposium on the Packaging and Transportation of Radioactive Materials* (PATRAM 2001), Chicago, IL, 2001.

30. P, Millan et al., "Drop Test for the Licensing of the RA-3D Package in the Transport of BWR Fresh Fuel Assemblies," *Proceedings of 13th International Symposium on the Packaging and Transportation of Radioactive Materials* (PATRAM 2001), Chicago, IL, 2001.

31. S. Whittingham et al., "Effects of Impact Accidents on Transport Criticality Safety Cases for LWR Packages – A New Approach," *Proceedings of 13th International Symposium on the Packaging and Transportation of Radioactive Materials* (PATRAM 2001), Chicago, IL, 2001.

32. M. Asami and N. Odano, "New Approach to Evaluate Lattice Expansion of Light Water Reactor Fuel Elements on Criticality Safety of Transport Packages under Impact Accidents," *Packaging, Transport, Storage & Security of Radioactive Material* **21**(2), 2010.

33. *Handbook of Neutron Absorber Materials for Spent Nuclear Fuel Transportation and Storage Applications: 2009 ed.*, EPRI Technical Report 1019110, Electric Power Research Institute, Palo Alto, CA, November 2009.

34. *SCALE: A Comprehensive Modeling and Simulation Suite for Nuclear Safety Analysis and Design*, ORNL/TM-2005/39, Version 6.1, Oak Ridge National Laboratory, Oak Ridge, TN, June 2011. Available from Radiation Safety Information Computational Center at Oak Ridge National Laboratory as CCC-785.

35. *RW-859 Nuclear Fuel Data*, Energy Information Administration, Washington, D.C., October 2004.

36. *Safety Analysis Report for the Holtec International Storage, Transport, and Repository Cask System (HI-STAR 100 Cask System),* Table of Contents to Chapter 1, Holtec Report HI-951251, Revision 10, Holtec International, August 2003, ADAMS Accession Number ML071940386.

37. *Safety Analysis Report for the Holtec International Storage, Transport, and Repository Cask System (HI-STAR 100 Cask System),* Chapter 2 through Chapter 4, Holtec Report HI-951251, Revision 10, Holtec International, August 2003, ADAMS Accession Number ML071940391.

38. *Safety Analysis Report for the Holtec International Storage, Transport, and Repository Cask System (HI-STAR 100 Cask System),* Chapter 5 to end, Holtec Report HI-951251, Revision 10, Holtec International, August 2003, ADAMS Accession Number ML071940408.

39. J. C. Wagner, *Computation Benchmark for Estimation of Reactivity Margin from Fission Products and Minor Actinides in PWR Burnup Credit*, NUREG/CR-6747 (ORNL/TM-2000/306), prepared for the U.S. Nuclear Regulatory Commission by Oak Ridge National Laboratory, Oak Ridge, TN, October 2001.

40. C. V. Parks, M. D. DeHart, and J. C. Wagner, *Review and Prioritization of Technical Issues Related to Burnup Credit for LWR Fuel*, NUREG/CR-6665 (ORNL/TM-1999/303), prepared for the U.S. Nuclear Regulatory Commission by Oak Ridge National Laboratory, Oak Ridge, TN, February 2000.

41. R. J. Cacciapouti and S. Van Volkinburg, *Axial Burnup Profile Database for Pressurized Water Reactors*, YAEC-1937, Yankee Atomic Electric Company, May 1997.

42. J. C. Wagner and C. V. Parks, *Parametric Study for the Effect of Burnable Poison Rods for PWR Burnup Credit*, NUREG/CR-6761 (ORNL/TM-2000/373), prepared for the U.S. Nuclear Regulatory Commission by Oak Ridge National Laboratory, Oak Ridge, TN, March 2002.

43. C. E. Sanders and J. C. Wagner, *Study of the Effect of Integral Burnable Absorbers for PWR Burnup Credit*, NUREG/CR-6760 (ORNL/TM-2000/321), prepared for the U.S. Nuclear Regulatory Commission by Oak Ridge National Laboratory, Oak Ridge, TN, March 2002.

44. J. C. Wagner and C. V. Parks, *Recommendations on the Credit for Cooling Time in PWR Burnup Credit Analysis*, NUREG/CR-6781 (ORNL/TM-2001/272), prepared for the U.S. Nuclear Regulatory Commission by Oak Ridge National Laboratory, Oak Ridge, TN, January 2003.

45. Topical Report on Actinide-Only Burnup Credit for PWR Spent Nuclear Fuel Packages, DOE/RW-0472 Rev. 2, U.S. Department of Energy Office of Civilian Radioactive Waste Management, September 1998.

46. D. P. Henderson et al., *Summary Report of Commercial Reactor Criticality Data for Quad Cities Unit 2*, B00000000-01717-5705-00096 Revision 01, Civilian Radioactive Waste Management System Management & Operating Contractor, September 1999.

47. D. P. Henderson et al., *Summary Report of Commercial Reactor Criticality Data for LaSalle Unit 1*, B00000000-01717-5705-00138, Civilian Radioactive Waste Management System Management & Operating Contractor, September 1999.

48. D. E. Mueller et al., *Review and Prioritization of Technical Issues Related to Burnup Credit for BWR Fuel*, NUREG/CR-XXXX (ORNL/TM-2012/261), prepared for the U.S. Nuclear Regulatory Commission by Oak Ridge National Laboratory, Oak Ridge, TN, to be published.

49. M. G. Natrella, *Experimental Statistics*, National Bureau of Standards Handbook 91, August 1963.

50. Fuel Cycle Safety and Safeguard Interim Staff Guidance-10, *Justification for Minimum Margin of Subcriticality for Safety*, Division of Fuel Cycle Safety and Safeguards, Office of Nuclear Material Safety and Safeguards, U.S. Nuclear Regulatory Commission, June 2006.

51. Spent Fuel Storage Transportation Interim Staff Guidance-19, *Moderator Exclusion under Hypothetical Accident Conditions and Demonstrating Subcriticality of Spent Fuel under the Requirements of 10 CFR 71.55(e)*, Division of Spent Fuel Storage and Transportation, Office of Nuclear Material Safety and Safeguard, U.S. Nuclear Regulatory Commission, May 2003.

52. L. E. Fennern, *ABWR Seminar – Reactor, Core & Neutronics*, GE Energy/Nuclear, http://www.ne.doe.gov/np2010/pdfs/ABWRReactorCoreNeutronics.pdf, retrieved April 16, 2012.

53. L. B. Wimmer, *BWR Axial Burnup Profile Evaluation*, Framatome ANP Document Number 32-5045751-00, July 16, 2004.

Appendix A

Fuel Assembly Modeling Details

A.1 WESTINGHOUSE 17 × 17 OFA

Westinghouse 17 × 17 OFA is a fuel design that has been commonly used in the commercial nuclear industry for more than 20 years. This common use makes it a good choice for a representative fuel assembly type for calculations in the PWR storage and transportation casks. For purposes of these analyses, the OFA fuel design encompasses all variations of cladding materials, grids, and assembly hardware which may lead to a different fuel product designation from Westinghouse, such as Vantage5 or Vantage+. The essential features are the fuel rod outer diameter of 0.9144 cm and fuel rod pitch of 1.2598 cm. The dimensions used to model the fuel assembly are provided in Table A-1.

The 17 × 17 OFA model is included in the MPC-24 and GBC-32 casks. The cladding is modeled as Zircaloy-4. The guide tube and instrument tubes are assumed to be identical and are also represented as Zircaloy-4. Unborated, unit density water fills the gap between the pellet and cladding. Water in the pellet/clad gap is conservative for criticality calculations because it causes a slight increase in calculated k_{eff} values. In irradiated fuel, pellet swelling closes this gap and causes this assumption to be nonphysical. A cross section of the 17 × 17 OFA model is shown in Figure A-1.

The fuel assemblies are modeled with a uniform initial enrichment in the axial and radial directions. No reduced enrichment and/or annular blanket pellets are included in any of the models. No integral burnable absorbers are modeled in the fuel, though the presence of wet annular burnable absorber (WABA) rods is considered during depletion to provide conservative used fuel isotopic compositions with respect to criticality calculations. The impact of the presence of removable and integral burnable absorbers is discussed in Refs. 42 and 43. The details of the depletion conditions are provided in Section 4.4.1.

Several modeling simplifications have been incorporated that either have a negligible effect or increase assembly calculated k_{eff}. Some of these simplifications include omission of fuel assembly hardware beyond the ends of the active fuel as well as the omission of all structural and mixing grids, assembly nozzles, plenums, and end plugs. The hardware beyond the active fuel region has a small effect on k_{eff}, and minimal effect on the change in k_{eff} associated with fuel reconfiguration. Omitting the grids allows more effective neutron moderation due to less moderator displacement between rods.

For cases involving depleted fuel, the fuel rods are represented with 18 axial regions. Each region is 20.32 cm (8 in.) tall and contains average mixture number densities in each zone. All fuel rods contain the same composition.

Table A-1. Westinghouse 17 × 17 OFA dimensions used in these analyses [39]

Parameter	Dimension (cm)	Dimension (in.)
Pellet outer diameter	0.7844	0.3088
Fuel rod outer diameter	0.9144	0.360
Cladding thickness	0.0571	0.0225
Fuel rod pitch	1.2598	0.496
Active fuel height	365.76	144
Guide/instrument tube outer diameter	1.204	0.474
Guide/instrument tube thickness	0.0407	0.016
Fuel density	10.5216 g/cm^3 (96% theoretical density)	
Number of fuel rods	264	
Number of guide/instrument tubes	25	

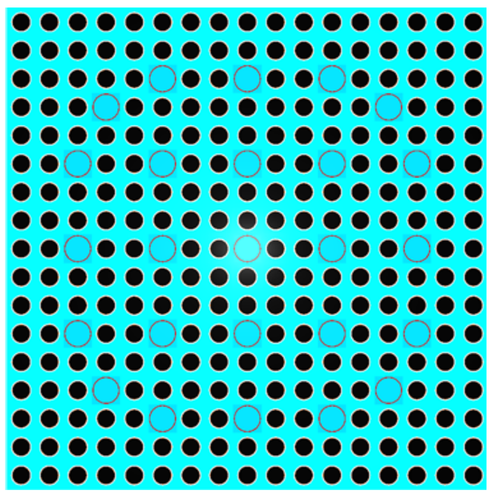

Note: Fuel shown in black; guide/instrument tubes are larger, water-filled tubes

Figure A-1. Cross section of 17 × 17 OFA assembly.

A.2 GENERAL ELECTRIC 10 × 10

General Electric 10 × 10 fuel assembly designs, such as the GE14 fuel product, are widely used in the commercial nuclear power industry. The 10 × 10 array is representative of existing BWR fuel assembly designs for use in the MPC-68 cask models. The GE 10 × 10 model included in the MPC-68 models uses dimensions shown in Table A-2. Unborated, unit density water fills the gap between the fuel pellet and cladding. The cladding and water tubes are modeled as Zircaloy-4. Each water tube occupies four unit cells in the lattice, displacing a 2 × 2 region of fuel rods. A cross section of the 10 × 10 model is shown in Figure A-2.

The fuel assemblies are considered with a uniform initial enrichment in the axial and radial directions. No reduced enrichment axial blanket pellets are included, and no part-length rods are represented in the fuel assemblies except in the explicit part-length rod sensitivity calculations.

Part-length rods are common in BWR assembly designs, including the GE14 design, making an investigation of the impact of part-length rods prudent as a part of these analyses. The pattern of part-length rods, taken from Ref. 52, is shown in Figure A-3. These shortened rods have fuel only in the bottom 220 cm of the fuel rods. As discussed in Section 5.2.4, only fresh 5 w/o fuel is considered in the part-length rod calculations presented in this report. Only fresh fuel is considered for these studies because no axial burnup profiles are available for fuel assemblies with part-length rods. The removal of some of the fuel in the upper portion of the assembly might cause a more bottom-skewed power shape, but the remaining sparser lattice will also be more reactive. The axial power shape could therefore also be about the same or even more top-skewed than that developed in Appendix E. The lower mass in the upper zone of the assembly also has the effect of increasing burnup since it is measured as energy released per unit mass of uranium. Given the unknown relative impact of these effects, depleted fuel is not considered in this study.

No burnable absorbers are modeled in the fresh fuel assemblies or during depletion. The impact of burnable absorbers is expected to be negligible on the results of this study. The details of the depletion conditions are provided in Section 4.4.2.

Several modeling simplifications that are consistent with industry practice for criticality safety have been incorporated that either have a negligible effect on system reactivity or increase assembly reactivity. Some of these simplifications include omission of fuel assembly hardware beyond the ends of the active fuel as well as the omission of all structural and mixing grids, assembly end fittings, plenums, and end plugs. The hardware beyond the active fuel region has a small effect on k_{eff}, and minimal effect on the change in k_{eff} associated with fuel reconfiguration. Omitting the grids allows more effective neutron moderation due to less moderator displacement between rods.

For cases involving depleted fuel, the fuel rods are represented with 25 axial regions. Each region is 15.24 cm (6 in.) tall and contains average mixture number densities in each zone. All fuel rods contain the same composition.

Table A-2. GE 10 × 10 assembly dimensions used in these analyses [34]

Parameter	Dimension (cm)	Dimension (in.)
Pellet outer diameter	0.876	0.3449
Fuel rod outer diameter	1.026	0.404
Cladding thickness	0.066	0.026
Fuel rod pitch	1.295	0.510
Active fuel height	381	150
Water tube outer diameter	2.522	0.993
Water tube thickness	0.1	0.039
Fuel density	10.5216 g/cm^3 (96% theoretical density)	
Number of fuel rods	92	
Number of water tubes	2 (each displaces four fuel rods)	

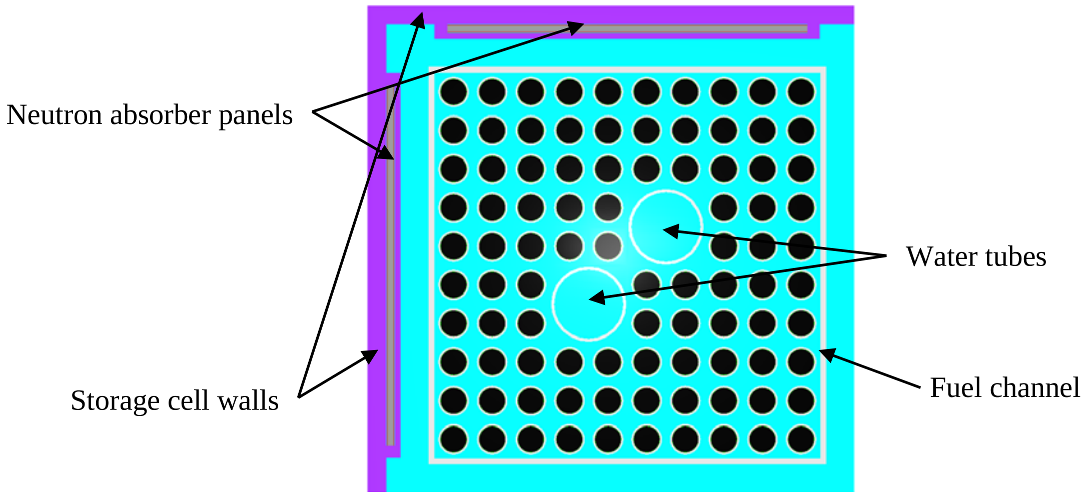

Figure A-2. Cross section of GE 10 × 10 fuel assembly in MPC-68.

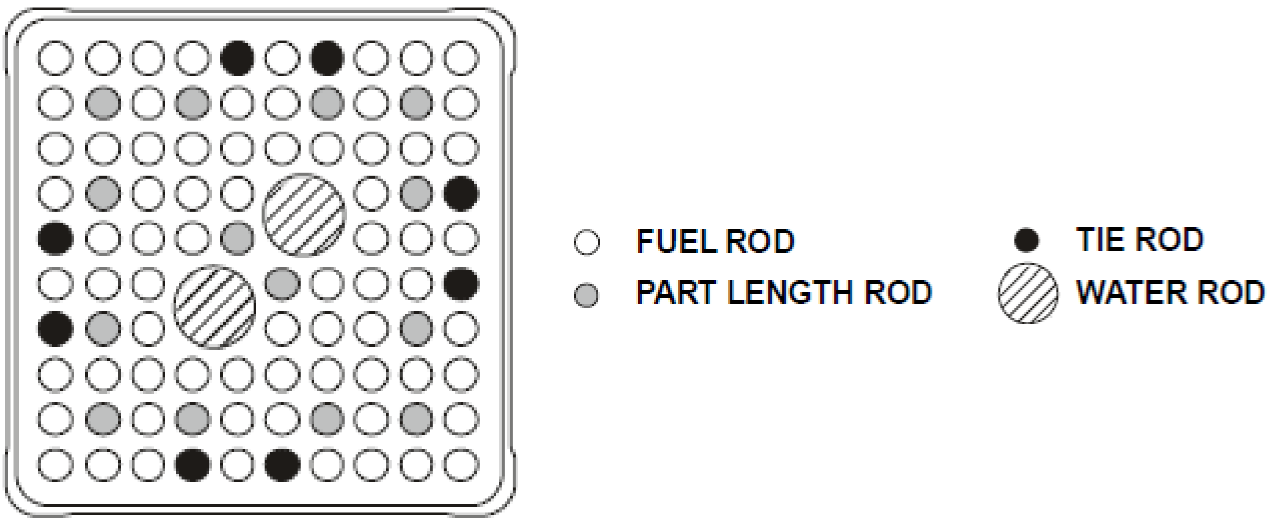

Figure A-3. Location of part-length rods in GE 10 × 10 fuel assembly.

Appendix B

MPC-24 Modeling and Results

The MPC-24 cask is designed for the storage and transportation of up to 24 PWR fuel assemblies. The nominal condition for this model is fully flooded with unit density, unborated water. A cross section of the MPC-24 model is shown in Figure B-1. It should be noted that the MPC-24 cask design in Refs. 36–38 has been updated from the design used in Ref. 7. The cask model is consistent with the description and drawings provided in the HI-STAR Safety Analysis Report (SAR), Refs. 36–38. More details of the modeling are provided in Appendix D.

Fresh 5 w/o ^{235}U enrichment Westinghouse 17 × 17 OFA is modeled in the MPC-24. This fuel represents a limiting case for analysis. It is unlikely that any fresh fuel assemblies would be placed in ES, but this condition is of interest to complete the parameter space to be covered in this study.

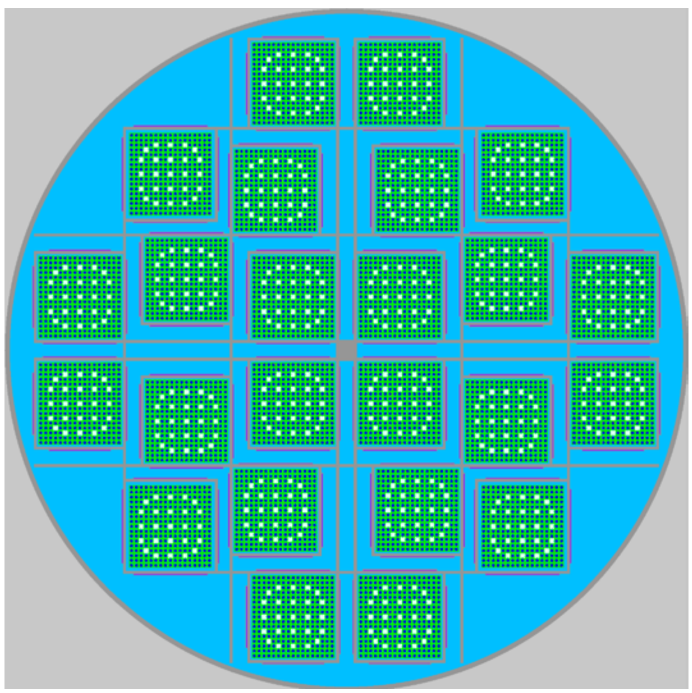

Figure B-1. Cross section of MPC-24 model.

B.1 ADDITIONAL CONFIGURATION CONSIDERED

The MPC-24 is the only cask design considered that integrates a flux trap into the design of the fuel storage basket. A flux trap is a region of typically water-filled space with neutron absorber panels on both sides of the trap and is positioned between fuel storage cells. The worth of the absorbers is greatly increased by allowing for additional moderation between the panels, thus allowing higher reactivity fuel to be stored safely. Fast neutrons escaping from one cell will be thermalized in the water between cells and are much more likely to be absorbed in the panel on the other side. For this design feature to be effective, the area within the flux trap must stay flooded in all cases in which the fuel storage cells are flooded. The primary design features that preclude the drainage of only the flux traps are an opening in the bottom of the storage basket walls and a small gap between the top of the storage cell walls and the cask lid. These openings allow water to flow into all regions of the basket. Preferential flooding (i.e., flooding of the fuel storage cells but not the flux traps) is considered here.

The modeling of preferential flooding configurations is straightforward. Two cases are considered: one in which only the flux traps are dry and one in which the area inside the fuel storage cell but outside the fuel assembly is also dry. The latter case is not credible but is included for completeness. No adjustments are needed to the cross section processing because the fuel assembly is always modeled as fully flooded. The orientation of the cask is not considered in the modeling of this configuration. It is not expected to influence the results of the calculations, though it would influence the progression of a flooding event if one occurred.

No preferential flooding cases are considered in Ref. 7.

B.2 RESULTS

The k_{eff} change associated with each of the configurations discussed in Section 3 and Section B.1 is presented in this section for the MPC-24 cask. All configurations assume a full loading of 24 fresh 5 w/o Westinghouse 17 × 17 OFA. The description of the fuel assembly modeling is provided in Appendix A. No used fuel configurations are considered in the MPC-24 model. The reference case k_{eff} results from both the KENO V.a and KENO-VI models are provided in Table B-1.

Table B-1. Reference case results for MPC-24

Burnup (GWd/MTU)	Cooling time (years)	KENO V.a		KENO-VI	
		k_{eff}	σ	k_{eff}	σ
0	0	0.95042	0.00010	0.95065	0.00010

B.2.1 Reconfiguration of All Assemblies

A summary of the k_{eff} consequences associated with each configuration is provided in Table B-2. Additional details for each configuration and the results for non-limiting cases are provided in the subsequent subsections.

Table B-2. Summary of k_{eff} increases for the MPC-24 cask

Configuration	Maximum increase in k_{eff} (% Δk_{eff})
Clad thinning/loss	
Cladding removal	5.24
Rod failures	
Single rod removal	0.15
Multiple rod removal	2.01
Loss of rod pitch control	
Expanded rod pitch, clad	2.88
Expanded rod pitch, unclad	6.83
Loss of assembly position control	
Axial displacement (maximum)	7.08
Axial displacement (20 cm)	0.03
Gross assembly failure	
Uniform pellet array	13.56
Homogeneous rubble	8.23
Preferential flooding	
Preferential Flooding (dry flux traps)	16.61
Neutron absorber degradation	
Missing neutron absorber (5-cm segment)	0.35
Missing neutron absorber (10-cm segment)	1.07
50% neutron absorber panel thinning	1.11

B.2.1.1 Clad Thinning/Loss

The loss of cladding configurations are modeled as discussed above in Section 3.1.1; the complete cladding removal configuration is shown in Figure B-2. The results of the calculations are provided in Table B-3, showing that the k_{eff} increase associated with complete cladding removal is 5.24% Δk_{eff}. The results as a function of fractional cladding thickness are shown in Figure B-3. The results presented here are somewhat higher than those presented in Ref. 7. This may be due to an updated cask model that includes the oversized fuel storage cells and the rotation of the standard storage cells relative to each other in the cask basket. These additional details may lead to a slightly more thermal spectrum and a correspondingly higher k_{eff} value for this configuration.

Table B-3. Increase in k_{eff} in MPC-24 due to reduced cladding thickness

Fraction of cladding thickness remaining	Increase in k_{eff} (% Δk_{eff})
0.90	0.62
0.75	1.51
0.50	2.87
0.25	4.06
0.00	5.24

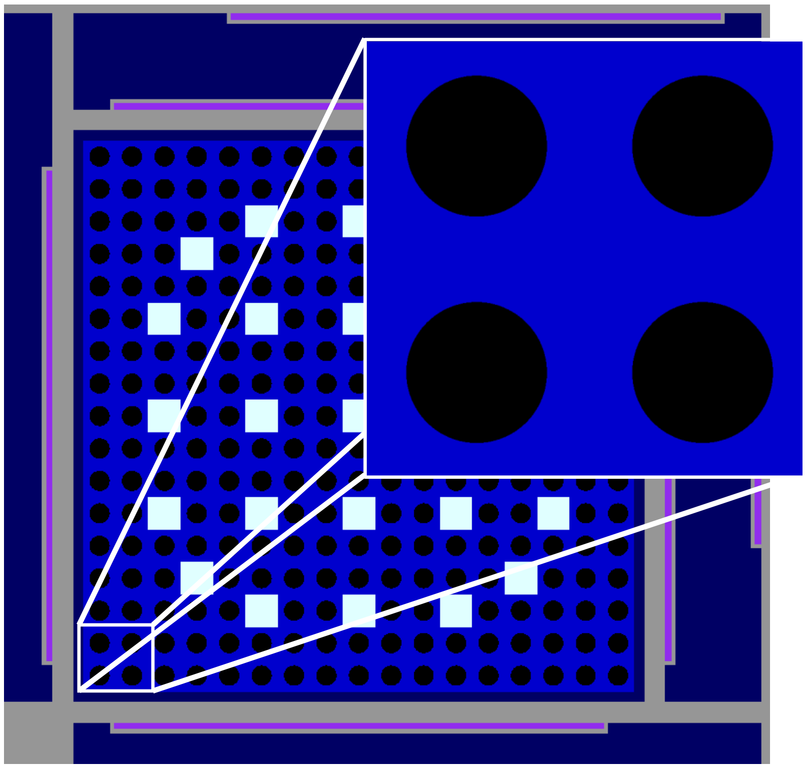

Notes: Fuel shown in black
Storage basket structural material is light grey
Neutron absorber panel is purple
Water is shown in blue, dark blue, and white
Guide/instrument tube locations contain water shown in white

Figure B-2. Loss of cladding model in MPC-24 storage cell.

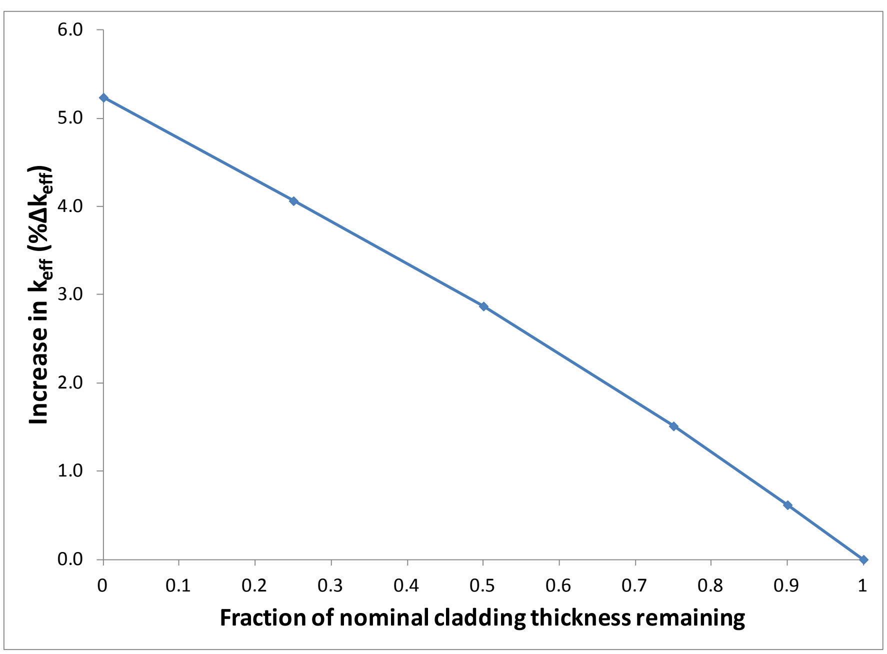

Figure B-3. Increase in k_{eff} in MPC-24 due to reduced cladding thickness.

B.2.1.2 Rod Failures

Each of the 39 unique eighth-assembly symmetric rods is removed individually to determine its worth, as discussed in Section 3.1.2.1. A sketch showing the eighth-assembly symmetry and row and column labels is provided in Figure 7. Table B-4 presents the rod locations whose best estimate worth is greater than 0.1% Δk_{eff}. Both the locations of these rods and the magnitude of the change in k_{eff} caused by rod failure are in good agreement with the previous work documented in Ref. 7. The columns in the assembly are designated with a letter, from A to Q, and the rows are designated with numbers, from 1 to 17, as shown in Figure 7. The maximum k_{eff} increase is associated with rod H8 and is 0.15% Δk_{eff}.

Multiple rods are removed in groups, as discussed in Section 3.1.2.2. Groups of 2, 4, 8, 12, 16, 24, 32, 40, 44, 48, and 52 rods are considered. The k_{eff} increase is shown as a function of rods removed in Figure B-4. The limiting lattice is shown in Figure B-5. The maximum k_{eff} value occurs for 48 rods removed and corresponds to a k_{eff} increase of 2.01% Δk_{eff}.

Table B-4. Single rod removal results for 17 × 17 OFA in MPC-24

Rod location	Increase in k_{eff} (% Δk_{eff})
H8	0.15
H5	0.13
H7	0.13
G5	0.12
I7	0.12
I8	0.12
I4	0.11
G7	0.11
G6	0.11

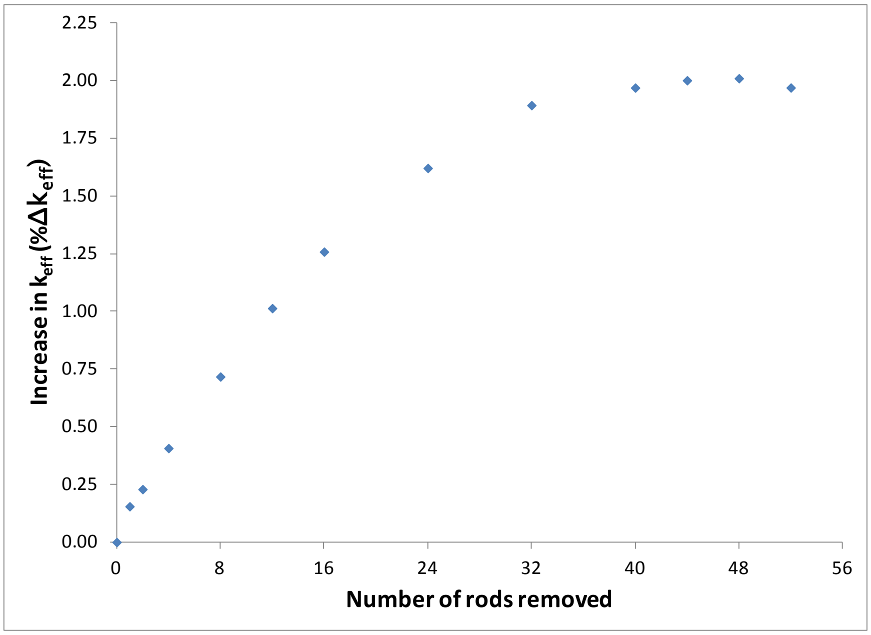

Figure B-4. Increase in k_{eff} in MPC-24 versus number of rods removed.

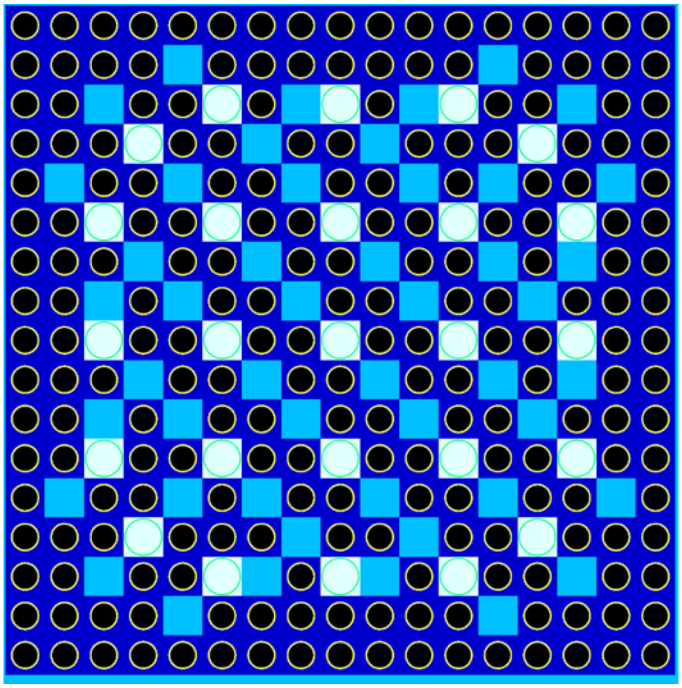

Notes: Fuel shown in black
Water is shown in light blue, dark blue, and white
Guide/instrument tubes contain water shown in white
Missing fuel rod locations shown in light blue

Figure B-5. Limiting multiple rod removal lattice (48 rods removed).

B.2.1.3 Loss of Rod Pitch Control

The loss of rod pitch control is modeled as a uniform increase in fuel assembly pitch, as discussed above in Section 3.1.3. Two different fuel storage cell sizes exist in the MPC-24 basket, as discussed in Appendix D. The four oversized storage cells allow for a larger uniform pitch than the 20 standard storage cells. The fuel assemblies in each type of cell are expanded to account for the larger possible pitch in the oversized storage cells. The maximum increase in k_{eff} is 2.88% Δk_{eff} with cladding intact and 6.83% Δk_{eff} with cladding removed. The increase in k_{eff} as a function of fuel rod pitch is shown in Figure B-6. The pitch used in the standard and oversized storage cells is the same until the pitch reaches approximately 1.31 cm. For the largest pitch, the assemblies in the oversized storage cells have a larger pitch than those in the standard cells so that the fuel rods are in contact with the cell walls in both cell types. A portion of the limiting configuration model with cladding intact is shown in Figure B-7. This result agrees well with the results provided in Ref. 7. Radial nonuniform pitch, as discussed in Section 3.1.3.1, is not considered in the MPC-24 cask.

The MPC-24 cask contains fresh fuel, so the most reactive axial portion of the assembly is the center. For that reason, the birdcage analysis, as discussed in Section 3.1.3.2, includes two compressed pitch sections symmetrically positioned above and below the mid-plane of the assembly. A range of center section and compressed section lengths is considered. A figure showing the axial pitch variation is included as Figure B-8. There is no k_{eff} increase associated with an axially variable fuel rod pitch for the MPC-24 model beyond the 2.88% Δk_{eff} resulting from uniform pitch expansion.

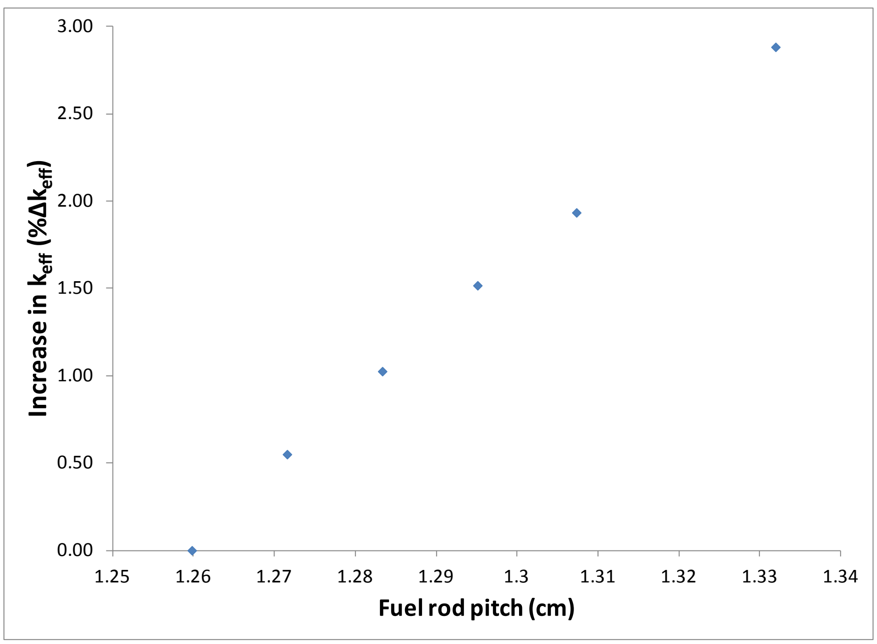

Figure B-6. Increase in k_{eff} in MPC-24 as a function of fuel rod pitch.

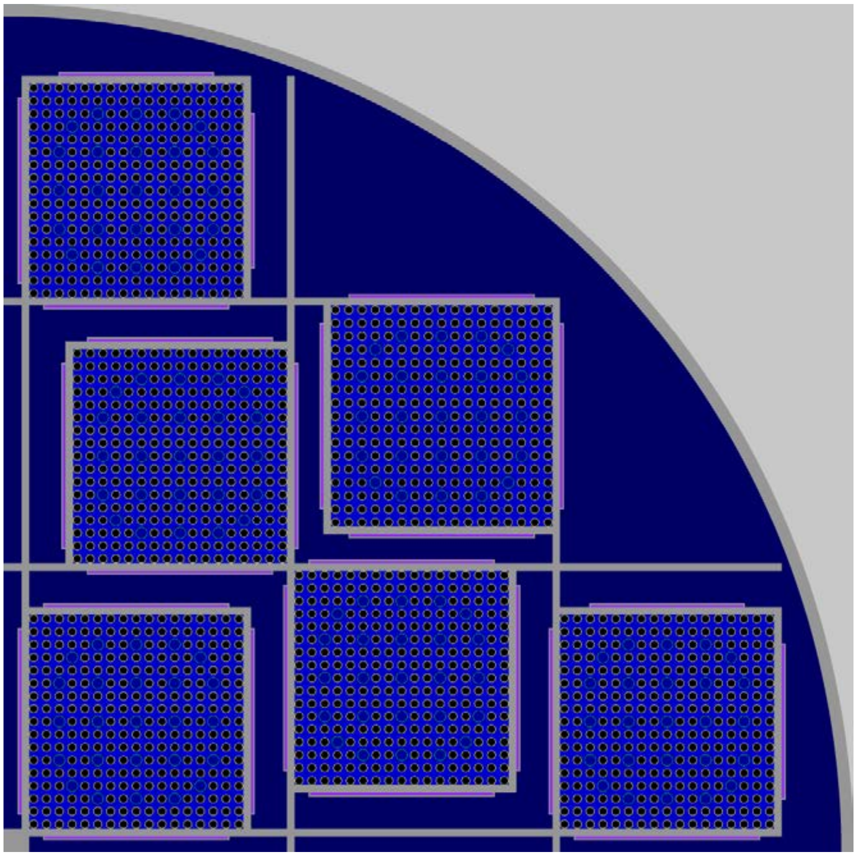

Figure B-7. Maximum pitch expansion case in MPC-24.

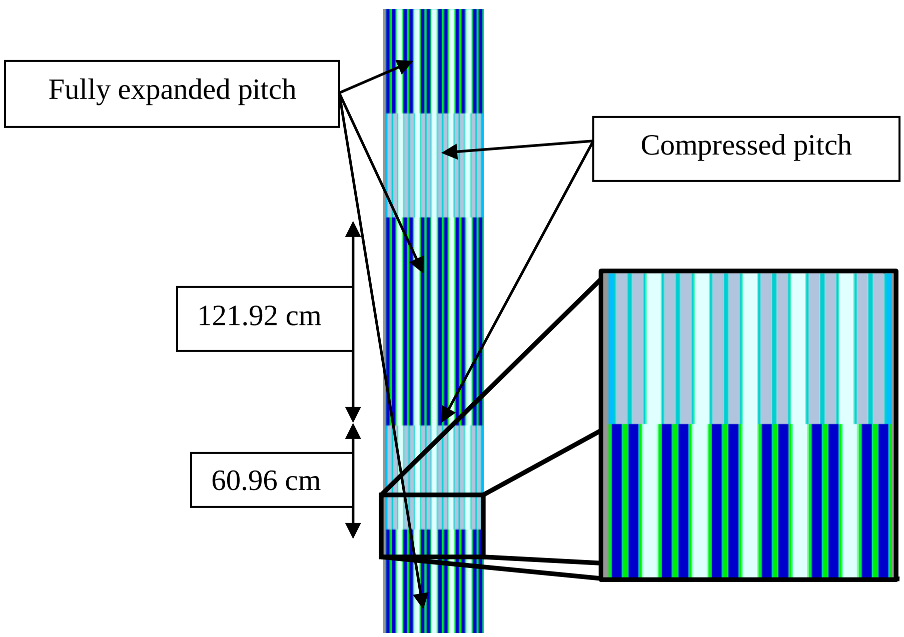

Figure B-8. Example axial variation of pitch expansion in MPC-24.

B.2.1.4 Loss of Assembly Position Control

Assembly misalignment is calculated over a range of displacements, as shown in Figure B-9. The consequence of the maximum misalignment is over 7% Δk_{eff}. A more limited misalignment case (20 cm) is also evaluated as a surrogate for potential degradation of assembly end fittings or the spacers used inside the cask to ensure proper assembly alignment. The consequence of this more limited misalignment case, shown in Figure B-10, is significantly less.

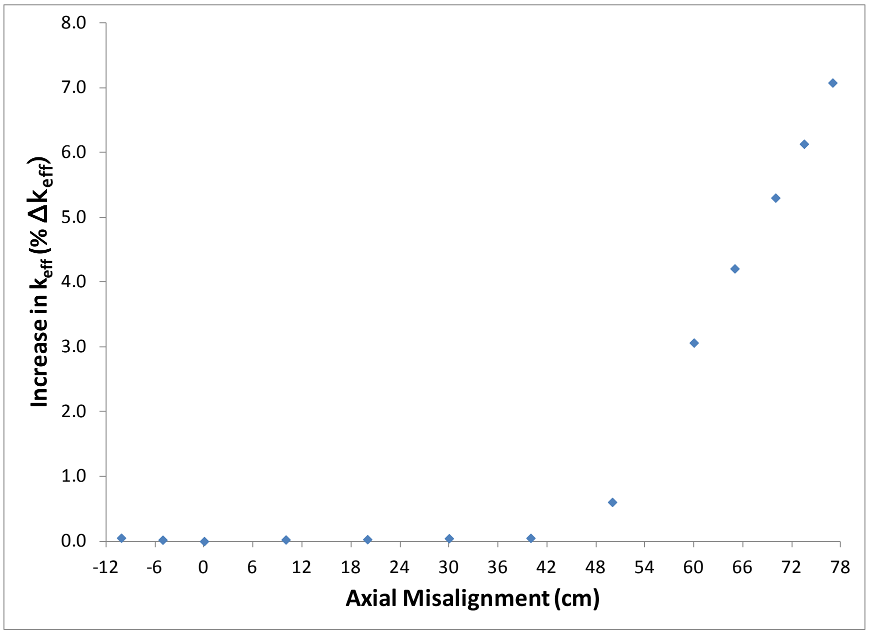

Figure B-9. Increase in k_{eff} as a function of axial assembly misalignment in MPC-24.

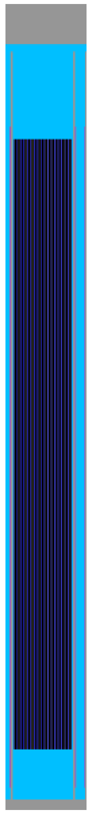

Figure B-10. Assembly in MPC-24 misaligned 20-cm toward cask lid.

B.2.1.5 Gross Assembly Failure

The two gross assembly failure configurations described in Section 3.1.5 are investigated in the MPC-24 cask. As expected, this configuration has the highest reactivity increase: the ordered pellet array case has a larger k_{eff} increase than the homogeneous rubble case. The k_{eff} increase in the homogeneous rubble case is over 8% Δk_{eff}, and the ordered pellet array case increases k_{eff} by over 13.5% Δk_{eff}. The gross assembly failure configurations are illustrated in Figure B-11 and Figure B-12. The configuration with homogeneous rubble contained only in the neutron absorber elevations is not considered in the MPC-24.

The results for the ordered pellet array case are significantly higher than those reported previously in Ref. 7. This is primarily because the array is also allowed to extend beyond the neutron absorber panel elevations. The homogeneous rubble case was not included in Ref. 7.

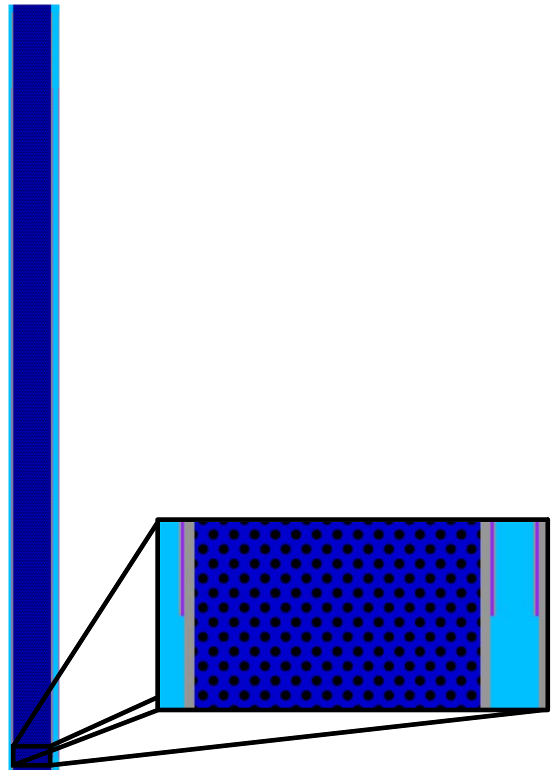

Figure B-11. Ordered pellet array configuration for gross assembly failure.

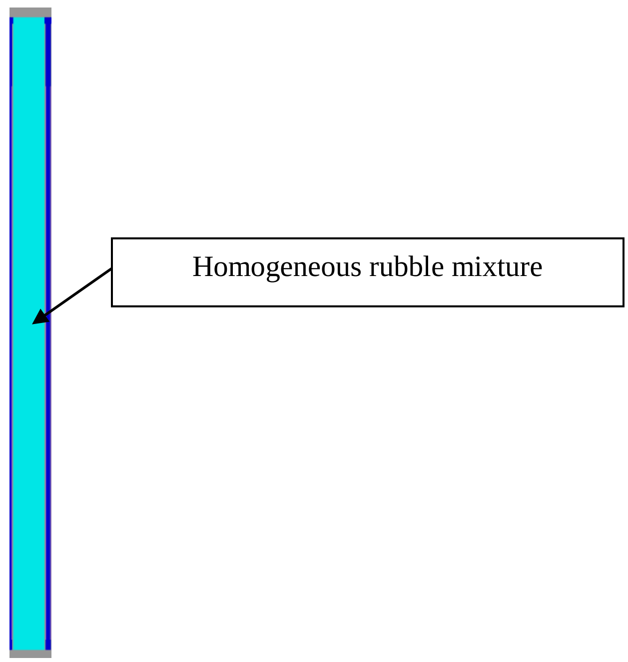

Figure B-12. Homogeneous rubble configuration for gross assembly failure.

B.2.1.6 Preferential Flooding

The preferential flooding configuration that leaves the flux traps dry in the basket is considered only for the MPC-24 cask, as mentioned in Section B.1. The results indicate an increase in k_{eff} of more than 16.5% Δk_{eff}. A preferential flooding configuration is shown in Figure B-13.

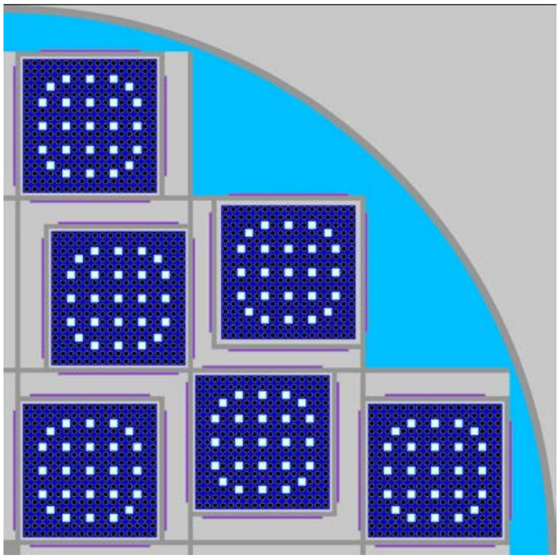

Notes: Fuel shown in black
Water is shown in light blue, dark blue, and white
Guide/instrument tubes contain water shown in white
Void in the basket and outside the cask is shown in light grey

Figure B-13. Preferential flooding with only the fuel assemblies flooded.

B.2.1.7 Neutron Absorber Degradation

The results of the calculations, described in Section 3.1.6.1, considering a 5-cm neutron absorber defect at varying elevations are presented in Table B-5. As expected, the limiting elevation is at the centerline of the active fuel height. The model containing the 5-cm gap is shown in Figure B-14. The k_{eff} increase for this location is 0.35% Δk_{eff} and increases to 1.07% Δk_{eff} if the defect size is increased to 10 cm. As discussed in Section 3, these defects are assumed to be present at the same elevation in all neutron absorber panels within the cask.

The results of the uniform absorber panel thinning calculations described in Section 3.1.6.3 are provided in Table B-6 and Figure B-15. A 50% decrease in panel thickness creates a 1.11% increase in k_{eff}. Complete removal of all neutron absorber material increases k_{eff} by over 11% Δk_{eff}, but the magnitude of the increase does not exceed 3% Δk_{eff} until more than 80% of the absorber has been eliminated.

Table B-5. Increase in k_{eff} in MPC-24 caused by a 5-cm neutron absorber defect at various elevations

Defect elevation midpoint (cm above bottom of active fuel)	Increase in k_{eff} (% Δk_{eff})
2.50	0.03
91.44	0.28
182.88	0.35
274.32	0.26
363.26	0.03

Table B-6. Increase in k_{eff} in MPC-24 caused by uniform neutron absorber panel thinning

Fraction of neutron absorber panel thickness remaining	Increase in k_{eff} (%Δk_{eff})
0.9	0.16
0.8	0.35
0.7	0.53
0.6	0.81
0.5	1.11
0.4	1.50
0.3	2.08
0.2	2.96
0.1	4.65
0.0	11.42

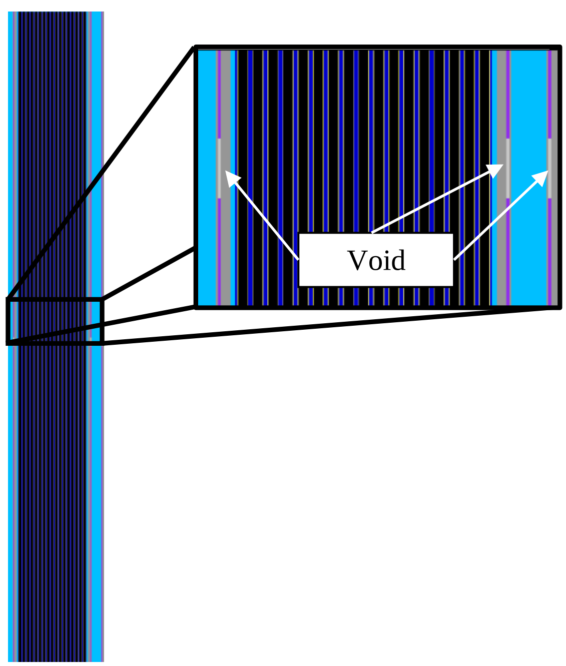

Figure B-14. 5-cm gap in neutron absorber panels in MPC-24.

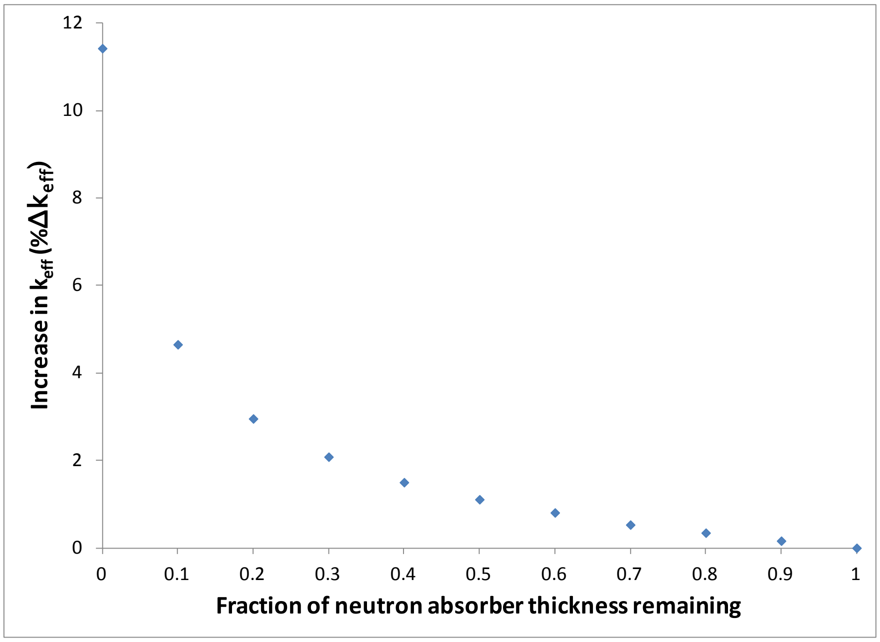

Figure B-15. Increase in k_{eff} in MPC-24 as a function of neutron absorber panel thickness.

B.2.2 Varying Number of Reconfigured Assemblies

The results presented in Section B.2.1 assume that all 24 fuel assemblies in the MPC-24 cask experience the same fuel or neutron absorber reconfiguration within the respective configuration of interest. For each of four of the configurations studied in Section B.2.1, a series of calculations is performed to establish the k_{eff} increase as a function of the number of reconfigured assemblies within the cask. The four configurations considered are the limiting conditions for single rod failure, multiple rod failure, uniform rod pitch increase, and homogeneous rubble resulting from gross assembly failure.

The first fuel assembly to experience the reconfiguration being examined is selected in an attempt to maximize the k_{eff} increase, and is therefore one near the center of the cask. Additional assemblies are added in mostly symmetric groups of equal distance from the first reconfigured assembly. For some low numbers of reconfigured assemblies, multiple combinations of assemblies are considered. Seven combinations of reconfigured assemblies less are considered in the MPC-24. One order in which the assemblies experience reconfiguration is shown in Figure B-16.

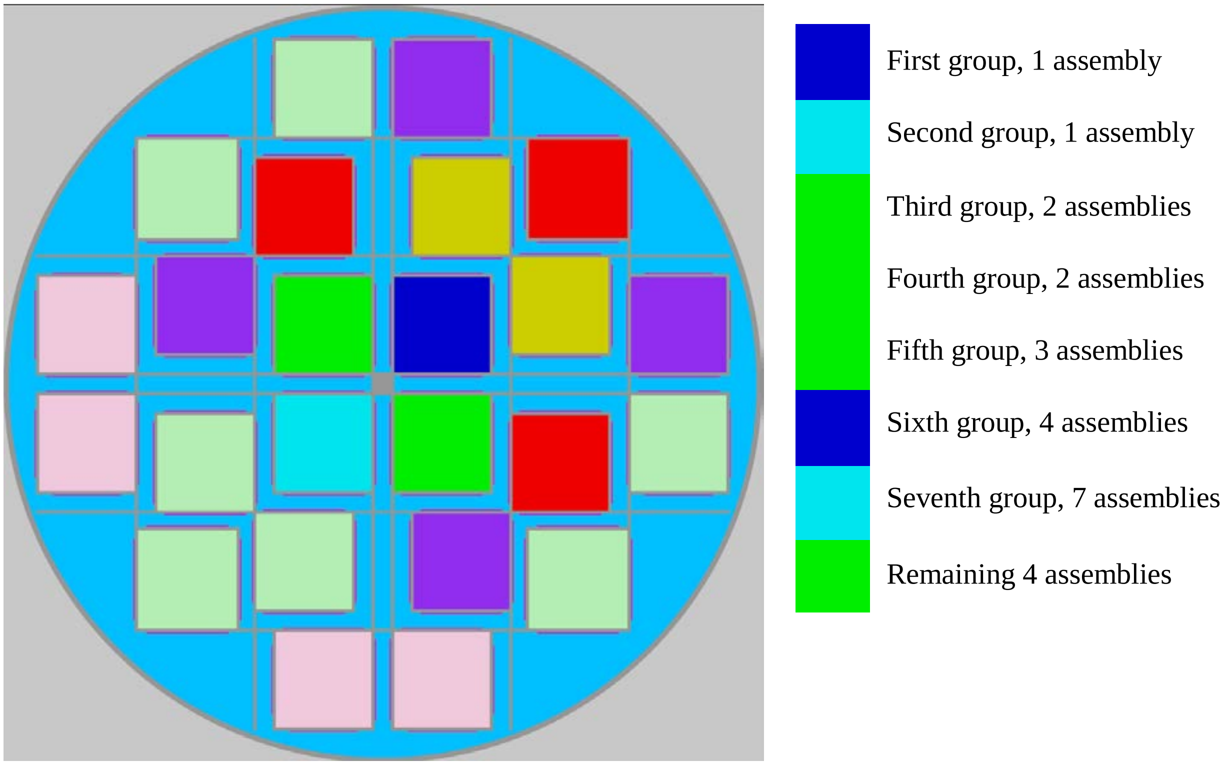

Figure B-16. One order of assembly reconfiguration in MPC-24 partial degradation configurations.

B.2.2.1 Rod Failures

The single and multiple rod failure configurations that result in the largest increase in k_{eff}, as discussed in Section B.2.1.2, are used to study the impact of some assemblies suffering reconfiguration while others in the cask remain intact. The results for single rod failure are shown below in Table B-7 and Figure B-17. The results for multiple rod failure are shown below in Table B-8 and Figure B-18. The portion of the k_{eff} impact introduced by each group of assemblies is similar for both configurations, with more than 50% of the reactivity change coming after only four assemblies experience reconfiguration. More than 75% of the k_{eff} change is caused by the first 13 assembly reconfigurations, which account for just over half the cask load. This indicates that a reduced number of reconfigured assemblies will not significantly reduce the k_{eff} increase associated with fuel reconfiguration if the degraded assemblies are in close proximity, and particularly if they are in the center region of the cask.

Table B-7. Increase in k_{eff} in MPC-24, single rod failure

Number of degraded assemblies	Increase in k_{eff} (% Δk_{eff})
1	0.04
2	0.06
2	0.06
4	0.08
5	0.09
9	0.11
13	0.12
20	0.14
24	0.15

Table B-8. Increase in k_{eff} in MPC-24, multiple rod failures (48 failed rods)

Number of degraded assemblies	Increase in k_{eff} (% Δk_{eff})
1	0.34
2	0.56
2	0.60
4	1.11
5	1.10
9	1.53
13	1.69
20	1.98
24	2.01

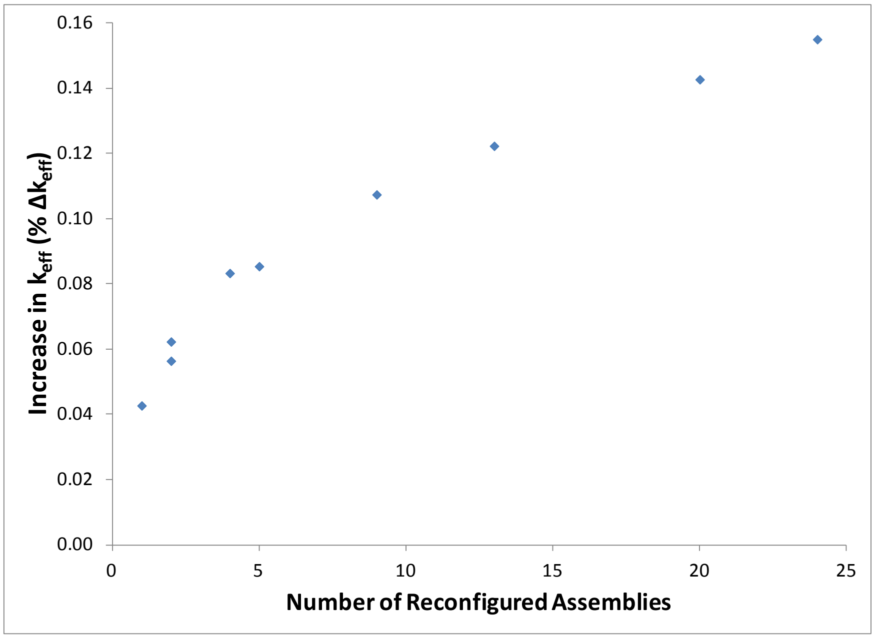

Figure B-17. Single rod failure results for a range of number of assemblies experiencing reconfiguration in MPC-24.

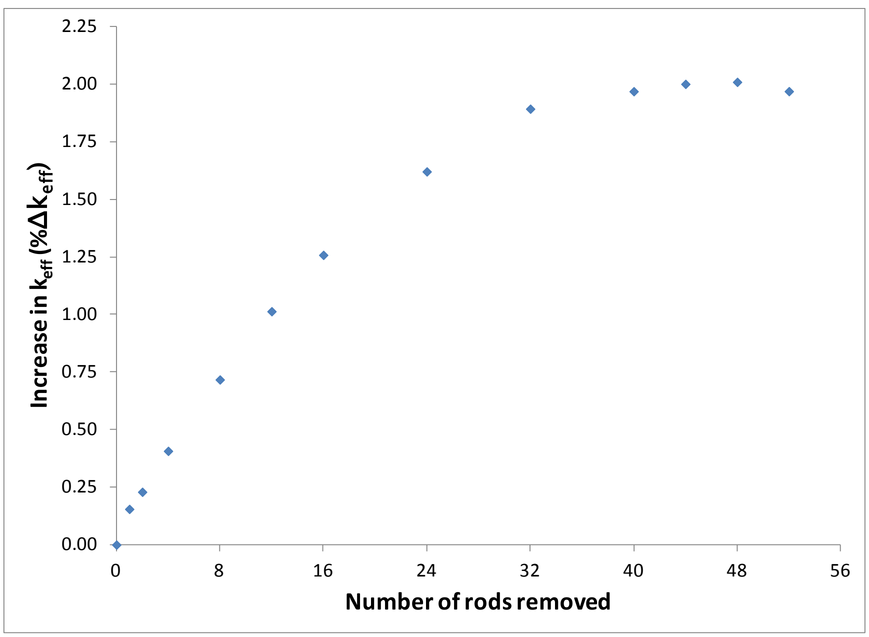

Figure B-18. Multiple rod failure results for a range of number of assemblies experiencing reconfiguration in MPC-24.

B.2.2.2 Loss of Rod Pitch Control, Uniform Pitch Increase

The maximum uniform pitch increase case is used to examine the k_{eff} impact of varying the number of assemblies that have experienced reconfiguration. The assembly configuration used for this study models

the outer row of fuel rods in contact with the inner wall of the fuel storage basket in each cell. The increase in k_{eff} for each number of reconfigured assemblies is provided in Table B-9 as well as Figure B-19. The general trend in the k_{eff} change for the uniform pitch increase cases is similar to that for single and multiple rod failure configurations presented in Section B.2.2.1. The first two reconfigured assemblies insert about 25% of the total k_{eff} increase, and 50% of the change has occurred with about five reconfigured assemblies. Approximately 80% of the increase in k_{eff} is caused by the first 13 reconfigured assemblies. This indicates that a reduced number of reconfigured assemblies will not significantly reduce the k_{eff} increase associated with fuel reconfiguration if the degraded assemblies are in close proximity, and particularly if they are in the center region of the cask.

Table B-9. Increase in k_{eff} in MPC-24, uniform pitch increase

Number of degraded assemblies	Increase in k_{eff} (% Δk_{eff})
1	0.37
2	0.73
2	0.70
4	1.39
5	1.54
5	1.41
9	2.08
13	2.32
20	2.77
24	2.88

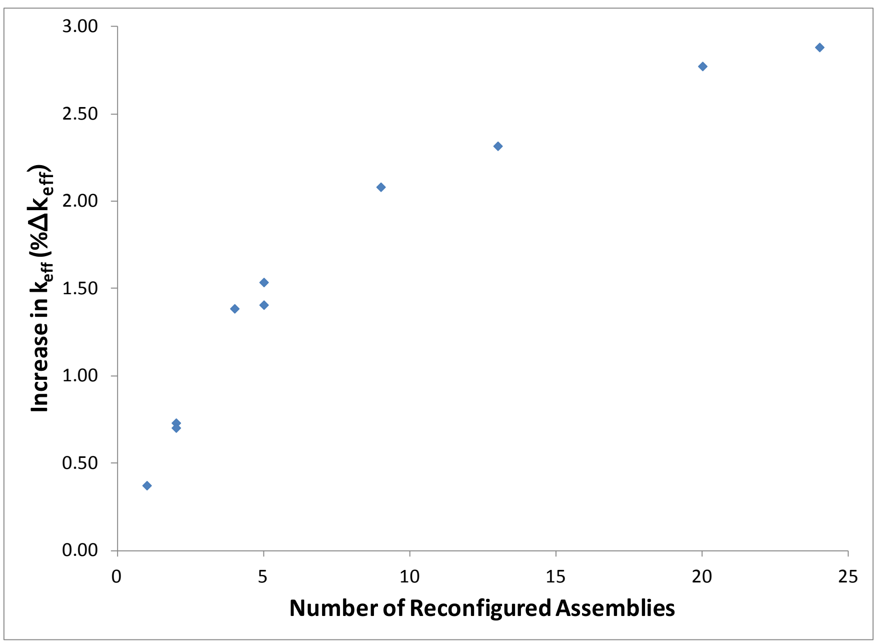

Figure B-19. Uniform pitch increase results for a range of number of assemblies experiencing reconfiguration in MPC-24.

B.2.2.3 Gross Assembly Failure, Homogeneous Rubble

The homogeneous rubble modeling of the gross assembly failure configuration is the final configuration used to examine the k_{eff} impact of varying the number of assemblies that have experienced reconfiguration. The configuration used for this study models the homogeneous smear of fuel, cladding, and water filling the entire inside volume of the storage cell from the base plate to the lid of the cask. This configuration resulted in the largest k_{eff} increase of the homogeneous rubble configurations used in Section B.2.1.5. The increase in k_{eff} for each number of reconfigured assemblies is provided in Table B-10 as well as Figure B-20. The general trend in the k_{eff} change for the uniform pitch increase cases is different from that for single and multiple rod failure and uniform pitch expansion configurations presented in Sections B.2.2.1 and B.2.2.2. The first two reconfigured assemblies lower the cask k_{eff} because of the effects of homogenization and fissile material relocation. An increase in k_{eff} is noted for four or more reconfigured assemblies after a sufficient number of assemblies are reconfigured to relocate the most reactive portion of the cask to the top of the homogeneous rubble. Nearly 70% of the increase in k_{eff} is caused by the first nine reconfigured assemblies, and more than 80% of the total k_{eff} increase results from the reconfiguration of 13 assemblies. This indicates that a reduced number of reconfigured assemblies will not significantly reduce the k_{eff} increase associated with fuel reconfiguration if the degraded assemblies are in close proximity, and particularly if they are in the center region of the cask.

Table B-10. Increase in k_{eff} in MPC-24, homogeneous rubble configuration of gross assembly failure

Number of degraded assemblies	Increase in k_{eff} (% Δk_{eff})
1	0.00
2	-0.04
2	-0.03
4	2.39
5	2.21
9	5.68
13	6.68
20	7.92
24	8.23

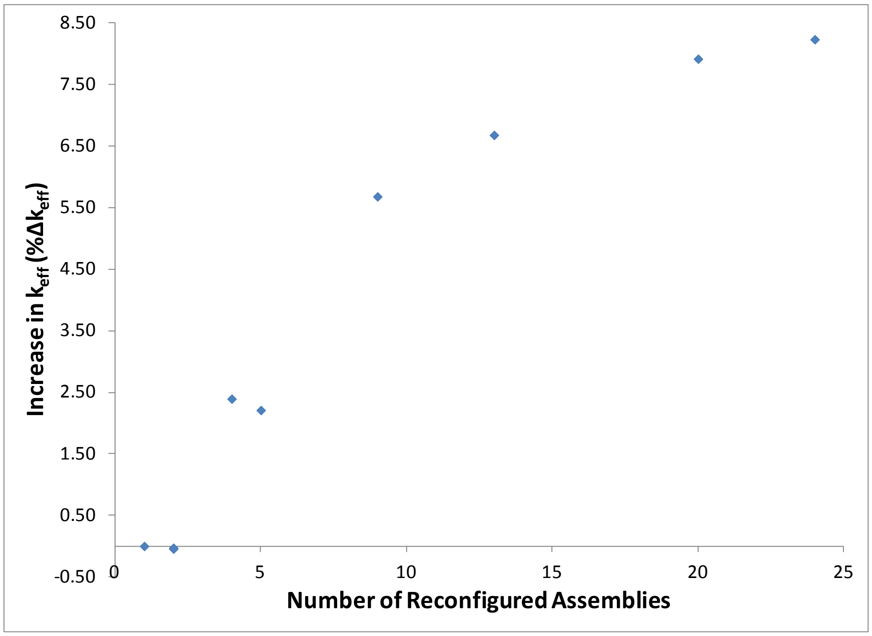

Figure B-20. Homogeneous rubble results for a range of number of assemblies experiencing reconfiguration.

B.2.3 Combined Configurations

As discussed in Section 3.3, some of the mechanisms that could result in fuel reconfigurations could result in a combination of reconfigurations. Combined configurations are evaluated including: 12 failed rods with 50% clad thinning and 12 failed rods with a uniform pitch increase of 0.023-cm.

The multiple rod failure results presented in Section B.2.1.2 indicate that the failure of 12 fuel rods results in an increase in k_{eff} of just over 1% Δk_{eff}. This is approximately half the maximum increase for multiple failed rod configurations and is therefore selected as an intermediate configuration. The pitch increase is approximately half of the maximum pitch increase in the 20 normal storage cells. Based on the results presented in Figure B-6, the k_{eff} increase associated with a fuel rod pitch increase of approximately 0.02 cm is around 1% Δk_{eff}. The cladding thickness on all intact rods in both combined configurations is represented with 50% of the nominal thickness.

The results of the two combined configurations considered in the MPC-24 cask are presented in Table B-11. For comparison, the k_{eff} increase assuming each degraded configuration separately and the sum of the two is provided. The increase in k_{eff} associated with explicit modeling of the combined configurations is less than the estimated increase based on summing the individual increases. The conservatism of adding the separate effects is less than 0.5% Δk_{eff}. It appears that the linear combination of the k_{eff} increases is conservative, but more combined configurations would need to be investigated prior to drawing general conclusions. If it is confirmed, the k_{eff} increase caused by combinations of degradations could be conservatively bounded by adding the increase associated with individual configurations where applicable.

Table B-11. Increase in k_{eff} in combined configurations for MPC-24

Case	Increase in k_{eff} (% Δk_{eff})
Multiple failed rods and clad thinning	
12 failed rods	1.01
50% clad thinning	2.87
Sum of k_{eff} increases	3.88
Combined configuration model	3.45
Overestimation of k_{eff} increase by summing individual effects	0.43
Multiple failed rods and 0.02-cm increase in fuel rod pitch	
12 failed rods	1.01
Uniform pitch increase	1.03
Sum of k_{eff} increases	2.04
Combined configuration model	1.88
Overestimation of k_{eff} increase by summing individual effects	0.16

B.3 MPC-24 CASK SUMMARY

The detailed results for each configuration considered in the MPC-24 are provided above in Section B.2 and summarized in Table B-2.

The highest k_{eff} impact involves the preferential flooding of the cask basket in such a way as to moderate the fuel but leave the flux traps dry. The flux traps are an essential feature of the cask, and the basket is designed to make this preferential flooding configuration impossible. The preferential flooding configuration is thus viewed as not credible for normal conditions of transport. The configuration is included here to emphasize the importance of maintaining flux trap integrity despite any degradation of fuel, basket, or cask materials that occur during ES.

Other significant k_{eff} increases result from the gross assembly failure configurations and large axial misalignments. The gross assembly failure and misalignment configurations are judged not to be credible, so the k_{eff} increase associated with these configurations does not require mitigation. Fuel assembly misalignment of as much as 50 cm results in a k_{eff} increase of less than 1% Δk_{eff}, as shown in Figure B-9. Fuel assembly axial position will be sufficiently controlled that the more extreme misalignments need not be considered. The remaining degraded configurations all have k_{eff} increases less than 3% Δk_{eff}. The consequences of potential fuel reconfiguration are therefore judged to be manageable. The k_{eff} increase is small enough that the cask will be subcritical considering a safety analysis with intact fuel, which demonstrates that k_{eff} will be less than 0.95. This would not, however, be in compliance with current regulations relating to transportation of fissile material.

Analyses of a range of assemblies experiencing reconfiguration are documented in Section B.2.2. Four configurations, listed in Section 3.2, are evaluated, and the relative increase in k_{eff} as a function of the number of assemblies experiencing reconfiguration is largely similar among all four configurations. This approach is unlikely to produce a significant reduction in the increase in k_{eff} because the majority of the increase is associated with a relatively small fraction of the fuel load suffering reconfiguration if the reconfigured assemblies are selected in a worst-case, deterministic approach.
Two configurations are also investigated in Section B.2.3 that are created by combining two different reconfiguration paths. An intermediate number of failed rods, in this case 12, is combined with clad thinning in one case and with uniform pitch expansion in another. In both cases, the sum of the k_{eff}

increases of each separate reconfiguration is slightly less than the increase determined from an explicit model of the combined configurations.

Appendix C

Sensitivity to Burnup and Cooling Time

A range of post-irradiation cooling times is considered in these analyses for both PWR and BWR fuel. Reference 44 provides details on the reactivity changes experienced by used fuel as a function of time since discharge. For the "Set 2" isotopes considered in these analyses, the reactivity of the depleted fuel decreases fairly steadily between 5 and about 100 years after discharge. The primary decays that drive this change are ^{241}Pu into ^{241}Am (14.4-year half-life) and ^{155}Eu into ^{155}Gd (4.8-year half-life). Beyond about 100 years after discharge, the reactivity of the fuel increases primarily due to the decay of ^{241}Am (433-year half-life) and ^{240}Pu (6561-year half-life). This increase continues until about 20,000 years after discharge. A plot for used PWR fuel considering the "Set 2" isotopes is shown in Figure C-1 and is expected to be similar for BWR fuel as well. Note that the maximum reactivity of used fuel considering "Set 2" isotopes occurs at discharge, and the reactivity after 5 years of cooling time is higher than the subsequent local maximum around 20,000 years later. These analyses considered cooling times ranging from 5 years to 300 years, with explicit reconfiguration calculations at cooling times of 5, 80, and 300 years. The effects of cooling time on the various configurations are considered, and they are discussed in more detail in the following subsections.

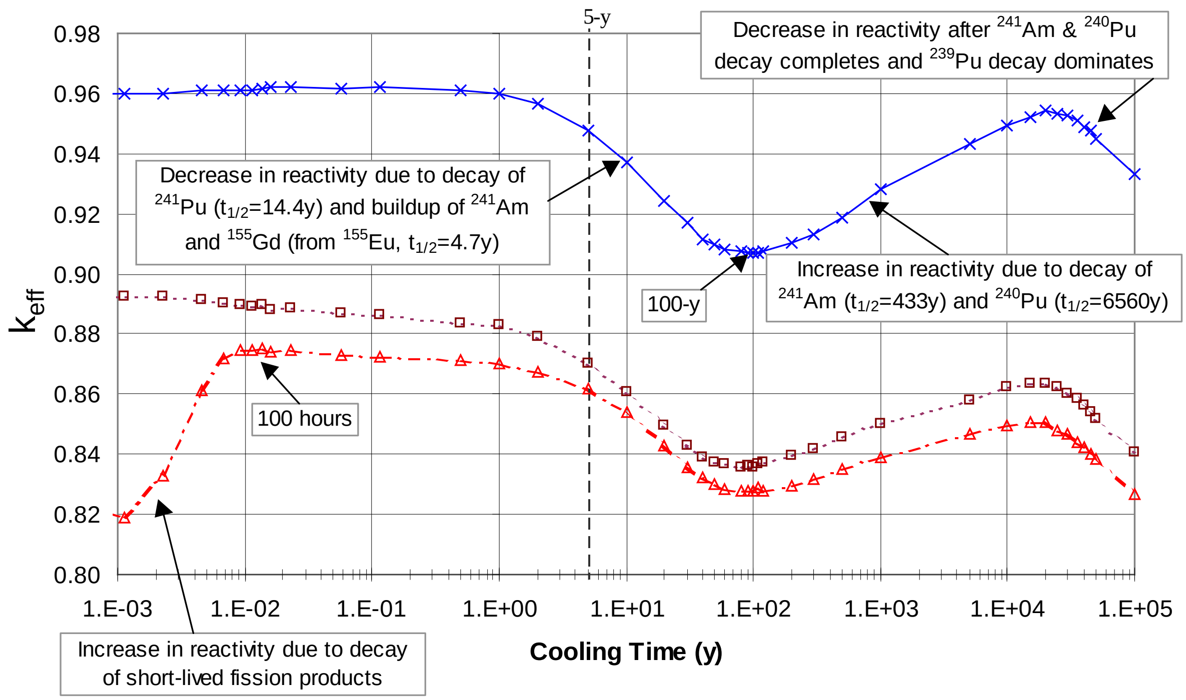

Figure C-1. Reactivity behavior of fuel with cooling time in a GBC-32 cask (4.0 w/o 40 GWd/MTU burnup) [44].

C.1 RESULTS FOR GBC-32 CASK

As discussed in Section 4.2.1, a range of initial fuel enrichments is considered to generate a representative loading curve for fuel to be stored in the GBC-32. The burnup limit for loading fuel with an initial enrichment of 5 w/o ^{235}U is determined to be approximately 44.25 GWd/MTU with 5 years of post-irradiation cooling time. Fuel with a discharge burnup of 70 GWd/MTU is also considered in the GBC-32 to investigate any potential sensitivity of the consequences of fuel reconfiguration to burnup. For both 5 w/o initial enrichment burnups, cooling times of 5, 80 and 300 years are considered to examine potential impacts of cooling time on the consequences of fuel reconfiguration.

The nominal condition k_{eff} values are provided in Table C-1. The reduction in k_{eff} caused by cooling time increases with burnup, which is expected given the larger inventory of ^{241}Am and ^{155}Gd at higher burnups. The 80-year cooling time also has the smallest k_{eff} for intact fuel, which is also expected as discussed above. It should be noted that the nominal k_{eff} values after 300 years of cooling time are still significantly lower than those after 5 years of cooling time. This decrease in k_{eff} for intact fuel would have to be exceeded by a larger k_{eff} increase due to reconfiguration before the longer cooling time case would represent a limiting condition. The results of explicit reconfiguration calculations are presented in subsequent subsections and compared to the differences in nominal k_{eff} values.

Table C-1. Nominal k_{eff} results for enrichment, burnup, and cooling time cases considered in GBC-32

Enrichment (w/o ^{235}U)	Burnup (GWd/MTU)	Cooling time (years)	KENO V.a		KENO-VI	
			k_{eff}	σ	k_{eff}	σ
5.0	44.25	5	0.94000	0.00010	0.93995	0.00010
		80	0.90003	0.00010	0.89991	0.00010
		300	0.90477	0.00010	0.90473	0.00010
	70.0	5	0.85040	0.00010	0.85048	0.00010
		80	0.78863	0.00010	0.78865	0.00010
		300	0.79472	0.00010	0.79478	0.00010

C.1.1 Clad Thinning/Loss

The increase in k_{eff} associated with clad thinning and removal is shown as a function of remaining cladding thickness in Figure C-2 for fuel of both burnups and all three cooling times. There is a trend that the increase in k_{eff} is smaller at 70 GWd/MTU than it is at 44.25 GWd/MTU. The increase in k_{eff} is approximately 0.04% Δk_{eff} larger after 300 years of cooling time than it is after 5 years, but this difference is very small compared to the change in nominal k_{eff}. These results show that the increase in k_{eff} shown in Section 5.1.1.1 is sufficiently large.

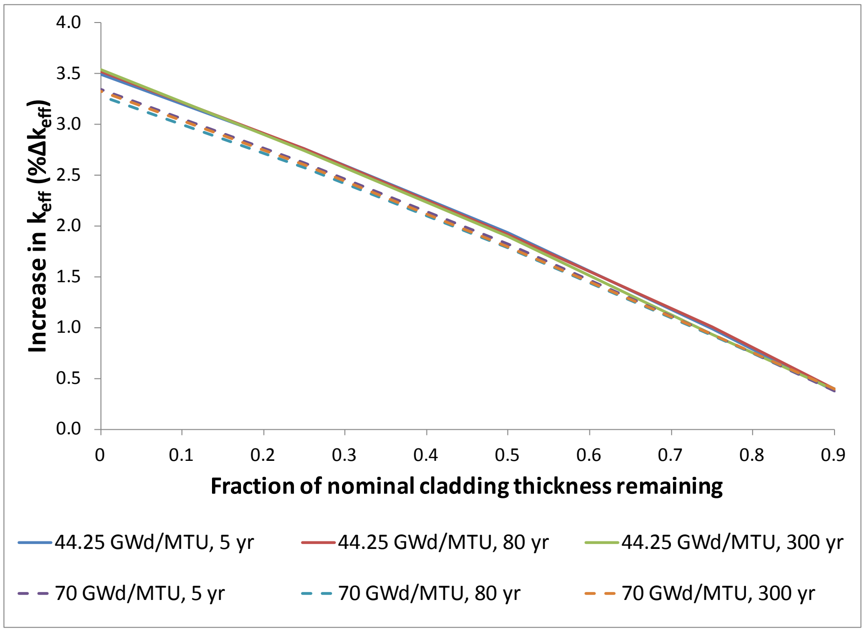

Figure C-2. Increase in k_{eff} as a function of cladding thickness remaining.

C.1.2 Rod Failures

The results of the single and multiple rod failure configurations of fuel rod failure are provided in Table C-2 and Table C-3, respectively. The variation of the increase in k_{eff} for single rod removal is small and shows no significant trends as a function of burnup or cooling time. The multiple rod removal results show a clear trend of reduced consequence at high burnup compared to moderate burnup; thus, the 44.25 GWd/MTU cases manifest a larger k_{eff} increase. The effect of cooling time appears to be significantly smaller, with essentially no sensitivity at 44.25 GWd/MTU, and only a reduction in the consequence of reconfiguration at longer cooling times for the high-burnup fuel. These results indicate that the k_{eff} increases identified in Section 5.1.1.2 are limiting.

Table C-2. Single rod removal results for 17 × 17 OFA in GBC-32

Burnup (GWd/MTU)	Cooling time (years)	Location	Increase in k_{eff} (% Δk_{eff})
44.25	5	H5	0.10
44.25	80	H7	0.09
44.25	300	G7	0.10
70	5	H5	0.09
70	80	G7	0.10
70	300	G5	0.10

Table C-3. Multiple rod removal results for 17 × 17 OFA in GBC-32

Burnup (GWd/MTU)	Cooling time (years)	Increase in k_{eff} (% Δk_{eff})
44.25	5	1.86
44.25	80	1.86
44.25	300	1.87
70	5	1.69
70	80	1.62
70	300	1.62

C.1.3 Loss of Rod Pitch Control

The increase in k_{eff} resulting from uniform pin pitch expansion for both burnups and all three cooling times is considered for the configuration in which the unit cell boundary contacts the inside surface of the storage cell wall. The use of this less extreme case provides an acceptable indication of the sensitivity of the consequence of this configuration to burnup and cooling time variations. The results of the fully expanded configuration, with cladding, are presented below in Table C-4. Moderate sensitivities are apparent that lower the impact of reconfiguration both with increasing burnup and with increasing cooling time for a fixed burnup. These results provide confidence that the results presented in Section 5.1.1.3 are limiting.

Table C-4. Increase in k_{eff} caused by uniform fuel pin pitch expansion

Burnup (GWd/MTU)	Cooling time (years)	Increase in k_{eff} (% Δk_{eff})
44.25	5	1.69
44.25	80	1.67
44.25	300	1.66
70	5	1.53
70	80	1.44
70	300	1.42

C.1.4 Loss of Assembly Position Control

The increase in k_{eff} caused by a 20-cm axial misalignment for both burnups and all three cooling times is presented in Table C-5. The results show that the consequence of fuel displacement increases with both burnup and cooling time. The maximum change relative to the 44.25 GWd/MTU and 5-year cooling is approximately 1.67% Δk_{eff}. This is a significant increase and occurs for 70 GWd/MTU and 300 years of cooling time. The reduction in base case k_{eff} due only to cooling time at this burnup is over 5.5% Δk_{eff}. The 300-year cooling time condition with only 44.25-GWd/MTU burnup causes an increase that is larger by 0.95% Δk_{eff}. For this case, the decrease in nominal (i.e., 44.25 GWd/MTU and 300-year cooling time) k_{eff} is more than 3.5% Δk_{eff}, when compared to the k_{eff} value for the case with only 5 years of cooling time. These results indicate that the results presented in Section 5.1.1.4 are large enough to account for additional impacts at high burnup and long cooling times.

Table C-5. Increase in k_{eff} for limited assembly axial displacement in GBC-32

Burnup (GWd/MTU)	Cooling time (years)	Increase in k_{eff} (% Δk_{eff})
44.25	5	10.82
44.25	80	11.82
44.25	300	11.77
70	5	11.74
70	80	12.46
70	300	12.49

C.1.5 Gross Assembly Failure

The results for both configurations of gross assembly failure are provided for both burnups and all three cooling times in Table C-6. Both the uniform pellet array and the homogeneous rubble configuration show little sensitivity to burnup but a larger increase in k_{eff} with increasing cooling time. The increases are smaller for the uniform pellet array configuration than for the homogeneous rubble configuration. The maximum difference is for fuel with 44.25-GWd/MTU burnup and 300 years of cooling time and is approximately 1.04% Δk_{eff}. The decrease in nominal k_{eff} for this fuel condition is more than 3.5% Δk_{eff}, so the results in Section 5.1.1.5 are sufficiently large to account for variations associated with higher burnups and longer cooling times.

Table C-6. Increase in k_{eff} caused by gross fuel assembly failure in GBC-32

Burnup (GWd/MTU)	Cooling time (years)	Increase in k_{eff} (% Δk_{eff})
Ordered pellet array		
44.25	5	21.37
44.25	80	22.21
44.25	300	22.21
70	5	21.43
70	80	21.63
70	300	21.77
Homogeneous rubble		
44.25	5	14.30
44.25	80	15.29
44.25	300	15.34
70	5	14.20
70	80	14.77
70	300	14.90

C.1.6 Neutron Absorber Degradation

The increase in k_{eff} caused by neutron absorber panel defects is shown in Table C-7 for both burnups and all three cooling times for defect sizes of both 5 and 10 cm. The results show an increase in the consequence of panel degradation at higher burnups and higher cooling times. The maximum change in

k_{eff} increase is approximately 0.3% Δk_{eff}, which is significantly smaller than the lower nominal k_{eff} at the higher burnups and cooling times. The results presented in Section 5.1.1.6 for the neutron absorber panel defect configuration are therefore large enough to account for the effects of higher burnups and cooling times.

The increase in k_{eff} increase due to uniform neutron absorber panel thinning at 44.25 GWd/MTU and 5 years of cooling time are shown in Table C-8. The increase in k_{eff} is smaller at the higher burnup, thus confirming that the results presented in Section 5.1.1.6 for uniform panel thinning are also conservative.

Table C-7. Increase in k_{eff} caused by neutron absorber panel defects

Burnup (GWd/MTU)	Cooling time (years)	Defect elevation (cm)	Increase in k_{eff} (% Δk_{eff})
5-cm defect			
44.25	5	348.86	1.05
44.25	80	348.86	1.22
44.25	300	348.86	1.21
70	5	348.86	1.17
70	80	348.86	1.24
70	300	348.86	1.24
10-cm defect			
44.25	5	348.86	2.33
44.25	80	348.86	2.59
44.25	300	348.86	2.56
70	5	348.86	2.54
70	80	348.86	2.59
70	300	348.86	2.63

Table C-8. Increase in k_{eff} caused by uniform neutron absorber panel thinning (44.25 GWd/MTU burnup, 5-year cooling time)

Fraction of neutron absorber panel thickness remaining	Increase in k_{eff} (%Δk_{eff})
0.9	0.25
0.8	0.53
0.7	0.87
0.6	1.26
0.5	1.72
0.4	2.30
0.3	2.99
0.2	3.94
0.1	5.36
0.0	8.46

C.2 RESULTS FOR MPC-68 CASK

As discussed in Section 4.2.2, a range of burnups and cooling times is considered to investigate the sensitivity of the consequence of reconfiguration to these parameters. Fuel with a discharge burnup of 70 GWd/MTU is considered in the MPC-68 in addition to the fresh fuel and 35-GWd/MTU burnup used discussed in Section 5.2. For fuel with 5 w/o initial enrichment and both 35-GWd/MTU and 70-GWd/MTU burnups, cooling times of 5, 80, and 300 years are considered to examine potential impacts of cooling time on the consequences of fuel reconfiguration.

The nominal condition k_{eff} values are provided in Table C-9. The reduction in k_{eff} caused by cooling time increases with burnup, which is expected given the larger inventory of ^{241}Am and ^{155}Gd at higher burnups. The 80-year cooling time also has the smallest k_{eff} for intact fuel, which is also expected as discussed above. It should be noted that the nominal k_{eff} values after 300 years of cooling time are still lower than after 5 years of cooling time. This decrease in k_{eff} for intact fuel would have to be exceeded by a larger k_{eff} increase due to reconfiguration before the longer cooling time case would represent a limiting condition. The reductions in nominal k_{eff} values for the BWR fuel in the MPC-68 are significantly smaller than those experienced by the PWR fuel in GBC-32, despite similar assembly average burnup values. This effect is the result of the extreme burnup profile, described in Appendix E, which has very low relative burnups in the top few nodes. These lower burnups lead to lower inventories of ^{241}Am and ^{155}Eu in the upper regions of the assembly which drive reactivity of the overall cask. These lower inventories lead to smaller changes in k_{eff} due to radioactive decay during the period of post-irradiation cooling. The results of explicit reconfiguration calculations are presented in subsequent subsections and compared to the differences in nominal k_{eff} values.

Table C-9. Nominal k_{eff} results for enrichment, burnup, and cooling time cases considered in MPC-68, channeled and unchanneled fuel

Channel present	Burnup (GWd/MTU)	Cooling time (years)	KENO V.a		KENO-VI	
			k_{eff}	σ	k_{eff}	σ
Yes	0	0	0.96800	0.00010	0.96828	0.00010
	35.0	5	0.83269	0.00010	0.83258	0.00010
		80	0.82425	0.00010	0.82416	0.00010
		300	0.82522	0.00010	0.82528	0.00010
	70.0	5	0.76709	0.00010	0.76693	0.00010
		80	0.75256	0.00010	0.75240	0.00010
		300	0.75412	0.00010	0.75405	0.00010
No	0	0	0.96768	0.00010	0.96763	0.00010
	35.0	5	0.83434	0.00010	0.83420	0.00010
		80	0.82615	0.00010	0.82621	0.00010
		300	0.82723	0.00010	0.82714	0.00010
	70.0	5	0.76994	0.00010	0.76971	0.00010
		80	0.75588	0.00010	0.75560	0.00010
		300	0.75731	0.00010	0.75705	0.00010

C.2.1 Clad Thinning/Loss

The increase in k_{eff} associated with clad thinning and removal is shown as a function of remaining cladding thickness in Figure C-3 for fresh fuel and fuel of both burnups and all three cooling times. There is a trend that the increase in k_{eff} is smaller with increasing burnup. There is no clear trend in the increase of k_{eff} as a function of cooling time. These results show that the increase in k_{eff} reported for fresh fuel in Section 5.2.1.1 bounds the effects of burnup and cooling time.

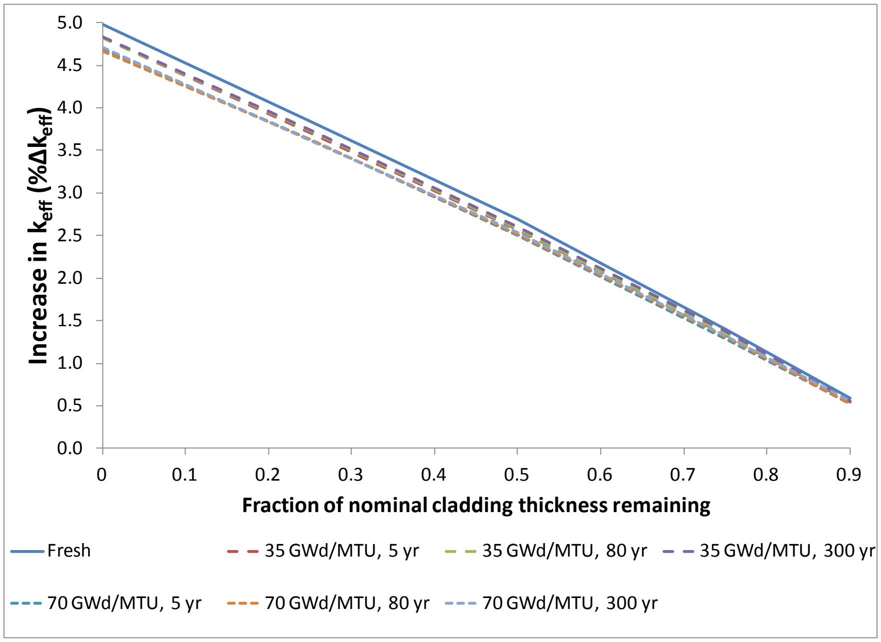

Figure C-3. Increase in k_{eff} as a function of cladding thickness remaining.

C.2.2 Rod Failures

The results of fuel reconfiguration calculations for the single and multiple rod removal configurations are shown below in Table C-10 and Table C-11, respectively. For single rod failure configurations, no sensitivity is apparent as a function of either burnup or cooling time. The fresh fuel single rod removal k_{eff} increase is larger than the results for UNF cases. For multiple rod failure configurations, a slight trend appears to cause small increases in k_{eff} change with cooling time but a decrease in k_{eff} change at high burnup. The largest difference compared to the results presented in Section 5.2.1.2 is approximately 0.02% Δk_{eff} and occurs for multiple rod failure and UNF with 300 years of cooling time. At this cooling time, the nominal k_{eff} is approximately 0.75% Δk_{eff} lower than the 5-year cooling time base case k_{eff} value. These results indicate that the increase in k_{eff} reported in Section 5.2.1.2 is sufficiently large to account for potential effects of additional burnup and cooling time for rod failure configurations.

Table C-10. Single rod removal results for GE 10 × 10 fuel in MPC-68, intact channel

Burnup (GWd/MTU)	Cooling time (years)	Location	Increase in k_{eff} (% Δk_{eff})
0	0	H7	0.29
35	5	G7	0.26
35	80	D4	0.27
35	300	G7	0.28
70	5	D3	0.26
70	80	G7	0.25
70	300	G7	0.26

Table C-11. Multiple rod removal results for GE 10 × 10 fuel in MPC-68, intact channel

Burnup (GWd/MTU)	Cooling time (years)	Increase in k_{eff} (% Δk_{eff})
0	0	2.24
35	5	2.40
35	80	2.40
35	300	2.42
70	5	2.30
70	80	2.31
70	300	2.32

C.2.3 Loss of Rod Pitch Control

The increase in k_{eff} resulting from uniform pin pitch expansion for fresh fuel as well as both burnups and all three cooling times is considered for the configuration in which the unit cell boundary contacts the inside surface of the storage cell wall. The use of this less extreme case provides an acceptable indication of the sensitivity of the consequence of this configuration to burnup and cooling time variations. The results of the fully expanded configuration, with cladding, are presented below in Table C-12. The increase in k_{eff} drops both as a function of burnup and cooling time, though the effect of burnup appears to be significantly larger. These results provide confidence that the results presented for fresh fuel in Section 5.2.1.3 bound the results for all burnups and cooling times.

Table C-12. Results for loss of rod pitch control with cladding intact in MPC-68

Burnup (GWd/MTU)	Cooling time (years)	Increase in k_{eff} (% Δk_{eff})
Channel intact		
0	0	11.00
35	5	9.55
35	80	9.46
35	300	9.49
70	5	8.68
70	80	8.51
70	300	8.52
Channel removed		
0	0	12.07
35	5	10.56
35	80	10.45
35	300	10.48
70	5	9.64
70	80	9.40
70	300	9.43

C.2.4 Loss of Assembly Position Control

The increase in k_{eff} caused by a 20-cm axial misalignment for both burnups and all three cooling times is presented in Table C-13. The results show that the consequence of fuel displacement increases with both burnup and cooling time. The 300-year cooling time condition with 35-GWd/MTU burnup causes an increase that is 0.37% Δk_{eff} larger than the 5-year cooling time. For this case, the decrease in nominal k_{eff} is more than 0.75% Δk_{eff}; thus, the cask with displaced fuel has a lower final k_{eff} value. The maximum change relative to the 35 GWd/MTU and 5-year cooling time is approximately 2.2% Δk_{eff} and occurs for 70 GWd/MTU and 300 years of cooling time. The reduction in base case k_{eff} due only to cooling time at this burnup is approximately 1.3% Δk_{eff}. The nominal k_{eff} for this high-burnup and high cooling time condition is significantly subcritical, so this fuel condition does not represent a challenge to the criticality safety of the cask.

Table C-13. Increase in k_{eff} for limited assembly axial displacement in MPC-68, intact channel

Burnup (GWd/MTU)	Cooling time (years)	Increase in k_{eff} (% Δk_{eff})
35	5	6.29
35	80	6.70
35	300	6.66
70	5	8.03
70	80	8.52
70	300	8.49

C.2.5 Gross Assembly Failure

The results for both configurations of gross assembly failure are provided for both burnups and all three cooling times in Table C-14. Both the uniform pellet array and the homogeneous rubble configuration show slightly larger k_{eff} increases at higher burnup, and a larger increase in k_{eff} with increasing cooling time. The increases are smaller for the homogeneous rubble configuration than for the uniform pellet array configuration. The maximum difference is for fuel with 70-GWd/MTU burnup and 300 years of cooling time and is approximately 1.23% Δk_{eff}. The decrease in nominal k_{eff} for this fuel condition is more than 1.30% Δk_{eff}, so the results in Section 5.2.1.5 are sufficiently large to account for variations associated with higher burnups and longer cooling times.

Table C-14. Increase in k_{eff} caused by gross fuel assembly failure in MPC-68

Burnup (GWd/MTU)	Cooling time (years)	Increase in k_{eff} (% Δk_{eff})
Homogeneous rubble, channel removed		
35	5	29.36
35	80	29.87
35	300	29.83
70	5	29.93
70	80	30.33
70	300	30.40
Uniform pellet array, channel removed		
35	5	34.40
35	80	34.88
35	300	34.87
70	5	35.22
70	80	35.57
70	300	35.63

C.2.6 Neutron absorber Degradation

The increase in k_{eff} caused by neutron absorber panel defects is shown in Table C-15 for both burnups and all three cooling times for a defect size of 5 cm and in Table C-16 for 10 cm defects. The results show an increase in the consequence of panel degradation at higher burnups and higher cooling times. The maximum change in k_{eff} increase is approximately 0.7% Δk_{eff}, which is smaller than the lower nominal k_{eff} at the higher burnups and cooling times. The results presented in Section 5.2.1.6 for the neutron absorber panel defect configuration are therefore large enough to account for the effects of higher burnups and cooling times.

The increase in k_{eff} increase due to uniform neutron absorber panel thinning at 35 GWd/MTU and 5 years of cooling time are shown in Table C-17. The increase in k_{eff} is smaller at the higher burnup, thus confirming that the results presented in Section 5.2.1.6 for uniform panel thinning are also conservative.

Table C-15. Maximum k_{eff} increase caused by a 5-cm neutron absorber defect in MPC-68, intact channel

Burnup (GWd/MTU)	Cooling time (years)	Defect elevation (cm)	Increase in k_{eff} (% Δk_{eff})
0	0	190.50	0.83
35	5	365.13	2.49
35	80	365.13	2.58
35	300	365.13	2.58
70	5	370.42	2.82
70	80	370.42	2.90
70	300	370.42	2.89

Table C-16. Maximum k_{eff} increase caused by a 10-cm neutron absorber defect in MPC-68, intact channel

Burnup (GWd/MTU)	Cooling time (years)	Defect elevation (cm)	Increase in k_{eff} (% Δk_{eff})
0	0	190.50	2.68
35	5	365.13	5.62
35	80	365.13	5.80
35	300	365.13	5.78
70	5	370.42	6.24
70	80	370.42	6.33
70	300	370.42	6.36

Table C-17. Increase in k_{eff} caused by uniform neutron absorber panel thinning (35-GWd/MTU burnup, 5-year cooling time)

Fraction of neutron absorber panel thickness remaining	Increase in k_{eff} (%Δk_{eff})
0.9	0.47
0.8	1.02
0.7	1.64
0.6	2.33
0.5	3.16
0.4	4.16
0.3	5.45
0.2	7.32
0.1	10.26
0.0	18.80

Appendix D

Details of Cask Modeling

This appendix provides additional details of the MPC-24 and MPC-68 cask models used in this analysis. Details of the GBC-32 cask are contained within Section 2.1 of Ref. 39.

D.1 MPC-24

The bottom of the active fuel is modeled 10.16 cm (4 in.) above the top surface of the cask base plate. The top of the active fuel is approximately 77 cm (30.3125 in.) from the bottom surface of the cask lid. The volume above and below the active fuel is normally occupied by spacers and fuel assembly hardware, but these are neglected in the model. The material in the spacers is not credited in any configuration, although the axial position control provided by the spacers is considered in assessing credibility of axial misalignment configurations. All fuel assemblies are modeled as nominally centered within the fuel storage cells in the MPC-24 basket.

The basket dimensions are provided in Table D-1. The basket is positioned on the cask base plate, creating a gap of approximately 4.60 cm (1 13/16 in.) between the top of the basket walls and the lower surface of the lid. The basket configuration consists of 20 standard storage cells and four oversized storage cells. The model is created with dimensions taken from the SAR for the HI-STAR 100 system, Refs. 36–38.

Two widths of neutron absorber panels are used in the MPC-24, and relevant dimensions are provided in Table D-2. The majority of the panels are “wide,” but 16 panels near the periphery of the basket are “narrow” panels. The locations containing narrow neutron absorber panels are indicated in Figure D-1. It is assumed that the entire panel thickness is neutron absorber; in other words, no face cladding is included in the panel models. The panels overlap the bottom of the active fuel by approximately 2.86 cm (1 1/8 in.) and overlap the top of the active fuel by approximately 27.6 cm (10 7/8 in.). The panel dimensions are taken from the SAR for the HI-STAR 100 system Refs. 36–38.

Table D-1. MPC-24 basket dimensions

Parameter	Dimension (cm)	Dimension (in.)
Wall thickness	0.79	0.3125
Basket height	448.31	176.5
Standard cell inner dimension	22.225	8.75
Oversized cell inner dimension	22.987	9.05

Table D-2. MPC-24 Neutron absorber panel dimensions

Parameter	Dimension (cm)	Dimension (in.)
Wide panel width	19.05	7.5
Narrow panel width	15.875	6.25
Panel thickness	0.26	0.101
Panel length	396.24	156
Panel axial position (from base plate)	7.30	2.875
Wrapper thickness	0.15	0.06
Neutron absorber areal density	0.0372 g $^{10}B/cm^2$	

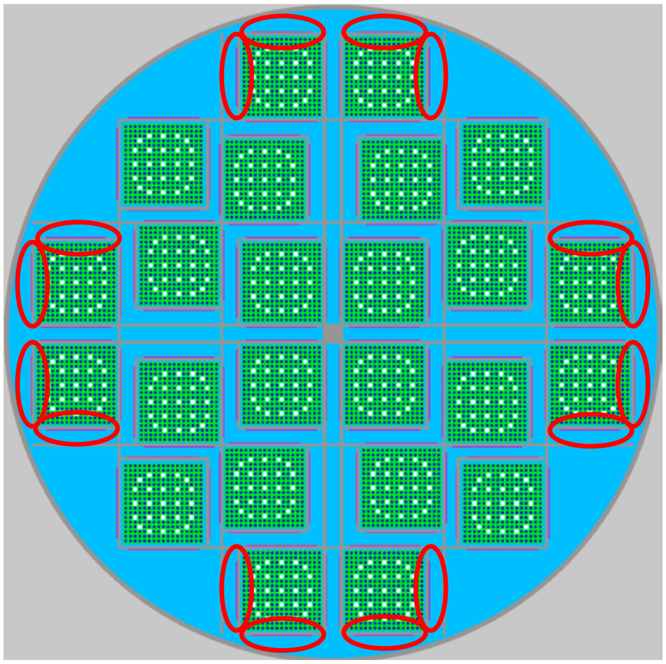

Figure D-1. Locations of narrow neutron absorber panels in MPC-24 basket.

D.2 MPC-68

The bottom of the active fuel is modeled 33.78 cm (~13.3 in.) above the top surface of the cask base plate. The top of the active fuel is approximately 38.13 cm (~15 in.) from the bottom surface of the cask lid. The volume above and below the active fuel is normally occupied by spacers and fuel assembly hardware, but these are neglected in the model. The material in the spacers is not credited in any configuration, although the axial position control provided by the spacers is considered in assessing credibility of axial misalignment configurations. All fuel assemblies are modeled as nominally centered within the fuel storage cells in the MPC-68 basket.

The basket dimensions are provided in Table D-3. The basket is positioned on the cask base plate. A gap of 5.87 cm (~2.31 in.) exists between the top of the basket walls and the lower surface of the cask lid.

The boron-based neutron absorber panels used in the MPC-68 are modeled with dimensions shown in Table D-4. The face clad is modeled as pure aluminum. The neutron absorber panel is modeled as centered in a channel with a thickness of 0.2844 cm (0.112 in.). The gaps between the neutron absorber panel faces and the wrapper walls are filled with water. The panels overlap the top and bottom of the active fuel by 6.35 cm (2.5 in.). The dimensions for the MPC-68 models are taken from Ref. 7.

Table D-3. MPC-68 basket dimensions

Parameter	Dimension (cm)	Dimension (in.)
Wall thickness	0.635	0.25
Basket height	447.04	176.0
Cell inner dimension	15.69	6.18

Table D-4. MPC-68 neutron absorber panel dimensions

Parameter	Dimension (cm)	Dimension (in.)
Panel width	12.065	4.750
Neutron absorber core thickness	0.2054	0.081
Face cladding thickness	0.0256	0.010
Panel length	393.7	155
Panel axial position (from base plate)	27.43	10.799
Wrapper thickness	0.1905	0.075
Neutron absorber areal density	0.0276 g $^{10}B/cm^2$	

Appendix E

Development of BWR Depletion Conditions

This appendix provides details about the selection of the axial burnup profile, the development of the axial moderator profile, and the calculation of the specific power used in the BWR depletion calculations. The data is selected from the CRC data available in Refs. 46 and 47.

The axial burnup profile modeled impacts the calculated k_{eff} of UNF. As discussed in Ref. 40, the gradient at the top end of the fuel assembly is the most important feature in driving reactivity in one profile relative to another. It is expected that BWR profiles are more severe than PWR profiles because the top of the assemblies experience high void fractions. This high void fraction and corresponding lack of moderation lead to lower relative burnups in the top section of a BWR assembly than a PWR assembly. The low-burnup region will also have a relative increase in plutonium generation at the same burnup. For these reasons, the axial burnup profiles in the PWR database [41] should not be used for BWR fuel. No analogous database of BWR axial burnup profiles exists, so axial burnup profiles from the CRC data for Quad Cities Unit 2 [46] and LaSalle Unit 1 [47] are surveyed for profile selection.

The relative burnup profiles for all assemblies presented in Refs. 46 and 47 are generated and compared to determine a potentially limiting burnup profile for use in these analyses. The two plants have different active fuel heights, so candidates are first selected from each plant, and then the potentially limiting profiles are compared to select the profile for use in these calculations. The relative burnup profiles are compared based on the integral relative burnup over two different axial extents from the top of the assembly. The relative burnups of the top three and top six nodes are summed, with lower sums indicating lower relative burnup leading to higher reactivity. The top three nodes include the top 45.72 cm (18 in.) and the top six nodes include the top 91.44 cm (36 in.) for each assembly. For Quad Cities Unit 2, assembly E7 has the lowest relative burnup in the top three nodes, but assembly F8 has the lowest relative burnup over the top six nodes. For LaSalle Unit 1, assembly C30 has the lowest relative burnup over both three and six nodes for all the assemblies considered. The relative burnup profile for assembly C30 is more severe over both the top three nodes and top six nodes than either E7 or F8 from Quad Cities Unit 2. The three potential profiles, including the integrated relative burnup over the top three and top six nodes, are provided in Table E-1. The LaSalle fuel has an active length of 150 in., compared to the 144-in. active length of fuel used at Quad Cities. This difference in length is not expected to cause a significant difference in calculated k_{eff}, so the use of LaSalle Unit 1 fuel data is acceptable for these calculations. A comprehensive study would be required to identify a limiting axial burnup profile for BWR fuel, though the profile used here is similar to a potentially limiting profile identified in Ref. 53.

The water density, which includes both the actual water density and the density reduction due to the presence of steam voids, is provided for each axial node at each case for each assembly in Refs. 46 and 47. This information is used to generate the axial moderator profile for the assembly with the limiting axial burnup profile: Assembly C30 from LaSalle Unit 1. The moderator profile that is used is the average of the water densities in each of the eight cases which include Assembly C30. This profile is presented in Table E-2. The simple average used varies by less than 0.3% at all elevations from a burnup-weighted average. The axial moderator density profile is also lower at nearly all elevations than the limiting distribution from the Quad Cities Unit 2 data in Ref. 46. The lower moderator density will lead to a harder neutron spectrum and more plutonium generation. The profile selected is therefore judged to be sufficiently conservative for use in these calculations.

Discharged assembly reactivity is not highly sensitive to operating history or specific power. The depletion calculations for these analyses model a specific assembly, C30, from a specific commercial BWR plant, LaSalle Unit 1. The specific power can be estimated from data provided in Ref. 47. The core power, number of assemblies, and MTU loading per assembly can be used to determine the average specific power in MW/MTU (W/g). The average burnup of the assembly compared to the cycle burnup can be determined for each case, and thus a relative power can be calculated. The burnup-weighted average specific power for assembly C30 is slightly greater than 30 MW/MTU. This specific power is used in the TRITON depletion calculations to generate the ARP libraries for the STARBUCS calculations. Both TRITON and STARBUCS depletion calculations assume a constant, full-power operating history. These assumptions provide realistic estimates of the UNF reactivity.

Table E-1. Potentially limiting relative burnup profiles from Quad Cities Unit 2 and LaSalle Unit 1

Axial zone midpoint elevation (cm)	Assembly C30 (LS U1)	Assembly E7 (QC U2)	Assembly F8 (QC U2)
7.62	0.2461	0.2141	0.2228
22.86	0.7879	0.7470	0.7500
38.10	1.0175	0.9788	0.9813
53.34	1.1026	1.0980	1.0996
68.58	1.1751	1.1518	1.1568
83.82	1.1942	1.1781	1.1877
99.06	1.2052	1.1967	1.2087
114.30	1.2168	1.2125	1.2270
129.54	1.2481	1.2522	1.2668
144.78	1.2535	1.2602	1.2743
160.02	1.2526	1.2589	1.2734
175.26	1.2485	1.2523	1.2657
190.50	1.2419	1.2458	1.2531
205.74	1.2320	1.2391	1.2361
220.98	1.2170	1.2306	1.2139
236.22	1.1955	1.2084	1.1843
251.46	1.1655	1.1651	1.1412
266.70	1.1260	1.1165	1.0940
281.94	1.0759	1.0555	1.0358
297.18	1.0118	0.9569	0.9425
312.42	0.9112	0.8369	0.8270
327.66	0.7873	0.6815	0.6773
342.90	0.6336	0.2968	0.3065
358.14	0.2886	0.1662	0.1742
373.38	0.1656	Not Applicable	
Top Three Nodes	1.0878	1.1446	1.1580
Top Six Nodes	3.7980	3.9939	3.9633

Table E-2. Average moderator density by axial node, based on Assembly C30 from LaSalle Unit 1

Axial zone midpoint elevation (cm)	Average moderator density (g/cm^3)	Axial zone midpoint elevation (cm)	Average moderator density (g/cm^3)
7.62	0.7396	205.74	0.3126
22.86	0.7396	220.98	0.2953
38.10	0.7288	236.22	0.2802
53.34	0.6875	251.46	0.2668
68.58	0.6349	266.70	0.2549
83.82	0.5798	281.94	0.2445
99.06	0.5284	297.18	0.2354
114.30	0.4831	312.42	0.2276
129.54	0.4434	327.66	0.2213
144.78	0.4089	342.90	0.2163
160.02	0.3794	358.14	0.2128
175.26	0.3539	373.38	0.2115
190.50	0.3317		